How Extreme Apparitions of the Volcanic and Anthropogenic South East Asian Aerosol Plume Trigger and Sustain El Niño Events. First Attribution and Mechanism using data from the Last Millennium Ensemble, Large Ensemble, MERRA-2 Reanalysis, four Satellites and the Global Volcanism Program.

Keith Alan Potts[1]

[1]Kyna Keju Pty Ltd

November 22, 2022

Abstract

Volcanic aerosols over south east Asia have always been the trigger and sustaining cause of ENSO events. In recent decades this natural plume has been augmented by the anthropogenic plume which has intensified ENSO events especially in SON. Data from the Last Millennium Ensemble (13,972 months), and Large Ensemble (3,012 months) demonstrate this connection with three ENSO indices and aerosol data derived from the same datasets correlating at 1.00 (LME), 0.97 and 0.99 magnitude (segmented and averaged). ENSO events are the dominant mode of variability in the global climate responsible for Australian, Indian and Indonesian droughts, American floods and increased global temperatures. Understanding the mechanism which enables aerosols over SE Asia and only over SE Asia to create ENSO events is crucial to understanding the global climate. I show that the South East Asian aerosol Plume causes ENSO events by: reflecting/absorbing solar radiation which warms the upper troposphere; and reducing surface radiation which cools the surface under the plume. This inversion reduces convection in the region thereby suppressing the Walker Circulation and the Trade Winds which causes the SST to rise in the central Pacific Ocean and creates convection there. This further weakens/reverses the Walker Circulation driving the climate into an ENSO state which is maintained until the aerosols dissipate and the climate system relaxes into a non-ENSO state. Measured aerosol data from four NASA satellites, estimates of volcanic tephra from the Global Volcanism Program (GVP) for over 100 years and the NASA MERRA-2 reanalysis dataset all confirm this analysis.

How Extreme Apparitions of the Volcanic and Anthropogenic South East Asian Aerosol Plume Trigger and Sustain El Niño Events. First Attribution and Mechanism using data from the Last Millennium Ensemble, Large Ensemble, MERRA-2 Reanalysis, four Satellites and the Global Volcanism Program.

K. A. Potts[1]

[1]Kyna Keju Pty Ltd.

Corresponding author: Keith Potts (Keith.Potts@bigpond.com)

Key Points:

- Volcanic aerosol plumes over SE Asia are and always have been the trigger and sustaining force for ENSO events
- The anthropogenic aerosol plume has intensified the volcanic plume and ENSO events in recent decades
- Analysis of the Last Millennium Ensemble, Large Ensemble, MERRA-2, 4 satellite's and Global Volcanism Program data confirms this

Abstract

Volcanic aerosols over south east Asia have always been the trigger and sustaining cause of ENSO events. In recent decades this natural plume has been augmented by the anthropogenic plume which has intensified ENSO events especially in SON. Data from the Last Millennium Ensemble (13,972 months), and Large Ensemble (3,012 months) demonstrate this connection with three ENSO indices and aerosol data derived from the same datasets correlating at 1.00 (LME), 0.97 and 0.99 magnitude (segmented and averaged). ENSO events are the dominant mode of variability in the global climate responsible for Australian, Indian and Indonesian droughts, American floods and increased global temperatures. Understanding the mechanism which enables aerosols over SE Asia and only over SE Asia to create ENSO events is crucial to understanding the global climate. I show that the South East Asian aerosol Plume causes ENSO events by: reflecting/absorbing solar radiation which warms the upper troposphere; and reducing surface radiation which cools the surface under the plume. This inversion reduces convection in the region thereby suppressing the Walker Circulation and the Trade Winds which causes the SST to rise in the central Pacific Ocean and creates convection there. This further weakens/reverses the Walker Circulation driving the climate into an ENSO state which is maintained until the aerosols dissipate and the climate system relaxes into a non-ENSO state. Measured aerosol data from four NASA satellites, estimates of volcanic tephra from the Global Volcanism Program (GVP) for over 100 years and the NASA MERRA-2 reanalysis dataset all confirm this analysis.

1 INTRODUCTION

1.1 The Hypothesis and Physical Model

This paper explores an explicit physical model and hypothesis to explain how the occurrence of ENSO events is and always has been triggered and sustained by the natural volcanic aerosol plume over south east Asia (SEAsia) which has, in recent decades, been intensified by the anthropogenic aerosol plume especially from September to November (SON).

The sequence of events is:

1. The volcanic tephra aerosol plume forms and, in recent decades, is intensified by the anthropogenic plume which is most intense from September to November (SON);
2. The aerosols absorb (and reflect) solar radiation which heats the atmosphere;
3. The aerosols reduce the solar radiation at the surface under the plume which cools the surface;
4. 2 and 3 create a temperature inversion compared to times without a plume and this reduces convection;
5. Reducing convection over SEAsia causes the Trade Winds blowing from east to west over the Pacific Ocean to reduce in intensity as there is no exit into the convection and the Hadley and Walker Circulation;
6. Reducing the Trade Wind speed over the Pacific Ocean cause the sea surface temperature to rise;
7. The increased temperature in the central Pacific Ocean causes convection in this region and the Walker circulation further relaxes or even reverses;
8. The SOI is forced into a negative phase by these changes
9. The western Pacific warm pool then migrates east as the wind stress on the ocean has reduced;
10. The ENSO event continues until the aerosol plume over SEAsia dissipates which is typically when the SEAsian monsoon starts;
11. With the revived Trade Wind speed over the Pacific Ocean the warm pool then migrates west again and the ENSO event ends.

1.2 ENSO

El Niño Southern Oscillation Index (SOI) (ENSO) events are defined in the Intergovernmental Panel on Climate Change (IPCC) Assessment Report Four (AR4) Glossary as a coupled atmosphere-ocean phenomenon with a two to seven year time scale during which "the prevailing trade winds weaken, reducing upwelling and altering ocean currents such that the sea surface temperatures warm, further weakening the trade winds. This event has a great impact on the wind, sea surface temperature and precipitation patterns in the tropical Pacific. It has climatic effects throughout the Pacific region and in many other parts of the world, through global teleconnections."

Three national meteorological organisations together with The National Aeronautics and Space Administration (NASA) define ENSO in similar ways on their websites and there is also an extensive body of literature which describes the characteristics of ENSO events including:

1. "All [El Niño or ENSO] events are preceded by westerly wind anomalies on the equator near the date line." [*Enfield*, 1989];
2. "El Niño (EN) is characterized by a large-scale weakening of the trade winds and warming of the surface layers in the eastern and central equatorial Pacific Ocean." *McPhaden et al.* [1998] in a review of the history of El Niño events;
3. "The onset of an El Niño is characterized by a decrease in wind power that leads to a decrease in available potential energy, and hence a flatter thermocline." [*Brown and Fedorov*, 2010];
4. "the principal factor that affected model ENSO behavior is the change in the basic-state equatorial winds and associated equatorial upwelling." [*B. Wang and An*, 2002];
5. "Our model experiments reproduce the empirical observations of a short-term ENSO response to explosive tropical eruptions" [*Mann et al.*, 2005]
6. "The El Niño–Southern Oscillation (ENSO) cycle of alternating warm El Niño and cold La Niña events is the dominant year-to-year climate signal on Earth. ENSO, originates in the tropical Pacific through interactions between the ocean and the atmosphere" [*McPhaden et al.*, 2006]
7. *Zebiak and Cane* [1987] in exploring the reproduction of ENSO events in a climate model noted that "ENSO is largely controlled by deterministic processes in the tropical Pacific atmosphere-ocean system".
8. *Timmreck* [2012] explored the impact of low latitude strong explosive eruptions on climate and ENSO finding that the climate response depends on the initial ENSO phase and the eruption season;
9. *S McGregor et al.* [2014] investigated the pause in global warming and suggested that the Atlantic SST increase contributed to the strengthening of the Walker circulation.
10. *Maher et al.* [2015] investigated the effects of large tropical eruptions on the Indian-Pacific variability and found they are associated with "co-occurring El Niño and positive IOD events" which peak "6-12 months after the volcanic forcing peaks";
11. *Predybaylo et al.* [2017] also investigated the large, low latitude Pinatubo eruption in 1991but only used SO_2 emissions and found that the ENSO response depends on season and initial ENSO state.
12. *Blake et al.* [2018] investigated the effects of the six largest tropical volcanic eruptions using the Last Millennium Ensemble (LME) data from 850 to 1850 on Australian rainfall, the IOD and ENSO finding that the eruptions "increased the likelihood of El Niño and a positive IOD condition for up to four years following an eruption".

It is therefore clear that the Trade Winds and therefore the Walker Circulation are intimately connected with ENSO events and determining the cause of the weakening of the Trade Winds and Walker Circulation may well reveal the cause of ENSO events.

It is also worth noting that many of the references above only include large eruptions at any location and SO_2 emissions. Whereas this paper examines the role the natural and anthropogenic (all eruptions and aerosols) South East Asian aerosol Plume (SEAP) plays in reducing convection, weakening the Walker Circulation and thus in initiating and maintaining ENSO events. Aerosol plumes can alter the major atmospheric circulation systems [*Solomon et al.*, 2007], [*Remer et al.*, 2009] and the SEAP is uniquely positioned to influence the Walker Circulation as it exists in the region of normal (non-ENSO) Walker Circulation convection.

1.3 ENSO Return Frequency

The literature describes ENSO events as exhibiting a return frequency of two to seven to ten years and the University Corporation for Atmospheric Research (UCAR) website at http://webext.cgd.ucar.edu/Multi-Case/CVDP_repository/cesm1.lm in the ENSO section shows the ENSO power spectra for all the LME runs and the same information for the HadISST_1 [*Rayner et al.*, 2003] and ERSST v5_1 [*Huang et al.*, 2017]. The HadISST_1 and ERSST v5_1 spectra are similar and Figure 1 shows the multiple peaks in the HadISST_1 data whilst all the LME runs show a single peak at about 5 years and are nearly identical even with different forcings whilst they are all very different to the two spectra based on real data as Figure 1 shows. The reasons for this variation are discussed in the results section.

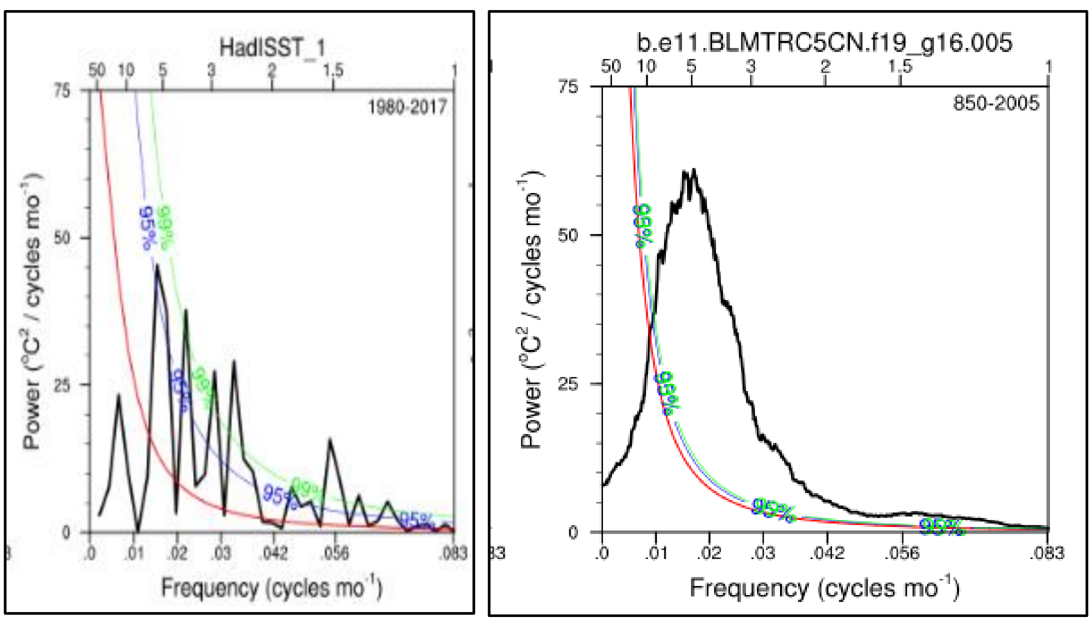

Figure 1: ENSO Power Spectra: Left: HadISST_1 and Right: run 5 LME all forcings

1.4 The SEAP and CSEAP Areas

In this analysis two areas are used which are shown in Figure 2:

1. The SEAP Area 10ºS-10ºN and 90ºE-160ºE which is the area covered by the SEAP;
2. The Central SEAP (CSEAP) Area 5ºS-5ºN and 100ºE-120ºE where the anthropogenic SEAP is most intense.

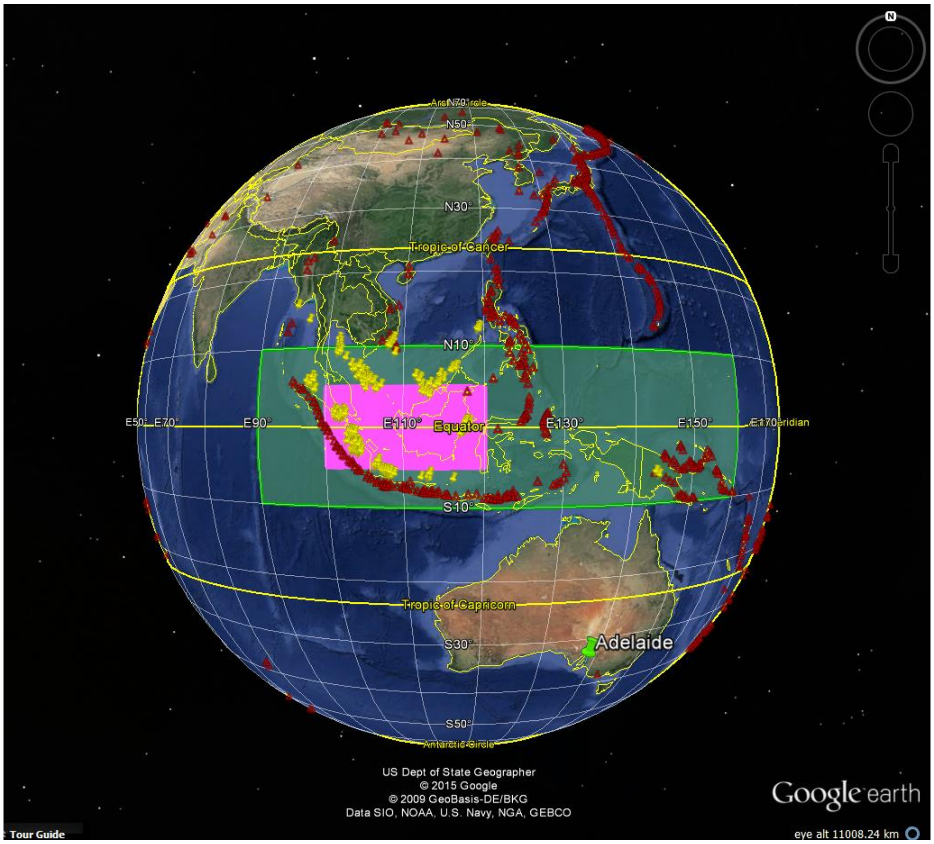

Figure 2: The SEAP Area, Green and CSEAP Area, pink with the locations of gas flares (from National Oceanic and Atmospheric Administration (NOAA) and the Global Gas Flaring Reduction Partnership (GGFRP)) in yellow and volcanoes (Global Volcanism Program (GVP)) in red. Image source: Google Earth.

1.5 The South East Asian Plume (SEAP)

This paper focuses on south east Asia as this region is where convection, which drives the Walker Circulation, occurs and is therefore where aerosols can have a significant effect. Appendix A describes the sources of aerosols in the SEAP Area, the Natural SEAP derived from volcanic eruptions and the Anthropogenic SEAP derived mainly from biomass burning and gas flares in the oil production industry.

1.5.1 The Natural SEAP

The SEAP Area, which covers about 3.4% of the globe, is the world's most tectonically active area with the United States Geological Survey (USGS) earthquake database showing 29% (5 of 17) of the major earthquakes (magnitude > 8.4) in the world since 1900 occurred in the SEAP Area and the GVP's database showing that from 1500 to 2018 over 18% of the global volcanic eruptions occurred in the SEAP Area. *Simkin and Siebert* [2000] state that 5 of 16 (31%) of the continuously erupting volcanoes in the world for the past 24 years are located in the SEAP Area and that one more, in Vanuatu, is just to the south east of the SEAP Area.

1.5.2 The Anthropogenic SEAP

The anthropogenic SEAP is one of eight continental scale, anthropogenic, aerosol plumes which occur annually and are shown in Figure 3. These extreme plumes typically exist for a few months each year at the end of the regional dry season when biomass burning can occur. The SEAP is easily identified on the monthly mean 0.55 micron Aerosol Optical Depth (AOD) data from MODIS [*Kaufman et al.*, 2000] on the NASA Terra and Aqua satellites. The monthly average AOD of the CSEAP Area observed by Terra is shown in Figure 4 to demonstrate the peak anthropogenic aerosol emission season is SON, the end of the dry season in SE Asia, and was extremely high (AOD > 0.6) in 2002, 2004, 2006, 2009, 2014 and 2015 compared with the intervening years. Peaks in the MODIS AOD in SON are attributed to seasonal biomass burning in south east Asia (Appendix A). CALIPSO (Cloud-Aerosol Lidar and Infrared Pathfinder Satellite Observations) [*Winker et al.*, 2009] profiles confirm a layer of smoke existed at about 3Km altitude in October 2015 in the SEAP Area and Figure 5 shows the geographic extent of the extreme October 2006 apparition of the SEAP. This paper analyses the effects of the SEAP on an annual, April to October (wet season in south eastern Australia) and SON (when the anthropogenic plume is at its most intense and will therefore have its greatest effect.) basis.

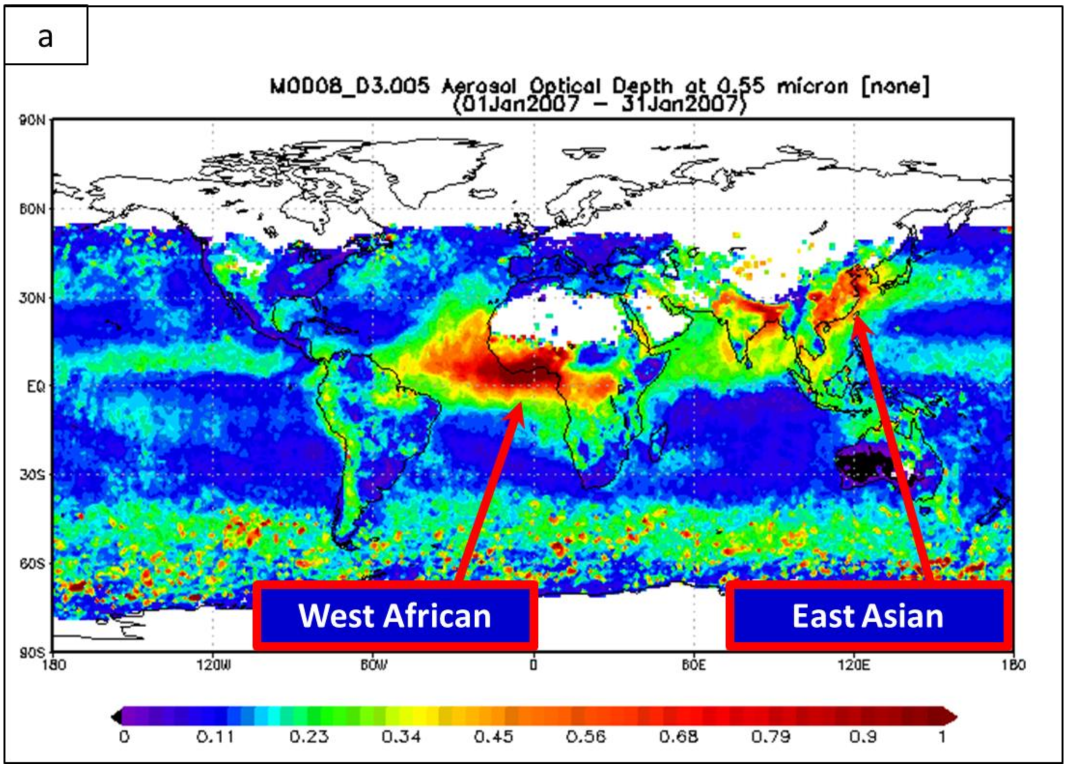

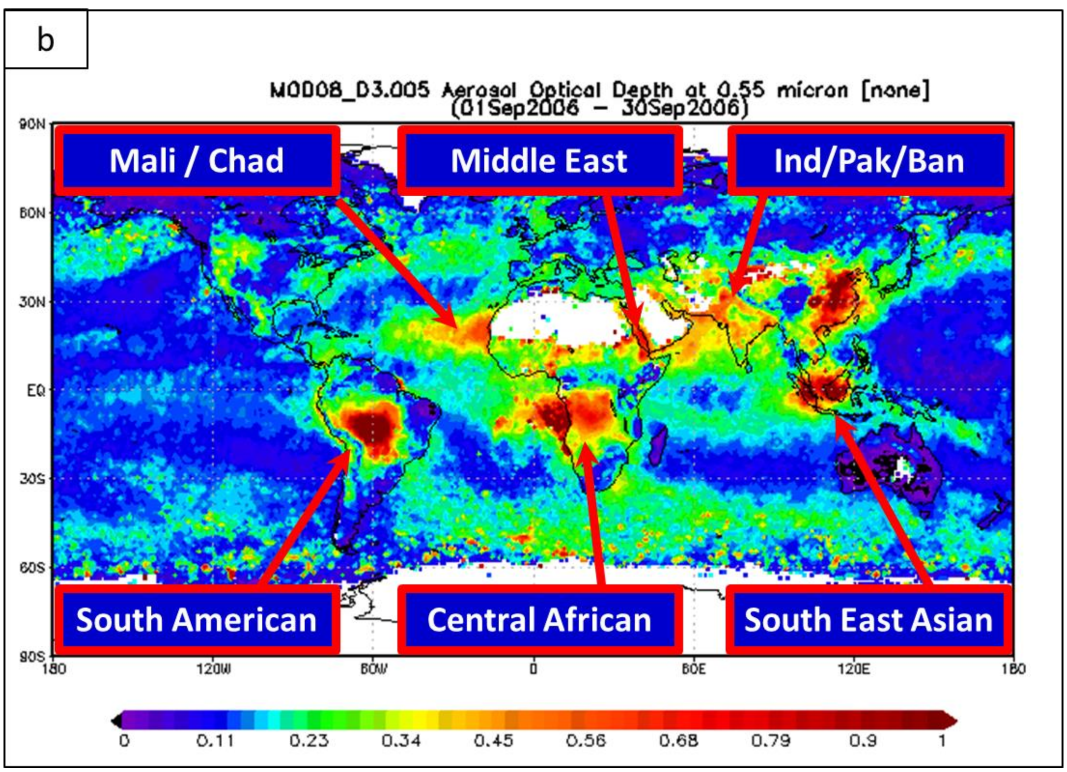

Figure 3: The Eight Continental Scale Aerosol Plumes. NASA Giovanni AOD (a) January 2007 (b) September 2006. Source: NASA Giovanni.

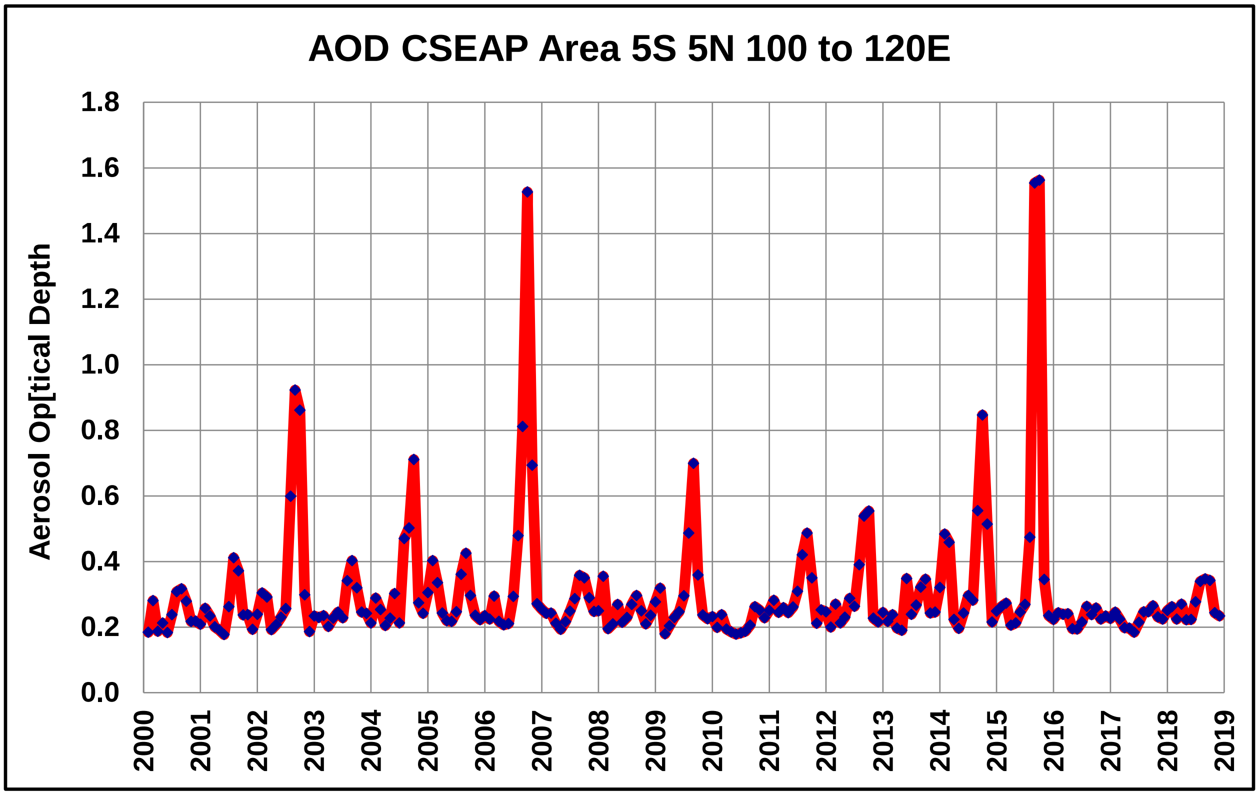

Figure 4: Monthly average MODIS Terra AOD in the CSEAP Area 5ºS-5ºN and 100ºE-120ºE.

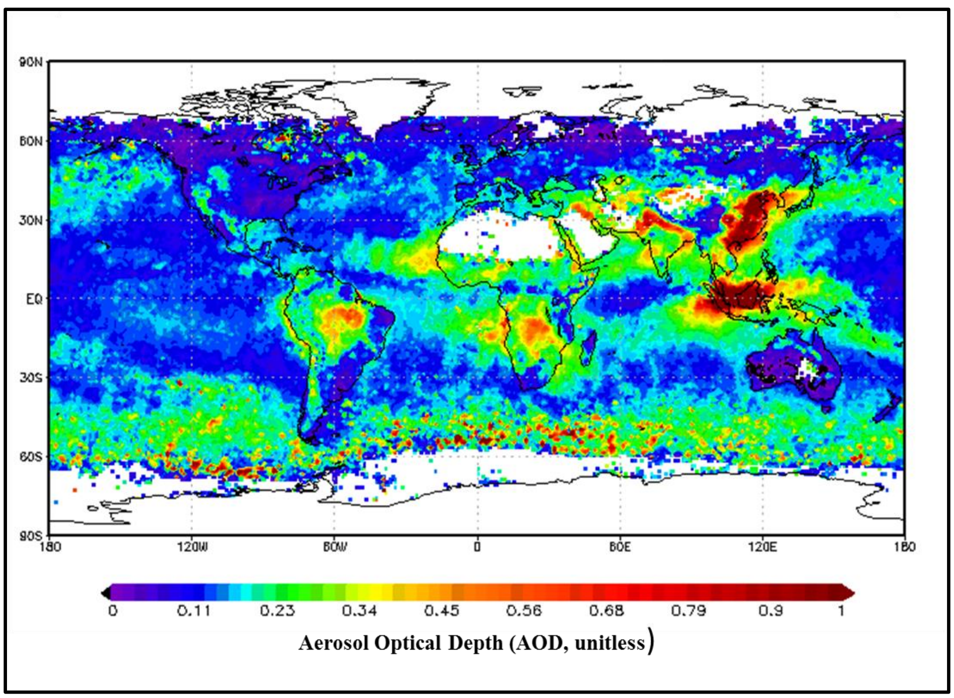

Figure 5: NASA MODIS monthly mean AOD data for October 2006. Source: NASA Giovanni.

The SON average Aerosol Index (AI) and AOD of the CSEAP Area from 1979 to 2018 in SON is shown in Figure 6. The maximum AOD was 1.60 (Oct 2015) and the maximum Nimbus 7 (N7) and Earth Probe (EP) AI was 1.81 (Sept 1997). The AI of the CSEAP Area increased from 0.050 in Sep 1979 to 0.297 in 1992 and to 0.396 in 2000 a 491% and 687% increase respectively in years without extensive biomass burning. From 1979 to 1997, a major biomass burning event year [*Applegate et al.*, 2001], the increase in September in AI is 3,499%.

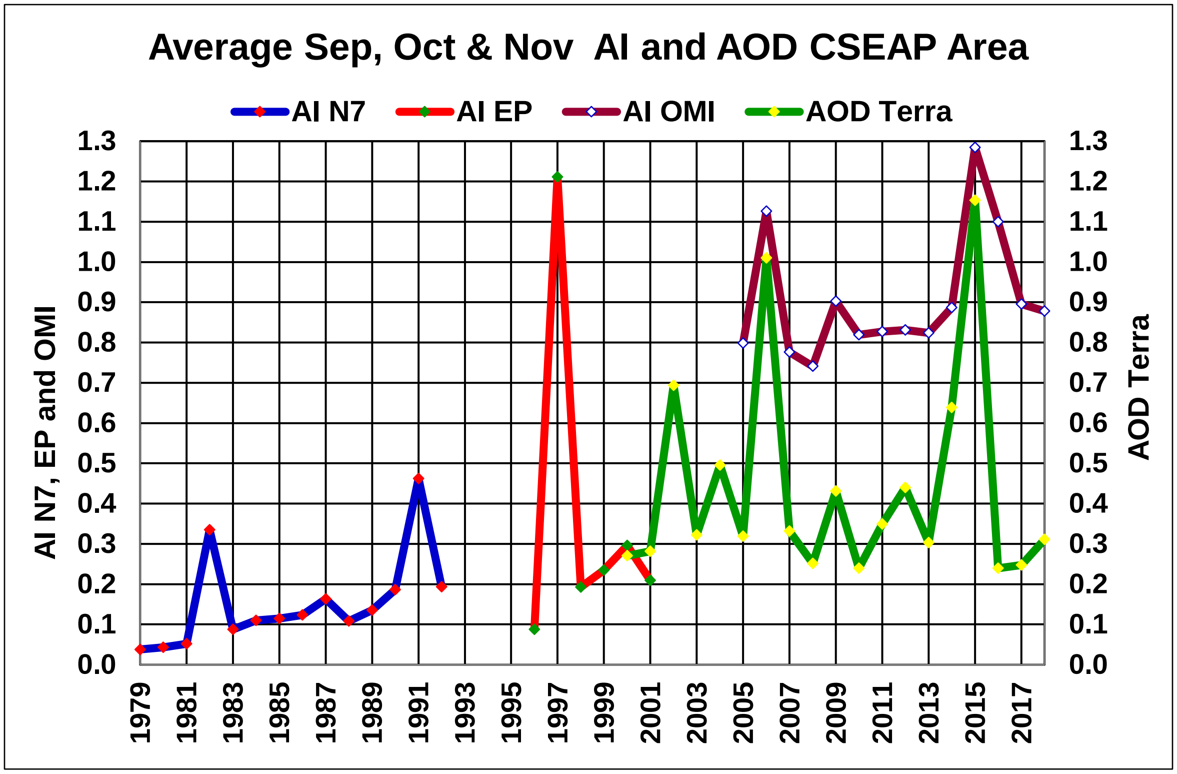

Figure 6: Average SON AI (N7, EP and OMI) and AOD (MODIS on Terra) CSEAP Area. (N7 – TOMS instrument, EP – TOMS instrument, OMI Ozone Monitoring Instrument)

The surface radiative forcing of the anthropogenic SEAP is significant and the literature includes:

1. A 10% to 30% reduction of Photosynthetically Active Radiation [Ramanathan, 2006];
2. -150 W m^{-2} [Duncan et al., 2003]; and
3. During ACE-Asia, ~-286.0 W/m^2/τα [*Hansell et al.*, 2003] (τα is the aerosol optical depth and its derivation is described in the paper in detail).

1.6 The Walker Circulation

The Walker Circulation is defined in the IPCC AR4 Glossary as "Direct thermally driven zonal overturning circulation in the atmosphere over the tropical Pacific Ocean, with rising air in the western and sinking air in the eastern Pacific" (See also [*Chunzai Wang*, 2002], [*Barry and Chorley*, 2010], [*Trenberth et al.*, 2000] and [*Sturman and Tapper*, 1996]).

The Australian Bureau of Meteorology (BOM) shows images of the atmospheric circulation during El Niño, La Nina and neutral seasons on its website at: http://www.bom.gov.au/climate/about/australian-climate-influences.shtml?bookmark=enso. It is clear from these figures that the "direct thermal drive" for the La Niña and neutral Walker Circulation must be located at ground level in the SEAP Area where solar radiation heats the Earth's surface which in turn heats the atmosphere as the rising limb of the non-ENSO Walker Circulation is located there in exactly the same location as the SEAP which is therefore uniquely positioned to directly affect the Walker Circulation and ENSO.

Since variations in the solar energy at the top of the atmosphere cannot explain the reduction in the surface heating in the SEAP Area which causes the Walker Circulation to relax the reduction must be caused by variations in the atmosphere where the SEAP reduces surface solar radiation. Indeed Figure 7 from the IPCC AR4 shows that, on a globally averaged basis, surface radiative forcing is controlled by aerosols with the net effect of long-lived greenhouse gases, ozone, aerosols and land use aligning nearly perfectly with the aerosol direct effect.

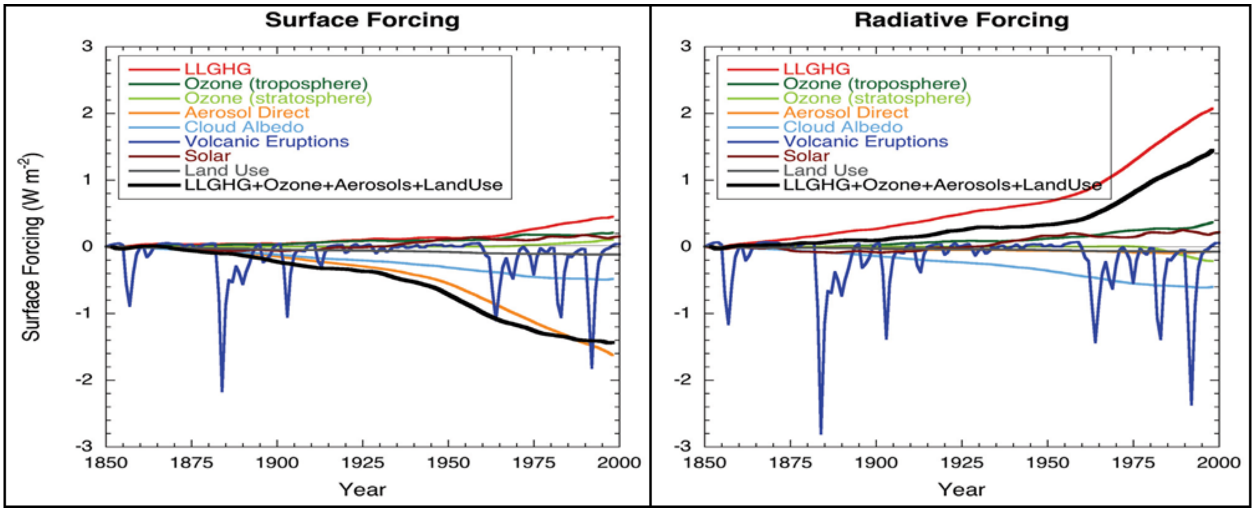

Figure 7: - Source: IPCC AR4 Figure 2.23. Globally and annually averaged temporal evolution of the instantaneous all-sky RF (right panel) and surface forcing (left panel) due to various agents, as simulated in the MIROC+SPRINTARS model (Nozawa et al., 2005; Takemura et al., 2005). This is an illustrative example of the forcings as implemented and computed in one of the climate models participating in the AR4. Note that there could be differences in the RFs among models. Most models simulate roughly similar evolution of the LLGHGs' RF. [*Nozawa et al.*, 2005] and [*Takemura et al.*, 2005].

Therefore, from the IPCC AR4 and literature it is a plausible hypothesis that the SEAP could force the Walker Circulation and trade winds to "relax" by reducing the surface solar radiation available to drive convection in the Walker Circulation in the SEAP Area and this paper examines the connection between the SEAP, convection in the SEAP Area, the trade winds, the Walker Circulation and ENSO events.

However, since the anthropogenic SEAP is a recent event driven by population growth as Appendix A and Figure 6 show and ENSO events have been occurring for many centuries to prove the hypothesis that the SEAP causes ENSO events it is necessary to show that the natural aerosols originating from volcanic eruptions in the SEAP Area can also trigger and sustain ENSO events.

1.7 Volcanic Eruptions and ENSO

The literature includes many attempts to connect volcanic eruptions and ENSO events. *Neville Nicholls* [1988] and *N. Nicholls* [1990] investigated volcanic eruptions and El Niño events and concluded there was no connection. *Hirono* [1988] investigated the possibility that the 1983 eruption of El Chichon in Mexico could have triggered the El Niño which followed. *Robock et al.* [1995] investigated the *Hirono* [1988] hypothesis and found that the eruption did not trigger the El Niño event which followed and also noted that "only trade wind collapses in the western equatorial Pacific can initiate El Niños". *Handler and Andsager* [1990] investigated the volcanic hypothesis which states that low-latitude volcanic aerosols are the immediate and only cause of warmer than normal SST or El Niño and its inverse using Monte Carlo techniques and found that both aspects of the hypothesis were satisfied to "a very high level of statistical significance". *Self et al.* [1997] investigated volcanic aerosol perturbations and the 16 strongest El Niño events over the last 150 years and found no general correlation. In discussing the evolution of ENSO events *Trenberth et al.* [2002] suggested that the effects of volcanic eruptions on ENSO events remained unanswered questions. *Emile-Geay et al.* [2008] focused on very large eruptions which were greater than the Pinatubo eruption in 1991 and found that small eruptions have no effect. *D Zhang et al.* [2013a] investigated the effects of large eruptions using AOD in latitudinal bands 0 to 30 and 30 to 90 in both hemispheres to force the climate model but did not consider the location or the intensity of the eruption and noted this should be done in the future. *Cane* [2005] reviewed forecasts of ENSO activity, found that there was no clear picture and suggested solar and volcanic variations in solar insolation and atmospheric aerosols might have a role. It is also worth noting that *Ammann et al.* [2003] found that including an improved volcanic eruption dataset in climate model simulations improved the correlation between the modelled data and observations whilst *Mann et al.* [2005] stated "Our model experiments reproduce the empirical observations of a short-term ENSO response to explosive tropical eruptions"

There is therefore obviously great interest in, but no general agreement on, the connection between volcanic eruptions and ENSO events.

2 METHOD AND DATA

Modelling, satellite and GVP data are used to show that ENSO and the climate variations commonly linked to ENSO events are accurately explained using mechanisms controlled by the SEAP.

2.1 Modelling – LME, LE and MERRA-2

The LME [*Otto-Bliesner et al.*, 2016] data from one member of each of the eight forcing simulations with run number in () (850 (3), All (13), Ozone and Aerosol (Aero) (2), Green House Gas (GHG) (3), Land use (Land) (3), Orbital (3), Solar (5) and Volcanic (5)) was used to create time series of 1,156 years and 13,872 months of: aerosol optical depth; air temperature; surface temperature; omega; wind speed; Oceanic Nino Index; and the global temperature as well as indices for the Nino 3.4 and 1+2 SST and the SOI (which the IPCC AR5 shows are used to monitor the status of ENSO). These series were correlated to demonstrate that these indices and parameters are directly connected to aerosols in the SEAP area.

A similar approach was used for the Large Ensemble (LE) [*Kay et al.*, 2015] using data from 1850 to 2005 with historic forcings and from 2006 to 2100 using RCP 8.5 projections (run 001) and with the NASA Modern Era Retrospective analysis for Research and Applications release two (MERRA-2) reanalysis dataset [*Gelaro et al.*, 2017] which includes assimilated aerosols.

LME and LE data is at https://www.earthsystemgrid.org/ and MERRA-2 data is at http://giovanni.gsfc.nasa.gov/giovanni/

2.2 Satellite Data

The same indices from that IPCC AR5 table were also correlated with four satellite-based measures of aerosols: The Aerosol Index (AI), obtained from the Total Ozone Mapping

Spectrometer (TOMS) instruments on the N7 and EP satellite platforms; the AOD from the MODIS instrument on NASA Terra; and the AI from the Ozone Monitoring Instrument (OMI) on NASA Aura.

Note: AI, unlike AOD, is "only sensitive to desert dust and elevated smoke layers. Therefore, it does not account for aerosols of industrial origin or any kind of aerosol in the lowest 2 km of the atmosphere" (Personal Communication - NASA). However in the SEAP Area it is useful as we are investigating biomass burning "smoke" in SON and the CALIPSO data at https://eosweb.larc.nasa.gov/project/calipso/calipso_table shows smoke at an altitude of 3Km in October 2015, above the lower limit of AI data.

The following datasets:

1. Sea Surface Temperature Niño 3.4 area (5ºS-5ºN, 170ºW-120ºW). http://www.cpc.ncep.noaa.gov/data/indices/ ;
2. Sea Surface Temperature Niño 1 and 2 areas (10°S–0°, 90°W–80°W). http://www.cpc.ncep.noaa.gov/data/indices/ ;
3. Southern Oscillation Index - Standardized difference of Sea Level Pressure (SLP) - Tahiti minus Darwin. http://www.bom.gov.au/climate/current/soihtm1.shtml ;

and the following:

1. Omega (vertical motion in the atmosphere) at 400mb level - CSEAP Area. http://www.esrl.noaa.gov/psd/cgi-bin/data/timeseries/timeseries1.pl (Source 1)
2. Rainfall – CSEAP Area. Data NCEP reanalysis (Source 1);
3. SST - SEAP Area. Data NCEP reanalysis (Source 1);
4. Interpolated OLR – CSEAP Area. Data NOAA NCEP reanalysis (Source 1);
5. Trade Wind Index (TWI) (850mb at 5ºN-5ºS, 175ºW-140ºW). http://www.cpc.ncep.noaa.gov/data/indices/cpac850 (source 2)
6. Oceanic Niño Index (ONI). Data NOAA (source 2); and
7. Air temperature at 650 hPa. Data MERRA-2 reanalysis.

2.3 Volcano Data

Volcanic eruption data from the GVP was processed using the methodology outlined in Appendix A and analysed against the main ENSO parameters.

3 RESULTS

The results in Figures 8, 9, 11 and 15 were calculated using the Excel correlation function with students two tail t test and colour coded for significance (yellow < 0.01, brown <0.02, green < 0.05 and blue < 0.1).

3.1 Modelling

Modelling from the LME and LE was analysed. Due to the significant variation in the mean and variability in the aerosol and temperature data from both the LME and LE data this data is non-stationary and must be pre-processed to achieve stationarity before correlating as this paper is investigating interannual variations. Acceptable stationarity, after testing using a variety of methods including PAST 3.22 [*Hammer et al.*, 2001], was achieved by the methods shown in Appendix B.

3.1.1 The Last Millennium Ensemble

The results of my analysis of the correlation between: the ENSO indices derived from TS (Skin Temperature) and PSL (Sea Level Pressure); temperature at level 609 and the surface, omega in the SEAP Area; the global temperature from TS; and the aerosol loading AODVIS (Aerosol Optical Depth 550 nm) in the SEAP and CSEAP areas averaged from one of each of the eight forcing regimes are shown in Figure 8. The LME TS from the atmosphere data was used instead of the SST from the ocean data to avoid having to regrid the ocean data to latitude and longitude (suggested by the UCAR help desk). The Oceanic Nino Index is a 3 month running average of the Nino 3.4 TS

Note: The volcanic forcing data in the LME cannot of itself demonstrate the connection between the natural volcanic SEAP and ENSO as it does not have the resolution required to do so. It is derived from ice cores in the Arctic and Antarctic [*Otto-Bliesner et al.*, 2016] and *Gao et al.* [2008] who provide the data as only stratospheric sulfate forcing in latitude bands (ten degrees wide), by altitude and month. For volcanic tephra to travel to the polar regions the tephra must be injected into the stratosphere requiring a minimum VEI of 3 to 4. Hence all the VEI 0,1,2 and some (50% assumed) of the VEI 3 eruptions in the SEAP Area must be missing from the dataset. Since this excludes over 94% of the eruptions in the SEAP Area since 1850 which are used in this paper the resolution of this LME volcanic forcing dataset is inadequate in itself in terms of eruption size, geo-space and aerosol type to prove the causation of ENSO by SEAP Area volcanic tephra described in this paper. Although these LME volcanic forcing runs do provide another independent LME aerosol forcing dataset which is useful.

3.1.2 The Large Ensemble

The LE data used includes historic data from 1850 to 2005 and RCP 8.5 data from 2006 to 2100. The data was analysed in these two parts and the results averaged and shown in the same way as the LME data in Figure 9.

Note some of the very high correlations from the LME and LE show significance levels much less than 0.01 due to the correlation magnitude and the length of the time series.

	SEAP T Level 609	SEAP Area TS	SEAP Area Omega	Nino 3.4 U10	Nino 3.4 TS	Nino 1+2 TS	ONI	SOI	Global TS	Nino 3.4 TS & U10 Wind
Monthly Segmented										**-0.89**
CSEAP	**0.94**	**-0.98**	**0.95**	**-0.82**	**0.96**	**0.91**	**0.95**	**-0.97**	**0.83**	
SEAP	**0.99**	**-0.99**	**0.76**	**-0.90**	**0.93**	**0.84**	**0.94**	**-0.98**	**0.78**	
Interannual Series (September to November Averages - No smoothing)										**-0.85**
CSEAP	**0.38**	**-0.88**	**0.82**	**-0.76**	**0.79**	**0.68**	**0.78**	**-0.79**	**0.42**	
SEAP	**0.50**	**-0.88**	**0.87**	**-0.79**	**0.77**	**0.70**	**0.76**	**-0.78**	**0.44**	
Interannual Series (April to October Averages - No smoothing)										**-0.88**
CSEAP	**0.58**	**-0.80**	**0.80**	**-0.73**	**0.85**	**0.70**	**0.83**	**-0.89**	**0.45**	
SEAP	**0.76**	**-0.73**	**0.81**	**-0.84**	**0.83**	**0.73**	**0.81**	**-0.80**	**.057**	
Annual Averages (No smoothing)										**-0.92**
CSEAP	**0.61**	**-0.77**	**0.79**	**-0.82**	**0.90**	**0.78**	**0.87**	**-0.86**	**0.58**	
SEAP	**0.80**	**-0.64**	**0.83**	**-0.87**	**0.84**	**0.80**	**0.81**	**-0.79**	**0.66**	
Annual Average - Segmented & Averaged (8 segments)										**-1.00**
CSEAP	**0.96**	**-0.95**	**0.92**	**-0.97**	**1.00**	**1.00**	**0.98**	**-1.00**	**0.98**	
SEAP	**0.99**	**-0.94**	**0.98**	**-0.99**	**0.99**	**0.98**	**0.98**	**-0.97**	**0.98**	

Figure 8: Average correlations of eight runs, one from each of the eight forcings described in the text, from the LME of AODVIS in the CSEAP and SEAP Areas with the ENSO indices, SEAP Area Surface and level 609 Temperature, omega, Nino 3.4 wind speed and the global temperature. Last column correlations of Nino 3.4 TS and U10 wind speed.

	SEAP T Level 609	SEAP Area TS	SEAP Area Omega	Nino 3.4 U10	Nino 3.4 TS	Nino 1+2 TS	ONI	SOI	Global TS	Nino 3.4 TS & U10 Wind
Monthly Series Segmented										-0.81
CSEAP Area	0.90	-0.93	0.96	-0.94	0.90	0.96	0.86	-0.86	0.90	
SEAP Area	0.88	-0.97	0.83	-0.91	0.93	0.80	0.93	-0.95	0.96	
Interannual Series (September to November Averages - No smoothing)										-0.85
CSEAP Area	0.68	-0.90	0.90	-0.85	0.78	0.75	0.81	-0.73	0.42	
SEAP Area	0.68	-0.85	0.85	-0.82	0.63	0.66	0.76	-0.72	0.44	
Interannual Series (April to October Averages - No smoothing)										-0.94
CSEAP Area	0.68	-0.89	0.91	-0.85	0.88	0.69	0.87	-0.84	0.47	
SEAP Area	0.84	-0.80	0.83	-0.81	0.76	0.57	0.80	-0.76	0.52	
Annual Averages (No smoothing)										-0.96
CSEAP Area	0.64	-0.89	0.92	-0.89	0.92	0.79	0.88	-0.82	0.60	
SEAP Area	0.84	-0.78	0.91	-0.85	0.86	0.73	0.82	-0.77	0.63	
Annual Average - Segmented & Averaged										-0.99
CSEAP Area	0.96	-0.99	0.98	-0.99	0.99	0.97	0.98	-0.97	0.89	
SEAP Area	0.99	-0.99	0.98	-0.99	0.99	0.99	0.99	-0.97	0.94	

Figure 9: Average correlations from the LE (1850 to 2005 and 2006 to 2100) of AODVIS in the CSEAP and SEAP Areas with the ENSO indices, SEAP Area Temperature at the surface and level 609, omega and the global surface temperature. Last column correlations of Nino 3.4 Area Skin Temp and U10 wind speed. Correlation significance shown is derived from the lowest significance of the two correlations. Red indicates one of the two correlations only included two points with the other showing <0.01 significance.

When the LME CSEAP Area AODVIS and Nino Index data from the TS, omega, U10 wind speed and surface pressure data are segmented and averaged the extraordinary correlations in Figure 8 results with graphs of the ENSO data shown in Figure 10 where the segmented and averaged data shows the Nino 3.4 TS rising by 3.0ºK from 297.9ºK to 300.9ºK from the segment with the lowest AODVIS to the highest. When the same analysis is applied to the LME SOI and CSEAP Area AODVIS the SOI falls from +8.7 to -12.4.

It is also worth noting that although the LME AODVIS data from one All Forcing run from 1979 to 2005 for the CSEAP Area ranges from 0.025 to 0.063 which is significantly lower than the Terra data from April to July from 2000 to 2018 which ranges from 0.18 to 0.35 the data still supports the hypothesis that the natural SEAP has always been the cause of ENSO events. (Note: April to July is used in this comparison as extreme biomass burning does not occur in these months and volcanic forcing is expected to dominate.)

It is therefore obvious with R^2 values of 1.00 in Figure 10 that the LME data proves the connection between the aerosol loading in the SEAP/CSEAP Areas and the ENSO indices. The causal relationship is discussed later.

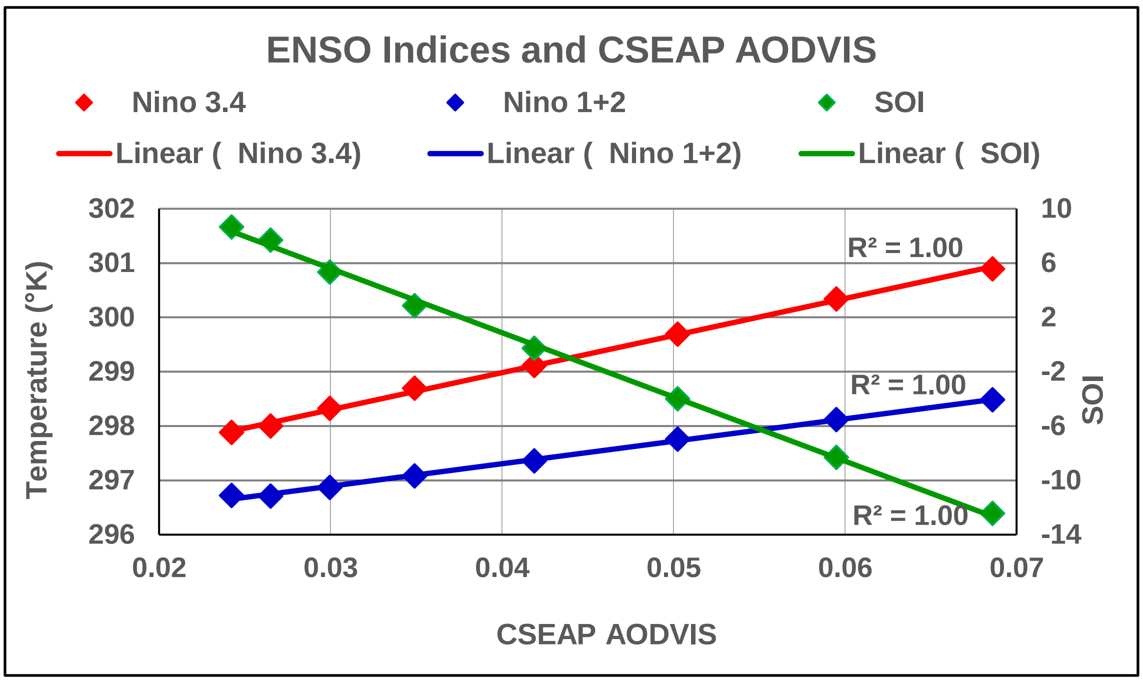

Figure 10: Last Millennium Ensemble segmented and averaged annual CSEAP AODVIS, Nino 3.4 and 1+2 Skin Temperature (TS) and the LME SOI from 850 to 2005 CE. Data averaged from the six of the forcings used – “All” and “Aero” not used as their segments are different.

It is also worth noting that in two columns of Figures 8 and 9:

1. The temperature in the Nino 3.4 area correlates at high levels with the U10 wind speed including at -1.00 and -0.99 when the data is segmented and averaged within the segments.

2. The average global temperature which is known to increase during El Nino events [*Foster and Rahmstorf*, 2011] is shown to correlate with the AODVIS in the SEAP and CSEAP areas at 0.98, 0.89 and 0.94 when the data is segmented and averaged

with the global average temperature rising by 0.4°C from the segment with the lowest AOD to the highest.

3.1.3 The NASA MERRA-2 Reanalysis

MERRA-2 which includes assimilated aerosols adds another independent model to the LME and LE. This dataset is continuous from 1980 to present and at the time of writing included thirty-nine full years of data.

The MERRA-2 analysis is included in two columns in Figure 11. The column labelled AOD MERRA-2 correlates the MERRA-2 AOD with the same parameters as the N7, EP, OMI and Terra AI and AOD. The column labelled AOD MERRA-2 & MERRA-2 was created by correlating the MERRA-2 AOD with the other parameters which were derived from the MERRA-2 dataset. Parameters such as the SOI which are not available in MERRA-2 were calculated using data from the MERRA-2 dataset. The SOI was calculated using the BOM formula available on their web site at: http://www.bom.gov.au/climate/current/soi2.shtml and the surface pressure near Darwin (130° to 131°E and 12° to 13°S) and Tahiti (149° to 150°W and 17° to 18°S). The easterly wind component from the same area as the NOAA TWI (140° to 175° W and 5°S to 5°N) from the MERRA-2 dataset was used as a proxy for the TWI.

For both the MERRA-2 columns in Figure 11 the parameters the IPCC listed as used to monitor ENSO events correlate at similar levels to the TERRA AOD data and at the same significance <0.01. The analysis of the SEAP in the column labelled AOD MERRA-2 & MERRA-2 is effectively a modelling analysis with near random forcings of extreme apparitions of the SEAP over 39 years which demonstrates exactly the same high correlations as the longer LME and LE datasets.

3.2 Satellite Data

As shown in Figure 6 the CSEAP AI data contains a significant trend and therefore the SON AI, AOD and other data was detrended using PAST 3 and then correlated both as a times series and a detrended time series. The resultant SON and annual correlations are reported in Figure 11 with the parameters listed in the IPCC AR5 as being used to monitor ENSO events highlighted in red.

a	Sept Oct Nov – Correlations								
		AOD Terra	AI N7	AI E Probe	AI OMI	AI N7 + EP	AI N7+EP+OMI	AOD MERRA-2	AOD MERRA-2 & MERRA-2
		2000-18	1979-1992	1996-2001	2005 - 18	1979...2001	1979…2018	1980-2018	1980-2018
1	Air Temp CSEAP Area MERRA-2 650 hPa	0.67	0.28	0.54	0.69	0.45	0.55	.019	0.12
2	CSEAP Area NCEP Omega	0.91	0.57	0.96	0.62	0.56	0.31	0.80	0.79
3	NOAA TWI	-0.72	-0.69	-0.97	-0.73	-0.76	-0.34	-0.86	0.87
4	SST Niño 3.4	0.77	0.56	0.91	0.65	0.61	0.34	0.74	0.73
5	SST Niño 1 and 2	0.78	0.48	0.96	0.77	0.76	0.34	0.79	0.77
6	SOI	-0.75	-0.64	-0.85	-0.69	-0.45	-0.13	-0.76	-0.73
7	ONI	0.77	0.51	0.92	0.65	0.57	0.26	0.74	0.77
8	SST SEAP Area	-0.66	-0.68	-0.85	-0.20	-0.41	0.11	-0.67	-0.54
9	Rainfall CSEAP Area	-0.58	-0.40	-0.88	-0.35	-0.38	0.18	-0.63	-0.68
10	NOAA Interpl'd OLR	0.85	0.64	0.99	0.50	0.60	0.21	0.82	0.73

b	Sept Oct Nov Detrended using PAST 3 – Correlations								
		AOD Terra	AI N7	AI E Probe	AI OMI	AI N7 + EP	AI N7+EP+OMI	AOD MERRA-2	AOD MERRA-2 & MERRA-2
		2000-18	1979-1992	1996-2001	2005 - 18	1979...2001	1979…2018	1980-2018	1980-2018
1	Air Temp CSEAP Area MERRA-2 650 hPa	0.63	0.08	0.59	0.67	0.25	0.16	0.31	0.37
2	CSEAP Area Omega	0.92	0.79	0.98	0.68	0.74	0.71	0.80	0.78
3	NOAA TWI	-0.71	-0.73	-0.97	-0.63	-0.80	-0.62	-0.87	0.88
4	SST Niño 3.4	0.77	0.67	0.92	0.61	0.73	0.63	0.75	0.75
5	SST Niño 1 and 2	0.77	0.67	0.98	0.71	0.88	0.73	0.79	0.78
6	SOI	-0.74	-0.76	-0.87	-0.65	-0.65	-0.60	-0.75	-0.73
7	ONI	0.76	0.65	0.93	0.61	0.73	0.63	0.74	0.77
8	SST SEAP Area	-0.67	-0.83	-0.83	-0.33	-0.75	-0.65	-0.70	-0.58
9	Rainfall CSEAP Area	-0.68	-0.79	-0.84	-0.58	-0.57	-0.55	-0.65	-0.68
10	NOAA Interpl'd OLR	0.87	0.83	0.97	0.62	0.75	0.69	0.82	0.74

c	Annual – Correlations								
		AOD Terra	AI N7	AI E Probe	AI OMI	AI N7 + EP	AI N7+EP+OMI	AOD MERRA-2	AOD MERRA-2 & MERRA-2
		2000-18	1979-1992	1996-2001	2004 - 18	1979...2001	1979…2018	1980-2018	1980-2018
1	CSEAP Area Omega	0.81	0.25	0.99	0.50	0.35	-0.13	0.75	0.71
2	NOAA TWI	-0.62	-0.54	-0.95	-0.85	-0.50	0.09	-0.79	0.74
3	SST Niño 3.4	0.67	0.47	0.95	0.82	0.38	0.11	0.73	0.70
4	SST Niño 1 and 2	0.58	0.36	0.85	0.63	0.55	0.06	0.61	0.59
5	SOI	-0.60	-0.45	-0.93	-0.66	-0.30	0.16	-0.73	-0.76
6	ONI	0.53	0.38	0.88	0.76	0.26	0.00	0.72	0.59
7	SST SEAP Area	-0.41	-0.07	-0.64	0.20	0.19	0.59	-0.47	-0.40
8	Rainfall CSEAP Area	-0.31	0.06	-0.64	0.06	-0.15	0.67	-0.42	-0.47
9	NOAA Interpl’d OLR	0.60	0.48	0.94	0.21	0.49	-0.35	0.70	0.60

d	Annual Detrended using PAST 3 – Correlations								
		AOD Terra	AI N7	AI E Probe	AI OMI	AI N7 + EP	AI N7+EP+OMI	AOD MERRA-2	AOD MERRA-2 & MERRA-2
		2000-18	1979-1992	1996-2001	2004 - 18	1979...2001	1979…2018	1980-2018	1980-2018
1	CSEAP Area Omega	0.81	0.80	0.99	0.71	0.77	0.37	0.74	0.70
2	NOAA TWI	-0.62	-0.77	-0.91	-0.68	-0.81	-0.21	-0.79	0.74
3	SST Niño 3.4	0.67	0.67	0.91	0.76	0.76	0.36	0.74	0.74
4	SST Niño 1 and 2	0.60	0.68	0.80	0.53	0.73	0.16	0.62	0.61
5	SOI	-0.60	-0.75	-0.89	-0.66	-0.75	-0.30	-0.72	-0.75
6	ONI	0.53	0.61	0.82	0.69	0.69	0.35	0.65	0.61
7	SST SEAP Area	-0.41	-0.56	-0.69	-0.05	-0.57	-0.37	-0.50	-0.41
8	Rainfall CSEAP Area	-0.31	-0.70	-0.47	-0.45	-0.32	-0.03	-0.40	-0.45
9	NOAA Interpl'd OLR	0.61	0.83	0.92	0.64	0.71	0.25	0.69	0.63

Figure 11: Correlations of (a) and (c) time series and (b) and (d) detrended time series of AOD and AI over the CSEAP Area with characteristics of ENSO in SON (a) and (b) and annual (c) and (d). The last column AOD MERRA-2 & MERRA-2 uses only aerosol and other data from the MERRA-2 reanalysis data set.

Air temp from MERRA-2 dataset at 650hPa. MERRA-2 MERRA-2 at 900 hPa.

MERRA-2 & MERRA-2 Easterly Wind Component is normally negative and reduces in El Niño periods - a positive increase c.f. the NOAA TWI which reduces under the same circumstances.

EP AI data was detrended using PAST 3 by excluding 1997 from the data set and reinserting it after detrending to avoid inserting a significant trend in the detrending process due to the extreme values of the EP data in 1997, the short duration and the proximity of 1997 to the start date.

3.2.1 Air Temperature CSEAP Area

Figure 11 (a), (b) (1) shows that when the SEAP exists the air temperature at 650 hPa rises and this correlation confirms that the SEAP is absorbing solar radiation and heating the upper atmosphere thereby contributing to the temperature inversion compared with periods when the SEAP does not exist.

3.2.2 SEAP Area SST and Rainfall

During an ENSO event the SEAP Area is prone to reduced rainfall and a cooler SST. These characteristics are shown to correlate with the AI/AOD of the SEAP in Figure 11.

3.2.3 Convection in the CSEAP Area

Tosca et al. [2015] investigated the effects of anthropogenic aerosols in West Africa and reported that anthropogenic aerosols in the tropics limit convection, dry the region under the plume and enable increased fire activity via human ignition due to a positive feedback effect. This paper also shows a reduction in convection when an aerosol plume exists and the CSEAP Area AOD and AI is correlated with the NCEP/NCAR reanalysis omega at the 400hPa level in the same area (Figure 11). Omega is a measure of vertical velocity in the atmosphere positive values indicate falling motion and negative values rising. A reduction in convection produces an increase in omega and if an increase in aerosols results in a decrease in convection the correlations will be positive. The Terra AOD correlates at 0.86 average magnitude and <0.01 significance. The N7, EP and OMI AI data show similar results. The N7 data correlates at lower magnitudes due to the lower levels of AI in the early part of the N7 data when the effects of the SEAP would have been greatly reduced. Figure 12 shows graphs of the data.

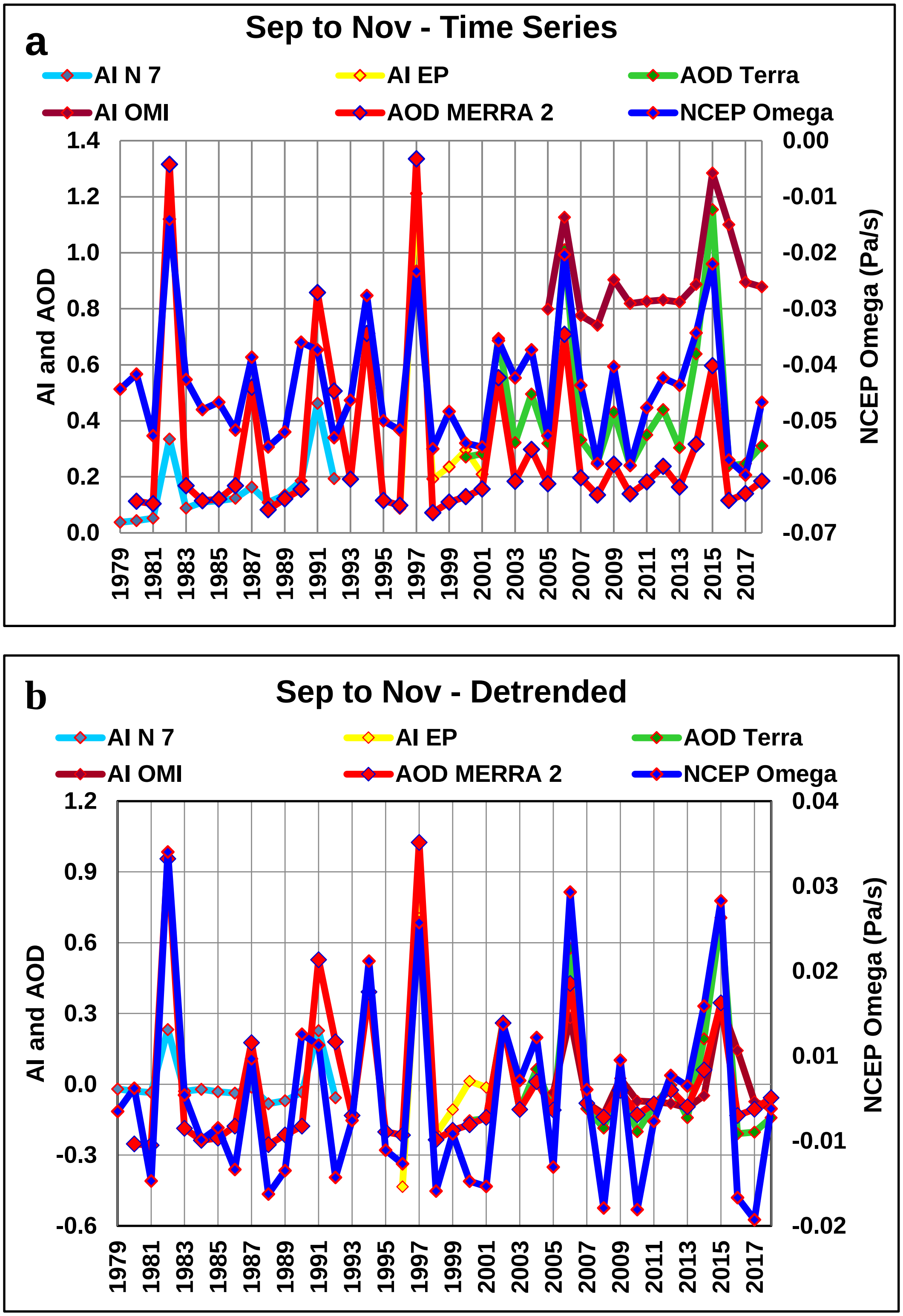

Figure 12: Average SON CSEAP Area AOD and AI and NCEP Omega (a) time series and (b) detrended using PAST 3.

3.2.4 Trade Wind Speed

The NOAA TWI in Figure 11 (2, 3) shows a significant negative correlation with the AI and AOD data implying that the Trade Winds and therefore the Walker circulation relax when the SEAP exists, a primary requirement for the onset of an ENSO event.

3.2.5 Niño Areas SST and the SOI

The prime indices used to monitor the onset and progress of an ENSO event are the SST in the Niño 1+2 and 3.4 areas and the SOI. Figure 11 shows that all these indices correlate with the AI and AOD of the SEAP and when the SEAP exists the Niño 1+2 and 3.4 area SST rises and the SOI declines – both of which indicate an ENSO event exists. Figure 13 shows AI, AOD and Niño 3.4 SST. Figure 14 shows the SOI data.

The ONI also shows the same characteristics.

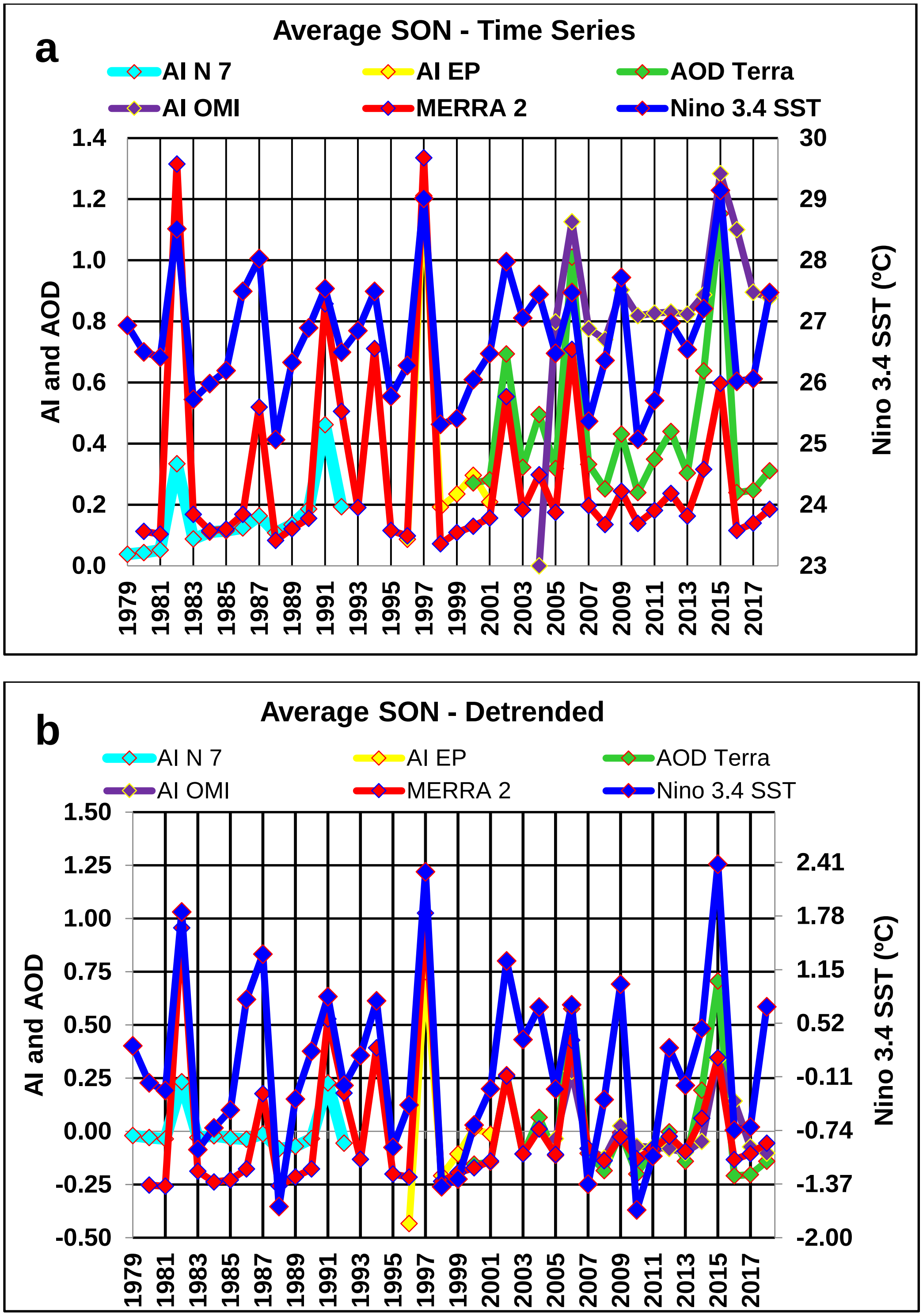

Figure 13: Average SON AOD and AI CSEAP Area and Niño 3.4 SST. (a) time series (b) detrended using PAST 3.

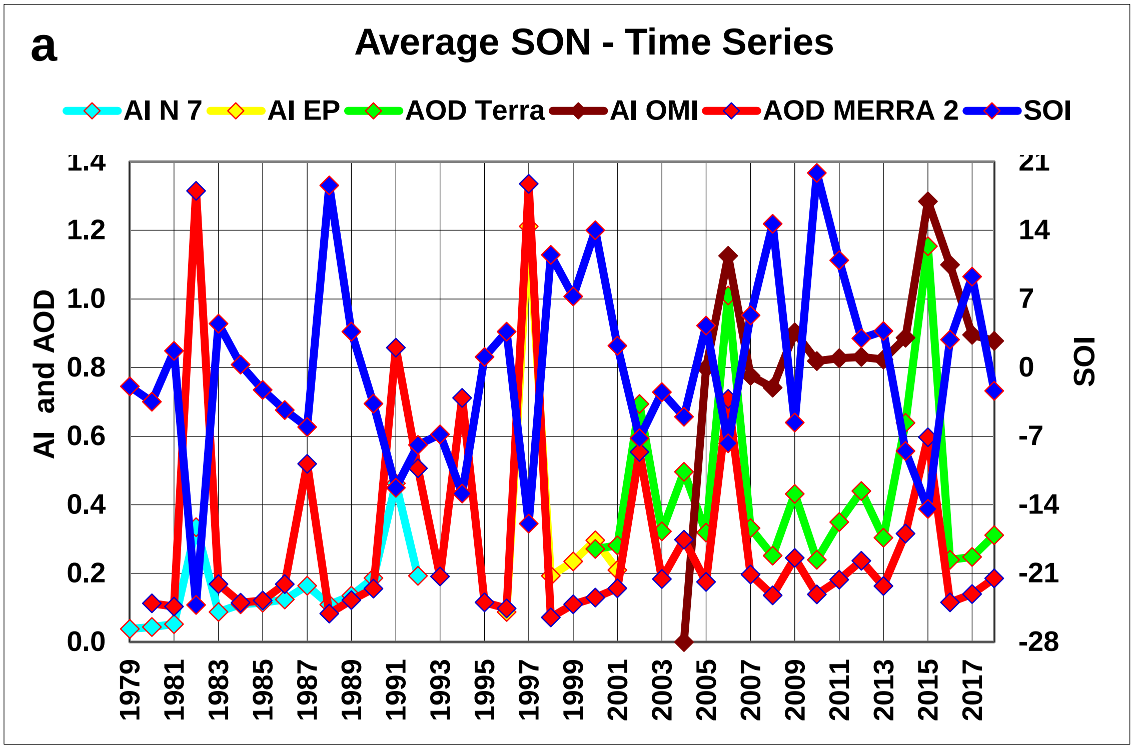

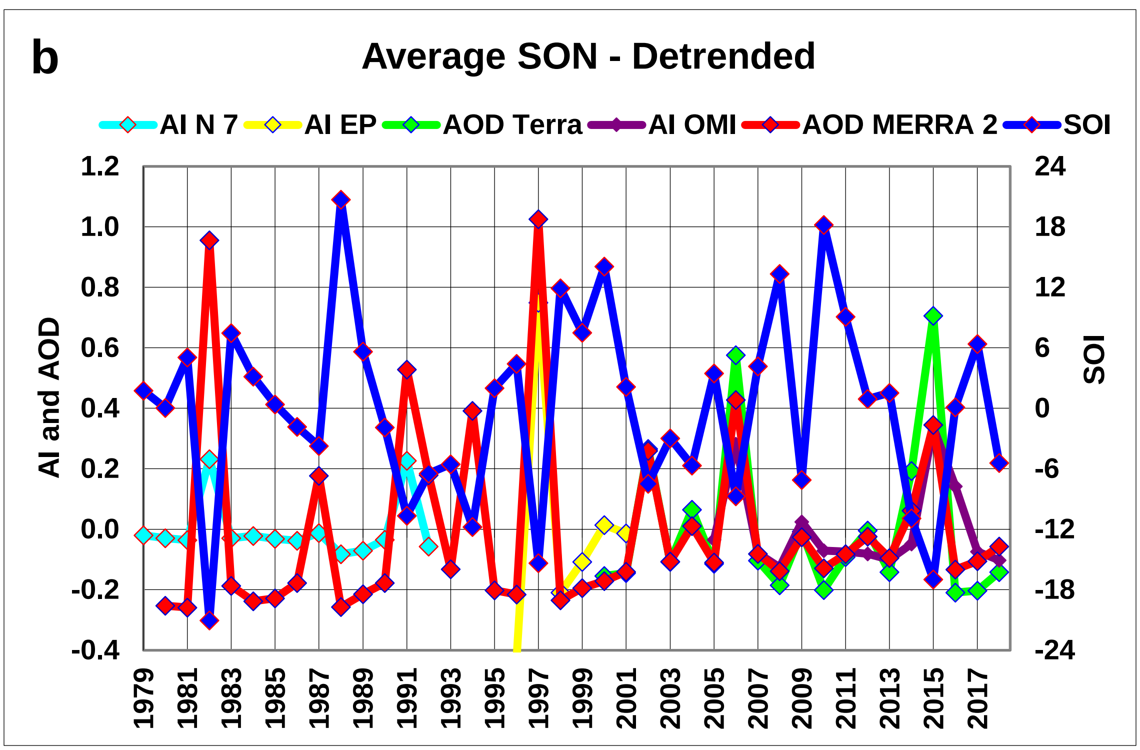

Figure 14: Average SON AOD and AI CSEAP Area and BOM SOI. (a) time series (b) detrended using PAST 3.

3.2.6 Outgoing Longwave Radiation

The CSEAP Area OLR correlates positively with the AI and AOD of the SEAP implying that the level of radiation at the surface of the SEAP Area reduces. In October 2015 the level of OLR was 244 W/m^2 compared with 209 W/m^2 in October 2016, a low month of CSEAP Area AOD.

3.3 Volcano Data

The level of VEI Tephra (VEIT) was calculated as shown in Appendix A.

3.3.1 Tephra, ENSO and CSEAP Area Convection

The anthropogenic SEAP has only existed in its current form since about 1980 (Figure 6, Appendix A) and as ENSO events have occurred for centuries the driver of historic ENSO events must be the natural SEAP which is created by volcanic eruptions (Appendix A).

Previous reported research failed to find a generally accepted link between volcanic eruptions and ENSO for two reasons:

1. In general, only large eruptions were considered and smaller eruptions which only eject tephra into the troposphere were ignored; and
2. A global analysis was undertaken rather than a specific geographic focus on the SEAP Area which is the only area which can create and sustain an ENSO event because of its location in the region which drives convection and therefore the entire non-ENSO Walker Circulation.

In this paper I report the correlation of the volcanic ash plumes emanating from within the SEAP Area, on a monthly segmented basis with two of the ENSO indices described in the IPCC AR5:

1. The Niño 3.4 SST; and
2. The SOI; and with
3. SEAP Area omega, vertical velocity in the atmosphere from the NCEP reanalysis;
4. The HADCRUT4 global temperature [*Morice et al.*, 2012]; and
5. Four monsoon indices

The correlations together with the relevant time periods are shown in Figure 15. The VEIT correlations show the same effects as the satellite and modelling data when the level of tephra ejected by the volcanoes in the SEAP area increases: the Niño 3.4 SST rises and the SOI decreases – both of which being indicative of an ENSO event; CSEAP Area omega and the global temperature increases and the monsoon indices fall. Figures 16, 17 and 18 show graphs of the data.

Correlations of VEIT (Monthly Segmented)		
Index	**Correlation**	**Period**
Niño 3.4 SST	**0.99**	1870 – 2018
SOI	**-0.99**	1876 – 2018
HADCRUT4 Global Temp Anomaly	**1.00**	1870 - 2018
Omega (400 hPa) (CSEAP Area)	**0.98**	1948 – 2018
Pre 1980 (Monthly Segmented)		
Niño 3.4 SST	**0.98**	1870 – 1979
SOI	**-1.00**	1876 - 1979
HADCRUT4 Global Temp Anomaly	**1.00**	1870 - 1979
Omega (400 hPa) (CSEAP Area)	**0.94**	1948 – 1979
Correlations Monsoon Index (Annual Average VEIT)		
Indian Summer	**-0.98**	1948 - 2018
Western North Pacific	**-0.98**	1948 - 2018
Webster and Yang	**-0.94**	1948 - 2018
Australian	**-0.99**	1948 - 2018

Figure 15: Correlations of segmented and averaged SEAP Area VEIT with indices shown. IPCC Indices highlighted in red.

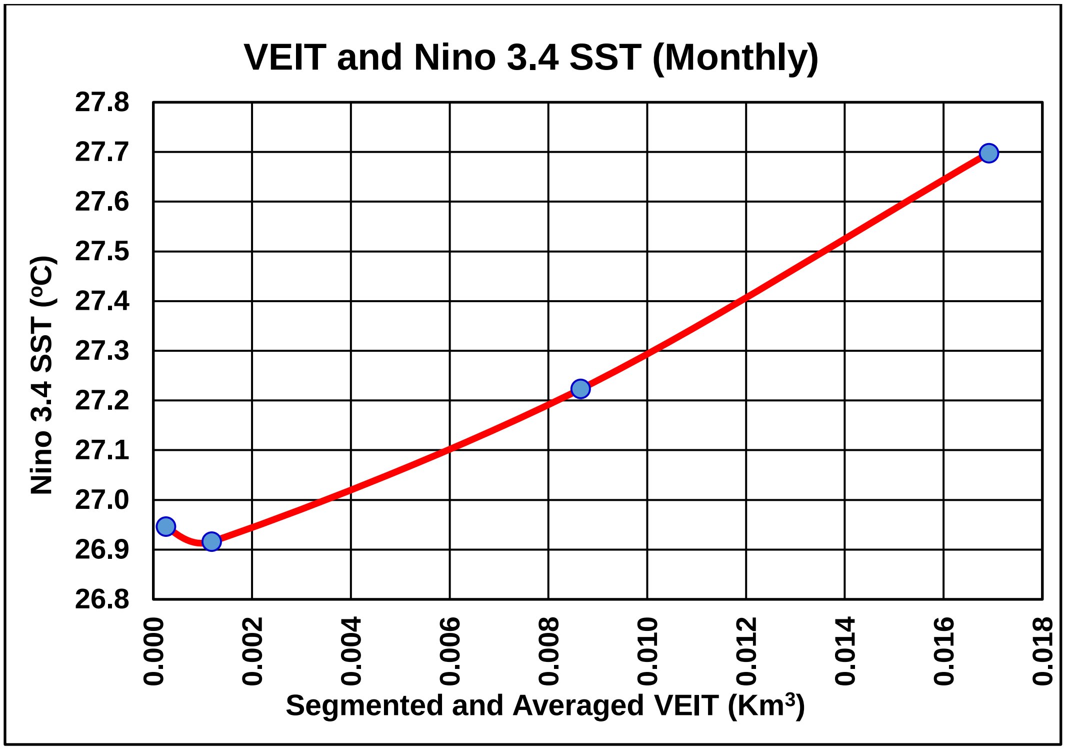

Figure 16: Monthly Segmented and Averaged Niño 3.4 SST and VEIT from Volcanoes in the SEAP Area. 1870 to 2018

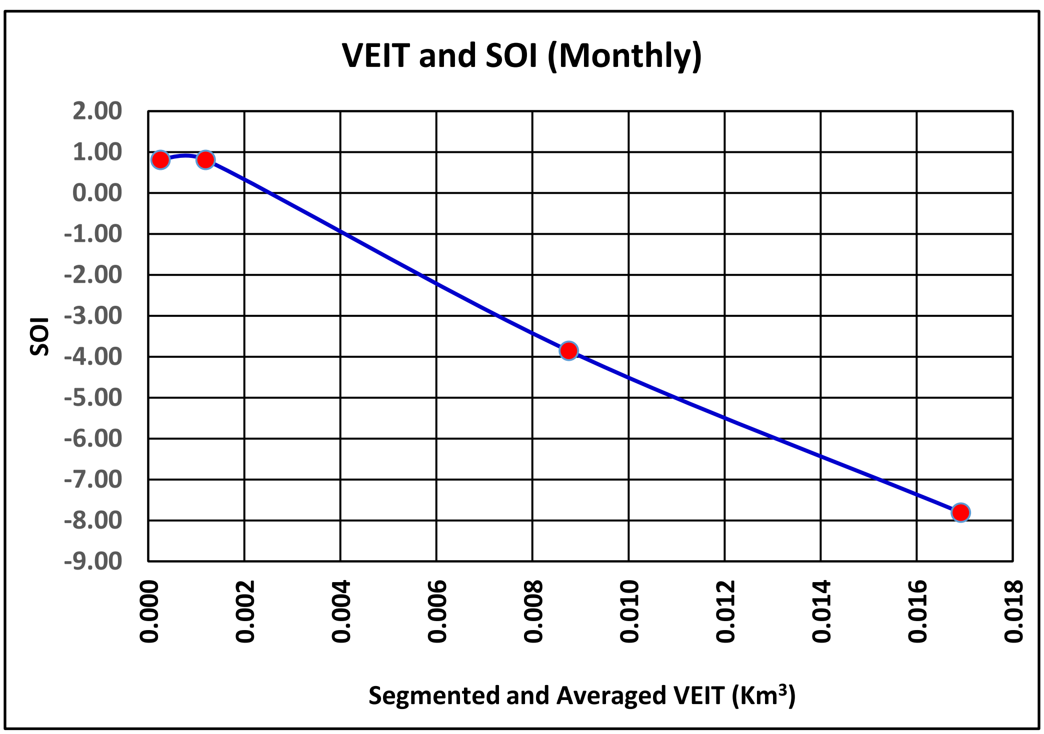

Figure 17: Monthly Segmented and Averaged BOM SOI and VEIT from Volcanoes in the SEAP area. 1876 to 2018.

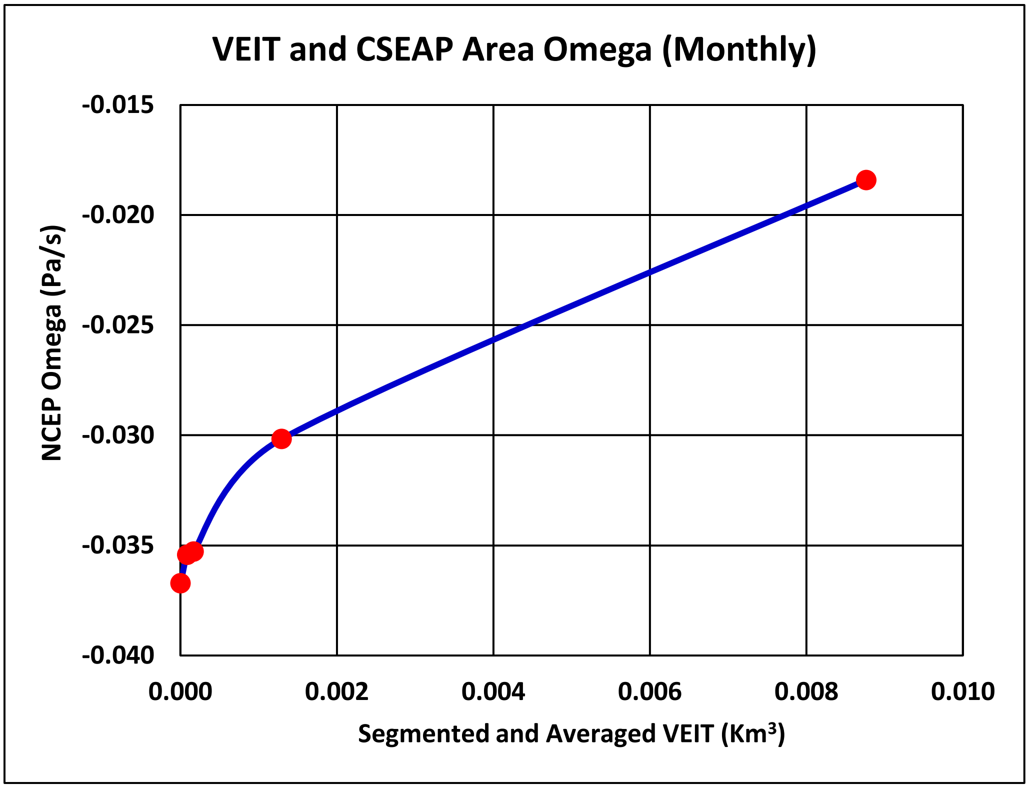

Figure 18: NCEP/NCAR Reanalysis CSEAP Area segmented and averaged Monthly Omega and VEIT 1948 to 2018.

Figure 15 includes correlations using only data prior to 1980 to demonstrate the volcanic connections to ENSO without the contamination of the anthropogenic SEAP in SON which the AI/AOD data and Figure 6 shows is much lower in intensity in 1979 and probably did not exist in its extreme form prior to this date. Indeed the Representative Concentration Pathways inventory version 2.0.5 of Asian black carbon emissions at http://tntcat.iiasa.ac.at/RcpDb/dsd?Action=htmlpage&page=compare confirms this as from 1850 to 1950 the emissions from land use change (deforestation), the major source of the SEAP, did not change at 0.063±0.02 Tg/year and from 1950 to 1970 increased by 300% [*Mieville et al.*, 2010].

3.3.2 ENSO Return Frequency

In the introduction it was noted in Figure 1 that the ENSO power spectra for the LME and HadISST_1 data are very different. The reason is that none of the forcings applied in the LME runs included forcing by the natural SEAP at the required resolution.

Figure 19 shows XLSTAT periodograms for the HadISST_1 and SEAP Area tephra data from 2 to 19 years with the time axis displayed on a logarithmic scale (base 2) as a linear scale compresses the higher frequencies (2 to 5 years) making the comparison difficult. This analysis is for the same period as the HadlISST_1 in Figure 1, 1980 to 2017, and the spectra are very similar with the same number of peaks and troughs which are closely coincident. This similarity should be compared with the LME data in Figure 1 which shows only one dominant peak at about 5 years.

Given the uncertainty in the tephra data which is based on GVP VEI data available as integer values on a logarithmic scale the similarity of the spectra in Figure 19 is impressive.

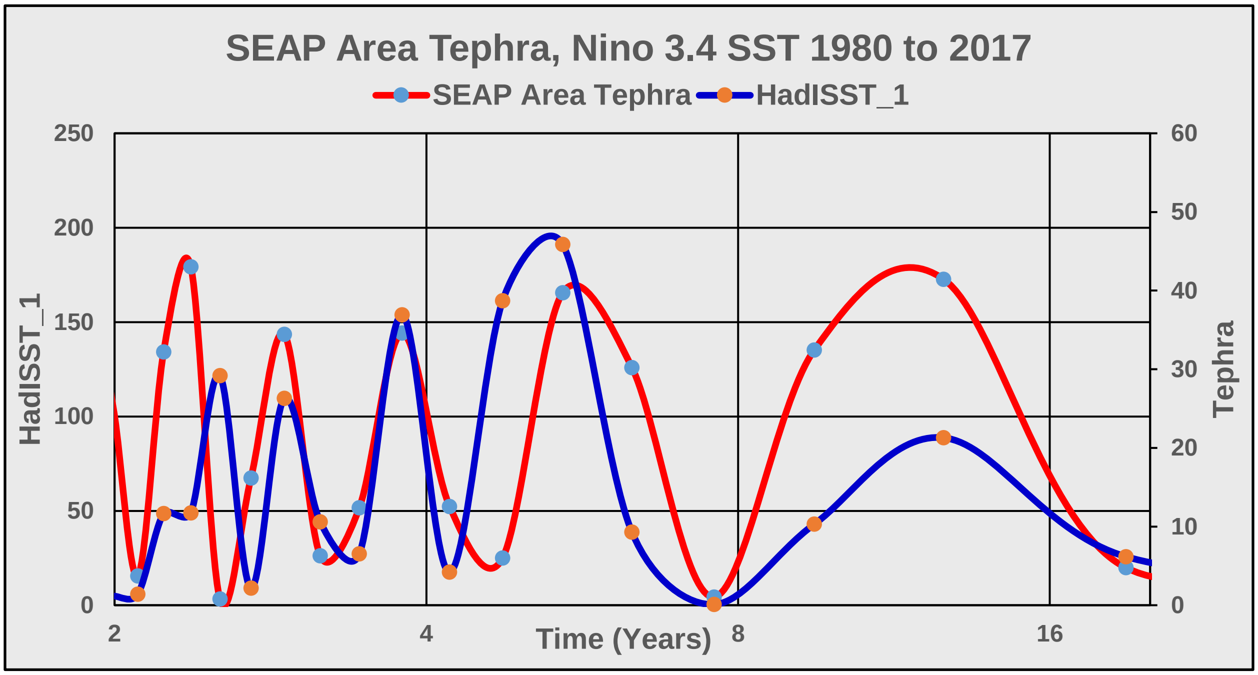

Figure 19: SEAP Area XLSTAT periodogram for the Nino 3.4 SST and SEAP Area Tephra from 1980 to 2017

3.3.3 Monsoon Indices

It was recognized by Sir Gilbert Walker a century ago that there was a connection between the Indian monsoon and the SOI and many subsequent papers have explored the relationship e.g. [*Shukla and Paolino*, 1983] , [*Maraun and Kurths*, 2005] and [*Cook et al.*, 2010]. With the high correlations between the volcanic tephra ejected within the SEAP Area and ENSO (Nino 3.4 SST and the SOI) four Asian monsoon indices were also correlated with the volcanic tephra on an annual basis. The correlations are for the same year for both annual VEIT and the monsoon index except for the Australian monsoon index which covers December to February where the tephra is the average of the year of the first month of the index. The indices used are:

1. Indian monsoon index (U850 (5°N -15°N, 40°E-80°E) – U850 (20°N -30°N, 70°E-90°E) [*Bin Wang and Fan*, 1999]
2. Webster-Yang monsoon index (U850-U200 averaged over 0-20°N, 40°E-110°E [*Webster and Yang*, 1992]
3. East Asia-WNP monsoon index (U850 (5°N -15°N, 100°E-130°E) – U850 (20°N -30°N, 110°E-140°E) [*Bin Wang et al.*, 2001]

4. Australian monsoon index (U850 averaged over 5°S-15°S, 110°E-130°E [*Kajikawa et al.*, 2010].

The data was calculated using the NCEP reanalysis dataset and the results are in Figure 15.

3.4 Recent Change in ENSO Character

ENSO has become more intense in recent decades as Figure 20 demonstrates using the Nino 3.4 SST which has risen by over 0.3°C in recent decades and especially in Aug-Nov when the anthropogenic SEAP is at its peak. From the hypothesis: the general rise in all months is due to the increase in the levels of both the natural and anthropogenic SEAP as Appendix A and Figure 6 show; and the anomalous rise from Aug to Nov is entirely due to the anthropogenic SEAP.

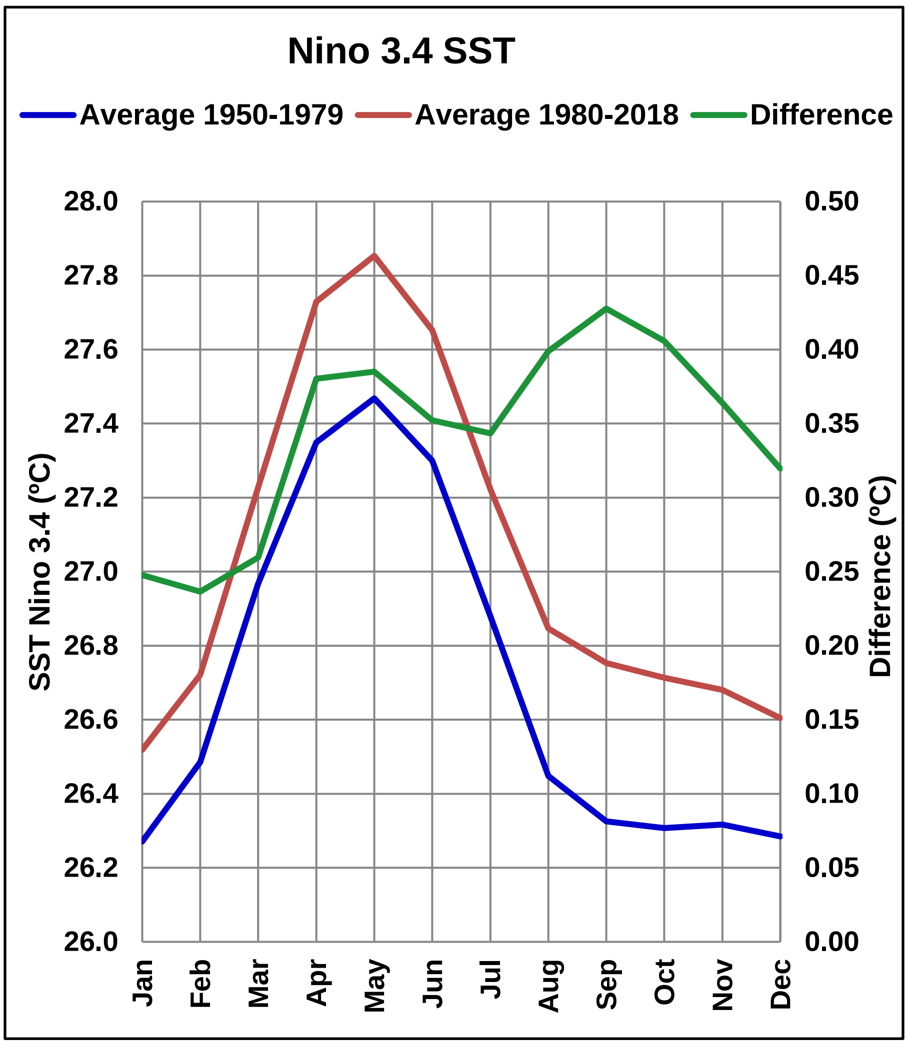

Figure 20: NCEP Reanalysis Nino 3.4 SST showing changes in the averages from 1950-79 and 1980-2018.

4 MECHANISMS FOLLOWING THE HYPOTHESIS AND PHYSICAL MODEL

The changes wrought on climate by extreme events can be shown visually by subtracting a “normal” year from the “extreme” year in a particular measurement. In this case 2015 was an extreme year for the AOD of the SEAP Area and 2016 was a “normal” year (Figures 4 and 6) and this section follows the steps outlined in the hypothesis and physical model using this technique. It is important to acknowledge that other events in 2015 and 2016 may also have affected the visualisation results, however as the visualisations show exactly the same effects as the segmented data and correlations these images are considered to be a reasonable demonstration of the effects of the SEAP in 2015. The images shown were assembled from the NCEP/NCAR Reanalysis directly and from the MERRA-2 dataset using NASA Panoply.

4.1 The SEAP Forms

The SEAP AOD in SON 2015 was at extreme levels and Figure 21 shows the variation from the “normal” 2016.

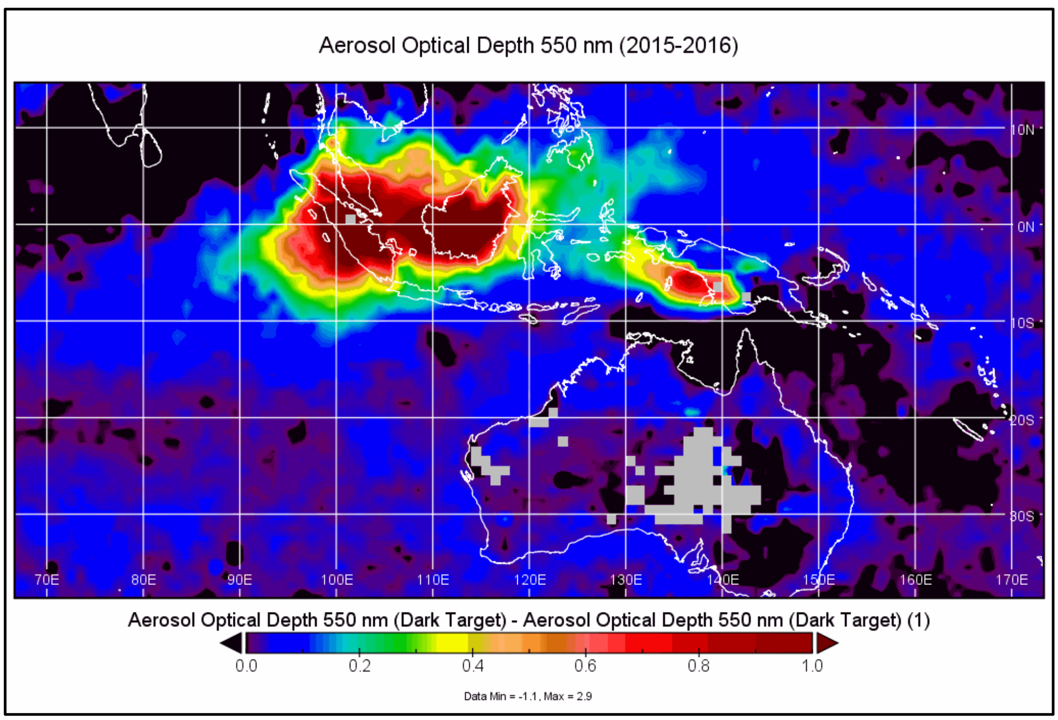

Figure 21: Terra AOD SON 2015-2016

4.2 Aerosols absorb solar radiation heating the atmosphere

The SEAP both absorbs and reflects solar radiation which warms the upper atmosphere as demonstrated in Figure 22 where the atmospheric temperature at 400 and 650 hPa has risen by about 0.5 and 1.0°K.

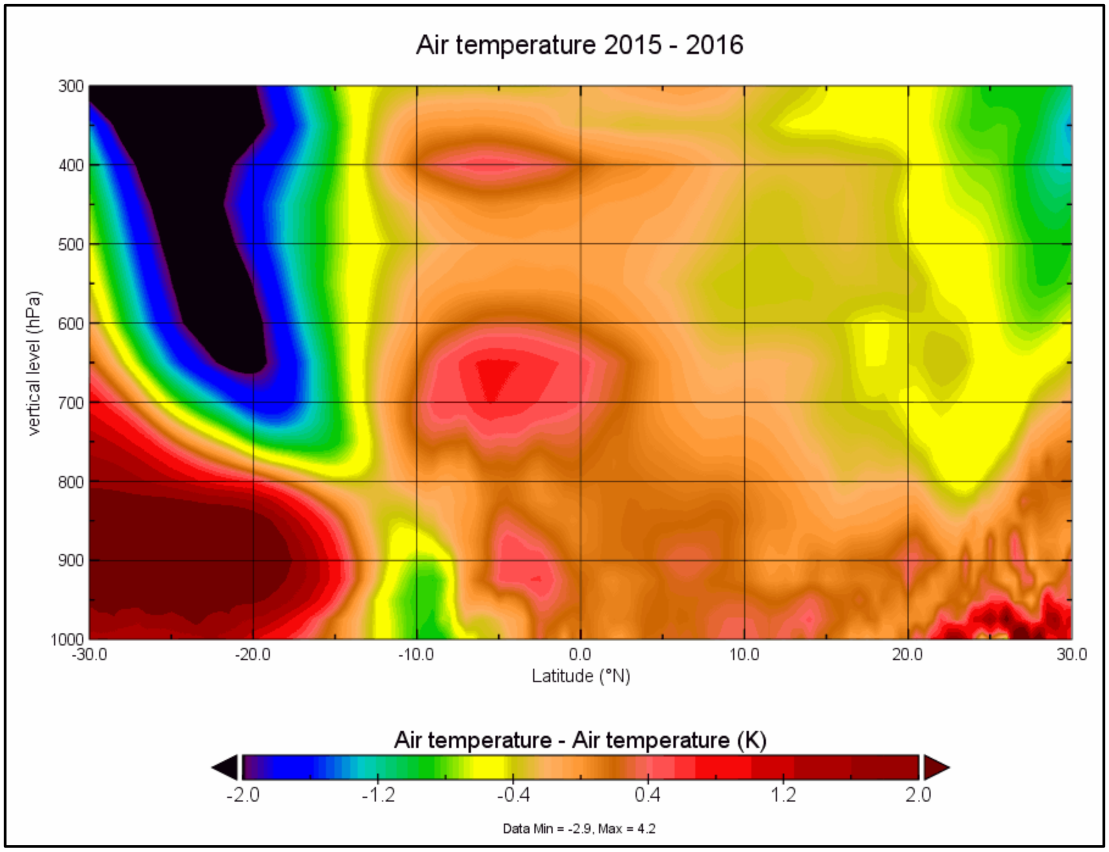

Figure 22: MERRA-2 SON Air Temperature 2015-2016 (Panoply) averaged across the CSEAP Longitudes

4.3 Aerosols reduce surface solar radiation cooling the surface

Figure 23 shows nearly all the SEAP Area sea surface is cooler except the extreme north and west by over 1°K.

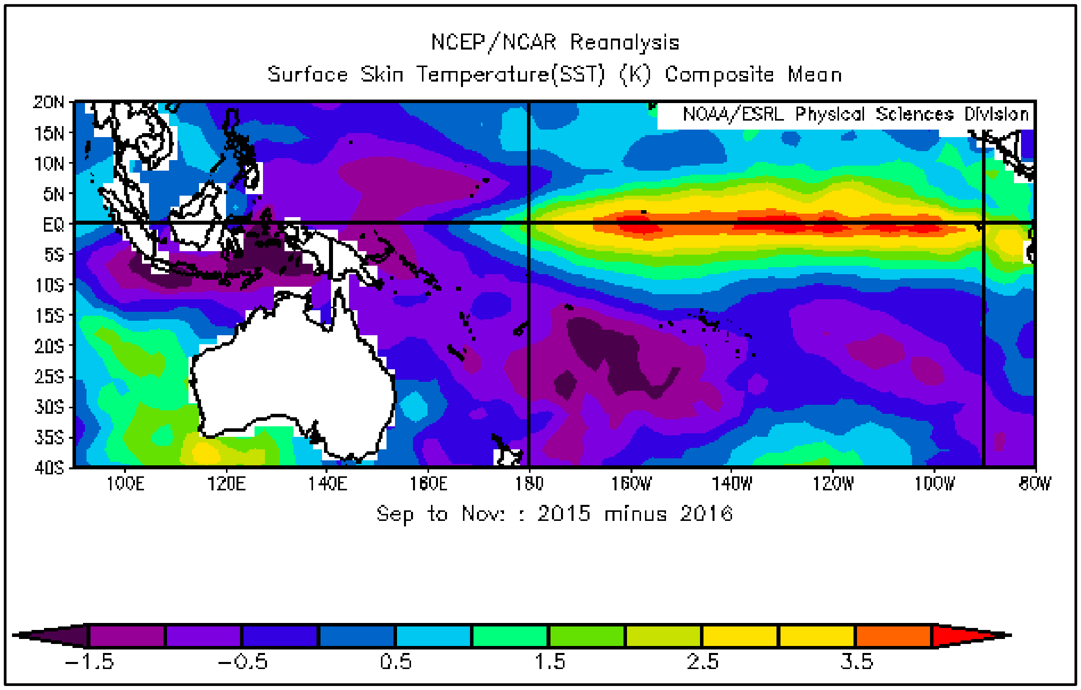

Figure 23: NCEP/NCAR Reanalysis SON SST 2015 - 2016.

4.4 This creates a temperature inversion which reduces convection

The effects of aerosols on convection and atmospheric circulation have been extensively described in the literature as discussed in the introduction. The SEAP absorbs solar radiation which warms the upper atmosphere and reduces solar radiation at the surface which cools the lower atmosphere. This alters the vertical temperature profile of the atmosphere with warmer air above cooler air (relative to the temperatures without the plume) and this stabilises the atmosphere and reduces convection. This well understood process is confirmed in the SEAP Area in this paper with the demonstrated correlation of omega with the AOD, AI and ejected volcanic ash in the area in Figures 8, 9, 11 and 15 and in Figure 24 where nearly all the SEAP Area is affected except the extreme north and west with omega increasing by up to 0.12.

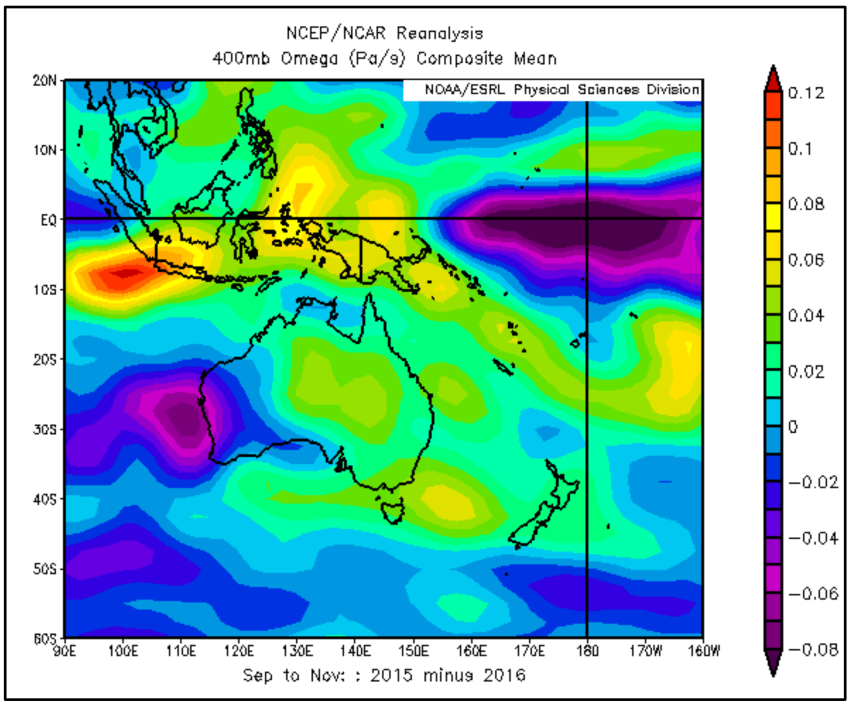

Figure 24: NCEP/NCAR SON omega (400 mb level) 2015-2016

4.5 Reduced convection in the SEAP Area causes the Trade Winds to relax

Figure 25 shows the changes in the surface vector winds caused by the SEAP in 2015. It is clear that the Trade Winds which normally blow east to west across the Pacific Ocean at about 6m/s have effectively stalled near the equator and the dateline in 2015 as an inspection of the data in the individual years which make up Figure 25 confirms.

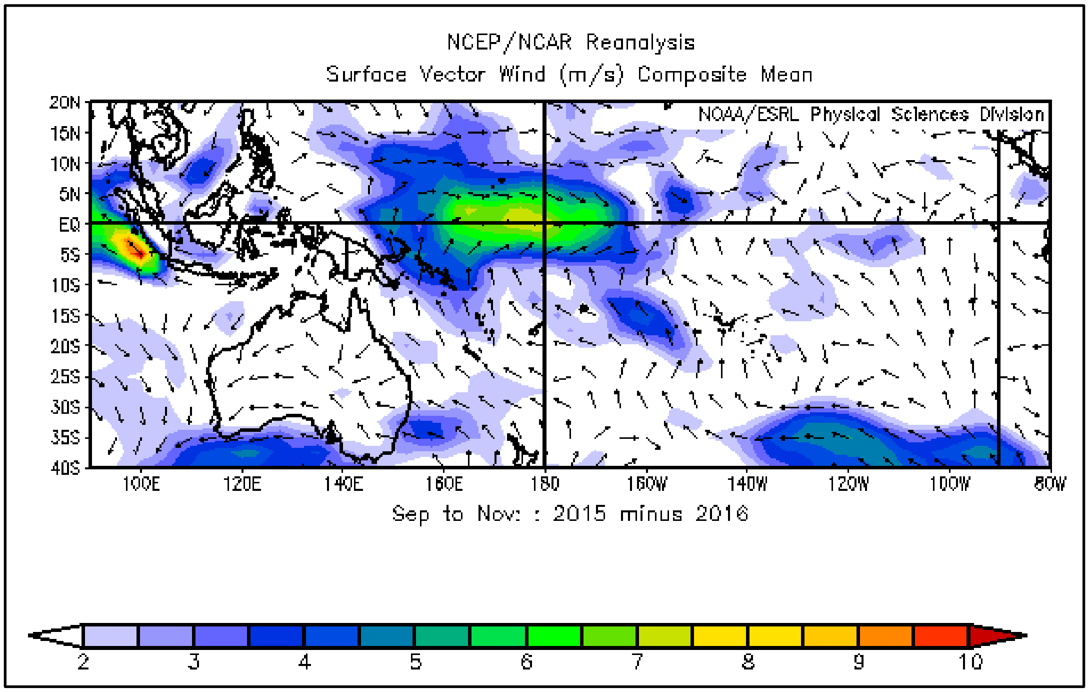

Figure 25: NCEP/NCAR Reanalysis SON Surface Vector Wind 2015-2016

4.6 Reduced Trade Wind speed causes the Nino 3.4 and 1+2 SST to rise

Figure 23 shows a classic warm tongue extending from South America across the Pacific Ocean with the Nino 3.4 SON SST rising between 2 and 4+°K in 2015 compared to 2016 which clearly indicates an ENSO event is occurring.

The Nino 1+2 also increases in Figure 23 by 1.5 to 3.5°K, a smaller increase than the Nino 3.4 Area

4.7 Higher Nino 3.4 SST causes convection and the Walker circulation relaxes

Figure 26 shows a vertical cross section of omega from the NCEP/NCAR Reanalysis from the SEAP Area across the Pacific Ocean averaged across the SEAP Area latitudes. Clearly Omega has fallen across the Nino 3.4 region indicating increased convection and the opposite has occurred over the SEAP Area forcing the Walker Circulation to relax/reverse.

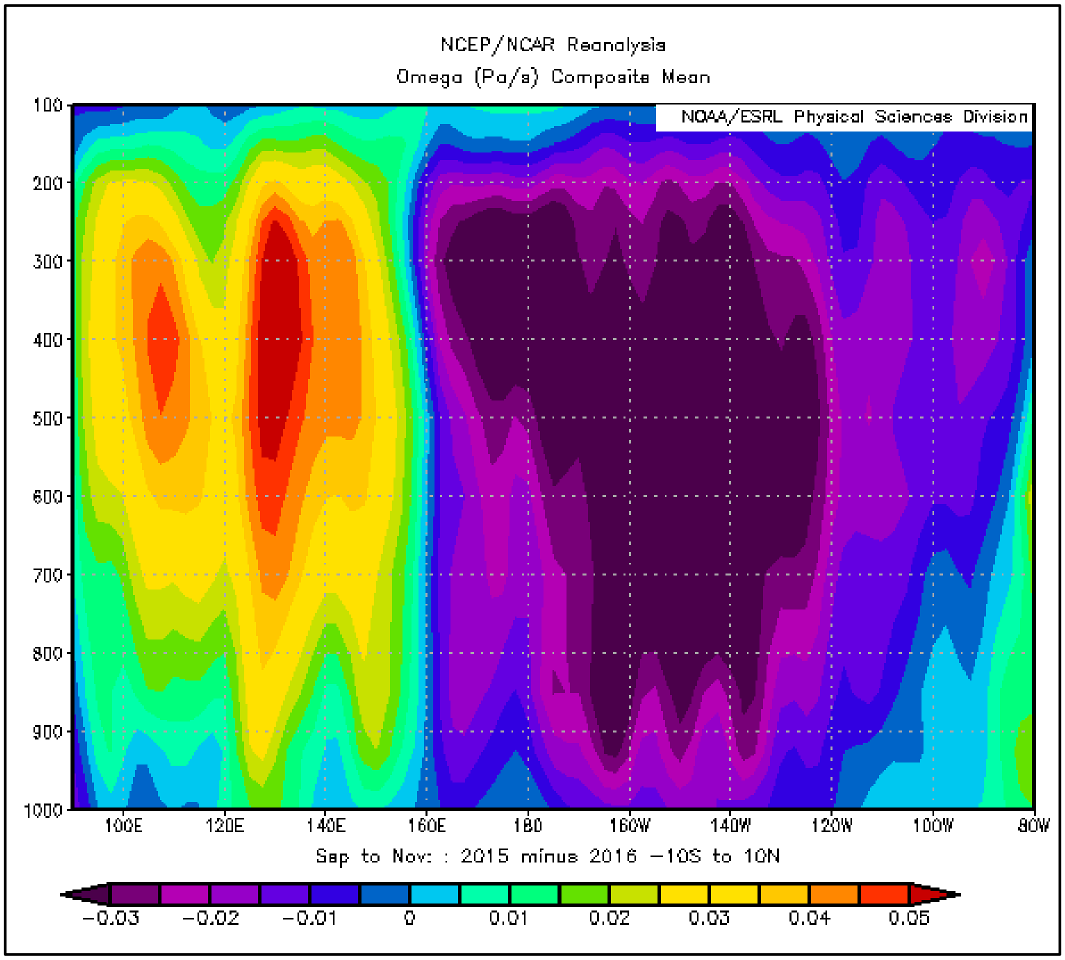

Figure 26: NCEP/NCAR Reanalysis SON Omega averaged across the SEAP Latitudes 2015-2016.

4.8 The SOI is forced into a negative phase by these changes

The increased convection in the central Pacific Ocean reduces surface pressure and the reduced convection in the SEAP Area raises surface pressure. Figure 27 clearly shows the increase in SLP in Darwin and a reduction in Tahiti which drove the SOI negative in 2015.

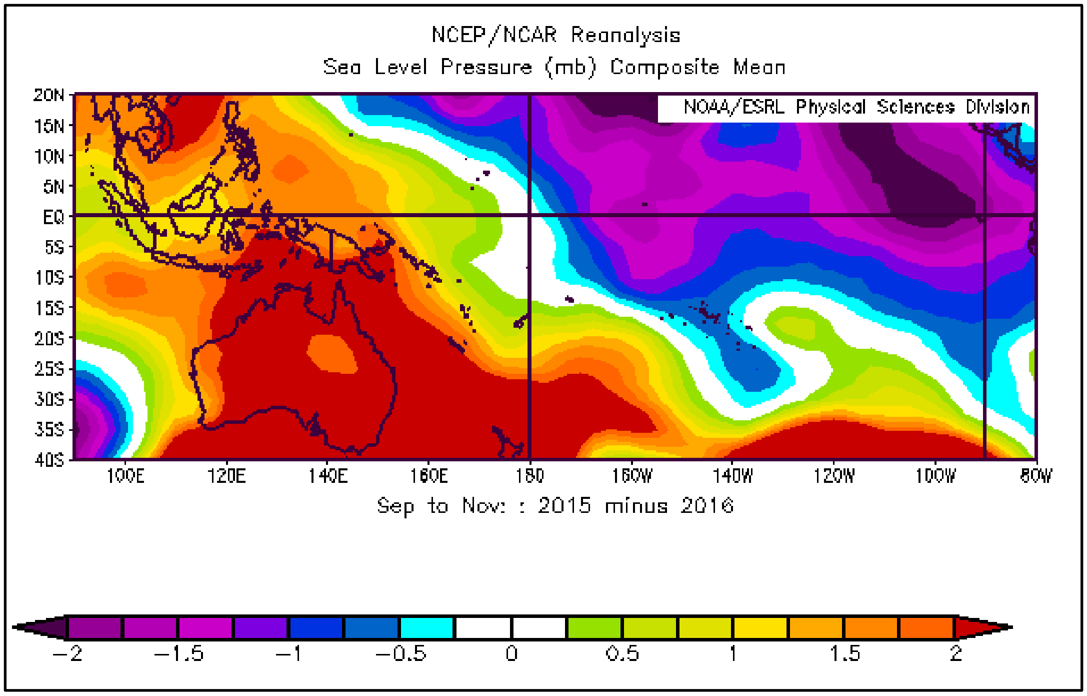

Figure 27: NCEP/NCAR Reanalysis SON Sea Level Pressure 2015 -2016

5 CAUSATION ANALYSIS

It is clearly understood that correlation between events A and B does not prove causation from A to B or vice versa. Thus, the causal relationship between the SEAP and the ENSO must be demonstrated in other ways.

5.1 Volcanic Eruptions

The similarity of the power spectra of the Nino 3.4 SST and the SEAP Area tephra and the clear correlations between volcanic tephra in the SEAP Area and ENSO demonstrated in this paper show a close relationship exists between the two and since volcanic eruptions are caused by deep earth tectonic processes and cannot be caused by ENSO events the causal direction must run from the volcanic eruptions to ENSO.

5.2 Analysis without Correlation

Figure 10 shows that the LME Nino 3.4 SST rises by 3.01°C from 297.88°C to 300.89°C and the SOI falls from +8.65 to -12.4 reflecting accurately the range of these indices from La Nina to El Nino events without using correlation.

5.3 Modelling

LME: the LME data used in this paper is forced by the eight agents described above and, in this modelling, there is no mechanism to create aerosols in south east Asia during an ENSO event and hence the causal direction must run from the aerosols to the ENSO events.

In addition, the aerosol forcings in all LME runs are fixed at 1850 values except for the "ozone and aerosol" and "all" runs and there can therefore be no forcing of the aerosols by any agent within these six runs and the causal direction must flow from the aerosols to the ENSO events.

LE: Aerosols are included as forcing agents in the LE. However, aerosol levels are specified at decadal intervals in RCP 8.5 and ENSO cannot therefore force the SEAP Area aerosols on an annual basis and the causal direction must run from the aerosols to the ENSO events.

MERRA-2: The MERRA-2 reanalysis assimilates measured aerosol data and as Appendix A shows the aerosol sources are volcanoes, gas flares and fires lit by the local population the causal direction must be from the aerosols to the ENSO events as the aerosols are assimilated and not generated within the model by ENSO.

5.4 Satellite Data and Recent Changes in the SEAP

Figure 20 clearly shown that the character of ENSO as measured by the Nino 3.4 SST has changed since 1980 when the extreme anthropogenic SEAP started to appear and with the high correlations of the anthropogenic SEAP in SON with ENSO it is clear that the change is driven by the SEAP and since Appendix A shows that the anthropogenic SEAP is caused by fires deliberately lit to clear land the causal direction must run from the SEAP to ENSO.

5.5 Seasonality of ENSO

ENSO is highly seasonal and this paper provides an explanation for the seasonality. Rainfall in the CSEAP area and the Nino 3.4 SST correlate at -0.59 significance <0.05 with the SST reducing when rainfall in the SEAP Area is high. This clearly supports the hypothesis that the SEAP is the major cause of ENSO events as the south east Asian monsoon rainfall washes the aerosols out of the atmosphere enabling convection to be re-established in the region to drive the Trade Winds and end the ENSO event.

5.6 Monsoon Indices

Three of the four monsoon indices in Figure 15 show a statistically significant relationship to the natural SEAP and since the monsoons cannot cause volcanic eruptions the causal direction must be from the volcanic tephra to the monsoon.

5.7 Multiple Independent Datasets

Seven of eight LME modelling runs (excluding the aerosol forced run as it correlates with the All forcing run) and the MERRA-2 reanalysis exhibit very low or negative correlations between the CSEAP AODVIS in the individual runs as shown in the correlation matrix in Appendix C with an overall average 0.0016. Hence the datasets are independent. The LE is excluded as the LE aerosols correlate with the LME ALL forcing run.

All these seven LME and MERRA-2 datasets show correlations with the ENSO indices at significance of <0.01 or less and the chance that all these seven datasets show the same result and are wrong is the product of the significances i.e. 0.01^{-8} or 10.0^{-16} a vanishingly small number.

5.8 Companion Paper

The companion paper [*K A Potts*, 2020a] demonstrates that drought in south eastern Australia (SEAus) which has commonly been attributed the ENSO and/or IOD events is also caused by the SEAP further confirms the causal relationship flows from the SEAP to all these events as drought in SEAus cannot create SEAP Area aerosols .

5.9 Segmented Data

The climate is a chaotic system and my preferred way to analyse climate data is to segment, average and compare similar elements as the averaging process will improve the signal to noise ratio of the analysis. The annual LME AODVIS and ENSO data is segmented on the basis of the AODVIS data and then averaged and correlated. The three major ENSO indices when analysed in this way with the CSEAP AODVIS deliver R^2 values of 1.00 (Figure 10) demonstrating clearly that the SEAP is the major and possibly the only driver of ENSO events.

5.10 Causal Direction

Therefore with:

1. The volcanic aerosols demonstrating conclusively that SEAP Area aerosols are the cause of ENSO events;
2. The LME data showing a clear connection between the SEAP and ENSO indices without correlation;
3. The LME and MERRA-2 time series analysis showing the same results with a vanishingly small chance of error;
4. The LME data showing, by a preferred analysis method, extremely high correlations which leave no possibility of other drivers;
5. The monsoon indices showing a clear connection to SEAP Area volcanic tephra;
6. The support of four satellite datasets showing the same results;

The inevitable conclusion is that the SEAP is the major driver of ENSO events and may even be the sole driver.

6 FUTURE RESEARCH

To finally confirm these conclusions, it is suggested that further LME style analyses are undertaken in which:

1. An aerosol plume is created in the model which ramps up from the naturally low level in January to reach the same AOD as the extreme SEAP of October 2006 or 2015 in February, continues at the same level to October and ramps down in November to the naturally low level in December. This plume to be applied in the model with random returns from 2 to 10 years to mimic the actual return frequency of ENSO;
2. Repeating 1 with reducing levels of AOD from February to October to determine the minimum AOD level over SE Asia which is required to cause an ENSO event.

These analyses will confirm the conclusions in this paper and conclusively demonstrate that ENSO events are caused by the SEAP and determine the AOD levels required to do so.

7 CONCLUSIONS

The LME with 1.156 annual and 13,872 monthly time series data points, LE with 251 years of data including 75 years of RCP 8.5 data, MERRA-2, measured aerosol datasets from four satellites and the GVP volcanic eruption data all confirm the direct connection between the SEAP and ENSO in multiple independent ways.

Causal analysis showing that the relationship must flow from the SEAP to ENSO.

Power spectra showing a clear, close relationship between the natural SEAP and the Nino 3.4 area SST derived from the HadlSST-1 datasets which is lacking in the LME data.

Correlations of the LME and LE CSEAP Area AOD with Nino 3.4 TS and the SOI show average R^2 values for these two major ENSO indicators at 0.79 and 0.72 (time series) and 1.00 (segmented) respectively.

I therefore conclude that the SEAP is unique and based on these values is the major and possibly the sole trigger and sustaining agent for ENSO events and that the hypothesis is proved.

This conclusion brings six important elements into climate change analysis:

First: Aerosol Regional Dimming, the Surface Radiative Forcing caused by the annual apparitions of continental scale aerosol plumes, the anthropogenic elements of which did not occur before the middle of the 20th century, is an important, recent element driving climate change. The eight plumes noted in this paper both reflect and absorb/reradiate solar radiation at levels depending on their aerosol chemistry and affect the local hydrologic cycle and large scale atmospheric circulation systems such as the Hadley and Walker Cells as this paper and its companion [*K A Potts*, 2020a] demonstrate. These plumes mainly exist in the tropics and the effects only occur in the season in which the plume exist as the residence time of aerosols in the troposphere is short – the IPCC AR5 [*Stocker et al.*, 2013] states “1 to 3 weeks” for volcanic aerosols.

Second: The natural volcanic tephra plumes from all volcanic eruptions and not just large eruptions must be included in climate modelling as they are the prime cause of ENSO events and are therefore the primary climate forcing agent on an interannual basis;

Third: All eight major continental scale, aerosol plumes shown in Figure 3 must be included in climate models as their effects are significant;

Fourth: Climate models must incorporate these plumes at temporal and geographic resolutions which will adequately model their effects. Global and seasonal or annual averages are not sufficient as the climate forcing effects of the plumes only exist when the plume exists and the averaging process reduces the intensity of the plumes and destroys their seasonal effects.

Fifth: Since the SEAP causes ENSO events it follows that this aerosol plume causes an increase in the global temperature, most likely through the modification of the large-scale atmospheric circulation systems (especially convection in SE Asia) instead of just cooling the region under the plume through direct surface forcing as is commonly assumed. It is also likely that the increases in the AI and AOD of the SEAP since 1980 in non-extreme years such as 1999 and 2001 will also have affected the global temperature. This requires further investigation.

Sixth: The effects of combinations of the eight anthropogenic, continental scale aerosol plumes require investigation as the combined effects of such plumes may be radically different to the effects of individual plumes.

Finally I concur with *Booth et al.* [2012] that emissions of carbonaceous aerosols are directly addressable by government policy actions and suggest that this is an urgent necessity to mitigate future anthropogenic ENSO events in the Austral spring which *Timbal and Drosdowsky* [2013] link to drought in Australia.

8 APPENDIX A - SOURCES OF THE SOUTH EAST ASIAN AEROSOL PLUME

8.1 Biomass burning

Biomass burning in the tropics is part of the annual agricultural cycle and usually occurs at the end of the dry season before the start of the local monsoon. In the SEAP Area the monsoon commences in November and the biomass burning aerosol plume is at its most intense in SON. The increase in biomass burning in the SEAP Area in recent decades has been driven by the increasing population of the SEAP Area. The population of Indonesia, Malaysia and Papua New Guinea has increased from 77 to 277 million between 1950 and 2010 (United Nations https://www.un.org/en/development/desa/population/publications/database/index.asp). This increasing population has forced: an increase in food production from tropical agriculture with its attendant smoke/aerosols; and increased rainforest clearing to provide living space and agricultural land. There has also been increasing levels of commercial activity including rainforest logging. In SON in 1982, 1991, 1997, 2002, 2004, 2006, 2009, 2014 and 2015 the AOD or AI increased significantly compared to the intervening years (Figure 6) due to the clearing of the rainforest for palm oil plantations.

Applegate et al. [2001] found that there were a number of direct causes of fire in the 1997-98 fires in Indonesia:

- Fire being used to assist with land clearing;
- Fire used as a weapon in land tenure or land use disputes;
- Accidental or escaped fires;
- Fire connected with resource extraction.

Neither climate change nor ENSO events are identified as a primary cause of fire in 1997-98 and the other major fire events in 1982/1983, 1987, 1991 and 1994 although this is commonly stated to be the case in the literature relating to ENSO events. ENSO is only noted as a reason for the spread of fire started by the causes noted above in certain years.

The 6th International Wildland Fire Conference held by the United Nations International Strategy for Disaster Reduction and their Food and Agriculture Organization in Korea, in 2015 released the Pyeongchang Declaration “Fire Management and Sustainable Development” (https://gfmc.online/allgemein/korea-2015.html) which stated in the Regional Statement for southeast Asia that “Most vegetation fires occurring in the member countries of the Association of Southeast Asian Nations are due to human interventions, notably by local communities and industrial corporations.”

Reports in the popular press as well as governments in the region attribute the cause of such fires to land clearing in Indonesia and on Nov 9 2006 Reuters reported “Environment ministers from five Southeast Asian countries endorsed a plan of action on Thursday to fight forest fires in Indonesia that have spread choking smoke across the region.” and “Indonesia's neighbours have grown increasingly frustrated by the fires, most of which are deliberately lit by farmers or by timber and palm oil plantation companies to clear land for cultivation.” In September 2015 the Times in London reported that “Singapore has taken legal measures against Indonesian businesses for the vast forest fires that are choking millions of people across southeast Asia.” See CIFOR at http://blog.cifor.org/37016/clearing-the-smoke-the-causes-and-consequences-of-indonesias-fires?fnl=en which suggests that 115,000 were burning in Indonesia in October 2015.

The connection between AOD in the CSEAP Area and fire is demonstrated in three ways:

One: The burned areas in Indonesia from NASA at https://search.earthdata.nasa.gov/projects?p=C1457414586-SEDAC!C1457414586-SEDAC&q=burned%20area%20indonesia&tl=1563231391!4!! [*Center for International Earth Science Information Network - CIESIN - Columbia University*, 2018] from 1997 to 2015 was extracted. Correlating the MERRA-2 AOD in SON, the burning season, with the areas burned in Indonesia gives 0.96. The data is shown in Figure 28

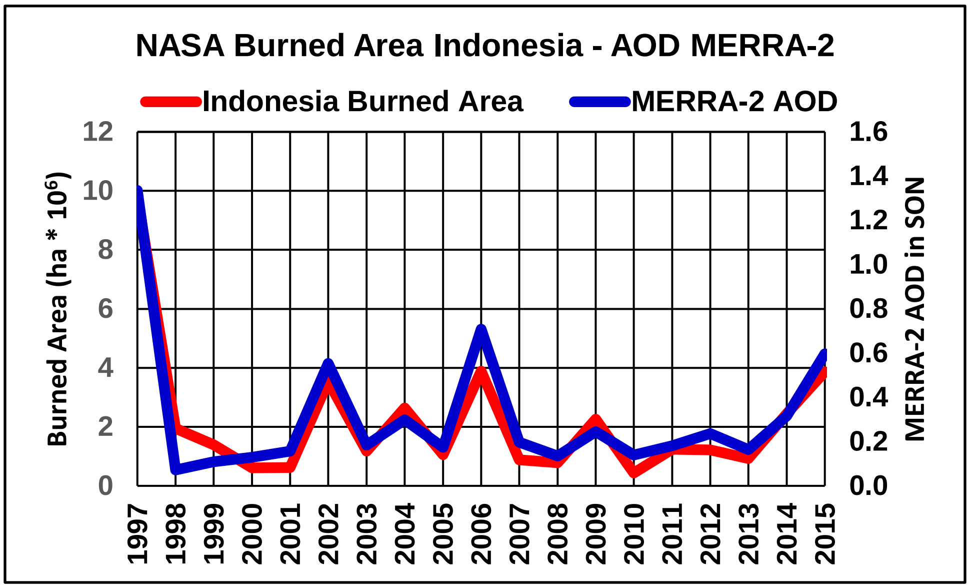

Figure 28: NASA MERRA-2 AOD in SON and Area Burned.

Two: The Indonesian archived active fires (NASA) from August 2013 to 2019 from the Global Forest Watch at https://data.globalforestwatch.org/datasets/de1fe5832831464cbd64aaa8f2d54781_0/data

was downloaded and the average number of fires locations each month were extracted which correlate with the MERRA-2 AOD at 0.95 (significance < 0.01) (Figure 29).

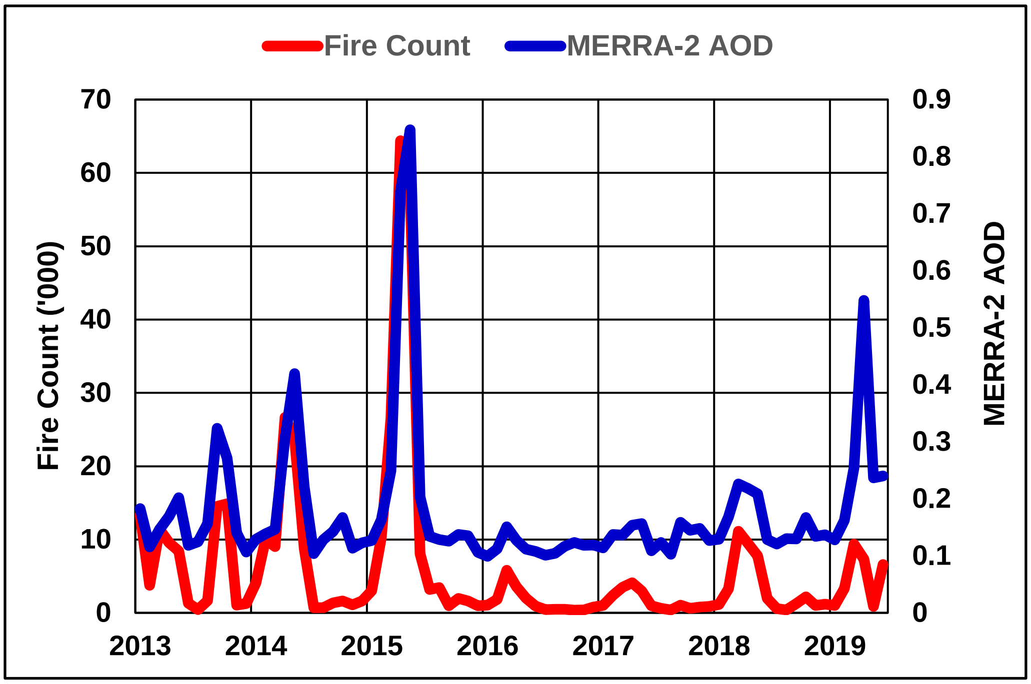

Figure 29: Indonesian Global Fire Watch Archived Fires (NASA) and NASA MERRA-2 AOD

Three: Correlating the Black Carbon (BC) Emissions from the Global Fire Emissions Database (GFED4.1) [*Randerson et al.*, 2017] for the Equatorial Asian (EQAS) Region and of similar extent to the SEAP Area) from fires at https://daac.ornl.gov/cgi-bin/dsviewer.pl?ds_id=1293 for the period 1997 to 2016 with the SON AOD of the CSEAP Area gives 0.96. The data is shown in Figure 30.

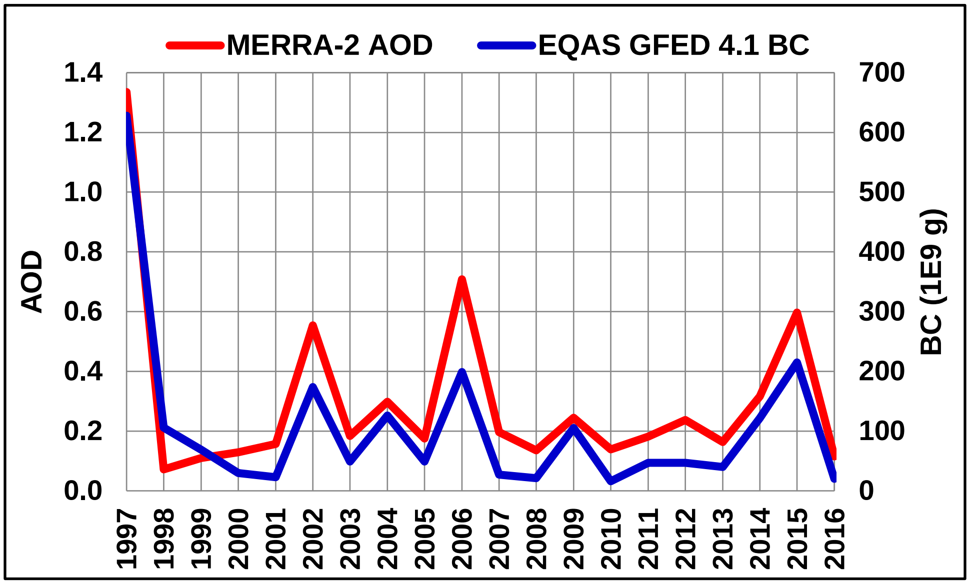

Figure 30: Equatorial Asian Region black carbon emissions from the GFED database 4.1 and the CSEAP Area SON MERRA-2 AOD.

Together the burned area, fire and BC data show that the extreme AOD in SON in some years was created by fire in south east Asia, mainly Indonesia.

8.2 Gas Flares

Gas Flares in the oil production industry increased in number over recent decades as oil production in south east Asia (Indonesia, Malaysia, Thailand and Brunei) increased from 567,000 to 2,087,000 barrels of oil per day between 1965 and 2018 (BP Statistical Review of World Energy 2019).

The World Bank has established the GGFRP which estimates SE Asia flares 4.03 billion m^3 of natural gas each year and the gas flare locations are shown in Figure 2. NOAA identifies about 387 flare locations in the SEAP Area. Images of such flares producing aerosols are easily found in Google Earth (Figure 31) or at the GGFRP web site.

Figure 31: LNG Badak. Credits: Left Ridho Akbari, Right Fauzi (from Google Earth)

8.3 Volcanoes

Figure 2 shows the GVP overlay of volcano locations, each red triangle is either one or a cluster of volcanoes.

The level of tectonic activity, shown by earthquakes, in the SEAP Area increased from the early 1980's to 2005, declined to 2009 and has since increased again. The USGS provides earthquake data from 1973 and Figure 32 and shows that the average number of earthquakes/month in the SEAP Area was 71 between 1973 and 1982. The red line marks this average plus 3 standard deviations calculated from the same period and shows that from 1995 to 2009 there was a significant (> 3 std deviations) increase in the number of earthquakes which peaked at 1,303 in January 2005 after the Boxing Day earthquake and Tsunami. In May 2009 the number of earthquakes fell below the red line for the first time since January 1995 but in 2013 started increasing again.

The GVP database of volcanic eruptions [*Venzke*, 2013] shows that the SEAP Area hosted over 18% of all the global volcanic eruptions from 1500 to 2018 whilst covering only 3% of the Earth's surface. *Simkin and Siebert* [2000] reported that 16 volcanoes have been erupting nearly continuously for 30 years and that 5 of these volcanoes are in the SEAP Area. Hence the SEAP Area hosts an unusually high percentage of the global volcanic activity and within it Indonesia is "the most volcanically active nation on Earth" (USGS) https://www.usgs.gov/center-news/revolutionizing-volcano-monitoring-indonesia).

It is also worth noting that the median duration of a volcanic eruption is 7 weeks [*Simkin and Siebert*, 2000]. The IPCC AR5 in Figure 1 of section FAQ 11.2 notes that the effect of volcanic eruptions on the lower atmosphere (and therefore the surface) is "cooling because the reduction of sunlight overwhelms any increased downward energy emitted by the volcanic cloud" and also states the residence time in the troposphere of "1 to 3 weeks" for volcanic ash. Hence a volcanic ash plume will have a median residence time of 8 to 10 weeks in the atmosphere – 7 weeks of eruption followed by 1 to 3 weeks of residence.

The volume of Tephra ejected by volcanoes in the SEAP Area was calculated as shown below. The VEIT data was summed for each decade from 1890 to the present and when restricted to the April to October Figure 33 shows the 2000 to 2009 VEIT level was 2.89 times the 20th century average.

AOD and Volcanic Tephra: The MERRA-2 AOD of the CSEAP Area averaged over the months January to August, which avoids the extreme plumes in SON, correlates with the tephra ejected by volcanoes in the same months at 0.73 from 1980 to 2014 (significance <0.1). For the full year from 1980 to 2014 the correlation is 0.83 (significance <0.05) and excluding the years of extreme SON aerosols (October AOD > 0.7) to avoid contaminating the analysis with the extreme plumes caused by biomass burning the correlation is the same, 0.83 (significance <0.05)

Spread of tropospheric Volcanic Tephra: Figure 34 shows an image of the eruption of the Sangeang Volcano in Indonesia which continued for 1.5 years from May 2014 to November 2015 (GVP database) at an estimated VEI of 3 (GVP) suggesting the majority of the tephra remained in the troposphere. This image demonstrates how quickly the aerosol plume spreads from a point source to about 250 km width in the lower right of the image after travelling about 400 Km. Noting that Indonesia, which covers a significant part of the SEAP Area, is "the most volcanically active nation on Earth” (USGS) it is easy to see how volcanic tephra from multiple simultaneous eruptions can significantly affect the AOD of the SEAP Area.

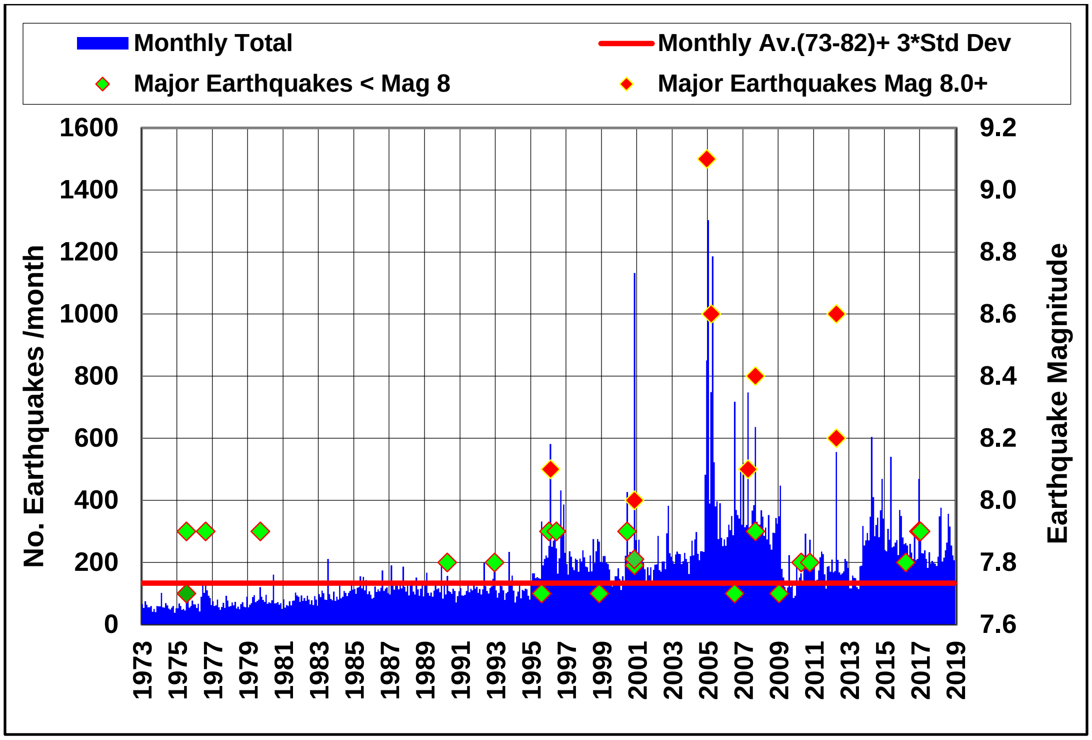

Figure 32: Total Monthly Earthquakes 1973 – 2018 SEAP Area with major events Magnitude 7.7+ shown. Source: USGS Earthquake database.

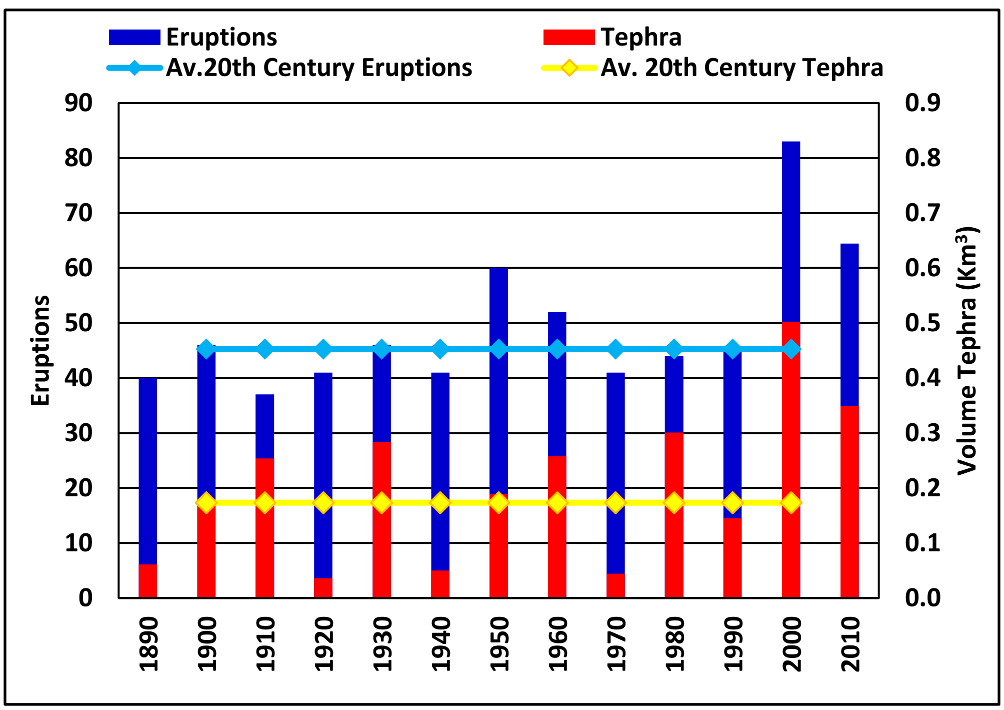

Figure 33: Decadal total and average volcanic eruptions and tephra volume in the SEAP Area from April to October. Averages from 1900 to 1999. Source GVP Database. (Note the 2010 column is for 2010 to 2018, 9 years, and has been increased pro rata to be comparable to the other decades).

Figure 34: Aerosol plume emanating from Sangeang Volcano May 2014. Source NASA.

8.4 Volcano Data Processing

The volcanic eruption data was downloaded from the Global Volcanism Program database at http://volcano.si.edu/list_volcano_holocene.cfm [*Venzke*, 2013]. Then:

- Eruptions from 1870 were extracted from the dataset;
- The VEI was extracted. Any eruptions with no VEI listed were allocated a VEI of 0;
- The VEIT in Km^3 was calculated using the table in *Newhall and Self* [1982];
- The eruption start year was extracted;
- The eruption start month was extracted and eruptions with no start month were allocated sequentially to January then February and so on;
- The end year and month was extracted. For eruptions with no end date the end date was calculated using the start date and the median eruption length in [*Simkin and Siebert*, 2000] of 7 weeks;
- The length of each eruption in months was calculated and the total VEIT for the eruption was allocated equally to each month of the eruption starting with the start month and ending with the end month.
- The VEIT for each month from 1870 to 2018 was summed;
- The summed monthly VEIT was then smoothed with a 12 month running average and carried forward to the various analyses;
- In the analyses of the Nino 3.4, 1+2 SST and the SOI (Nino Parameters) the VEIT data was allocated to segments 0 to 0.001, >0.001 to 0.004, >0.004 to 0.01 and >0.01 and averaged and the corresponding monthly Nino Parameter allocated to the same segment and averaged;
- The VEIT and Nino Parameters were then correlated and displayed on scatter plots.

Note:

- The BOM SOI data runs from 1876 to 2019
- The NOAA ESRL Nino 3.4 and 1+2 SST run from 1870 to 2018
- The NCEP Omega data runs from 1948 to 2018
- Due to the significantly different time periods of the Nino Parameter data and the omega data the segment boundaries for the omega data were: 0.00005, 0.0001, 0.0002, 0.00855 and >0.00855

9 APPENDIX B – PROCESSING SEQUENCE FOR LME AND LE DATA

The LME and LE data was processed through the following routes as required:

1. No Processing;
2. Deseasonalised;
3. Normalised: Some of the data exhibits a non-linear trend which was removed by dividing the data at time t by the running average from time t-3 to t+3 and then multiplying the result by the average of the whole data set;
4. Smoothed with a running 12 point average centered on time t (t-5 to t+6);
5. Note: the ONI, IOD and SOI include both negative and positive values and the normalising was carried out using the absolute values of these indices to avoid anomalies which occur when true averages resulted in values close to zero.

The processing route for each analysis is shown in Figure 35 and the key in Figure 36.

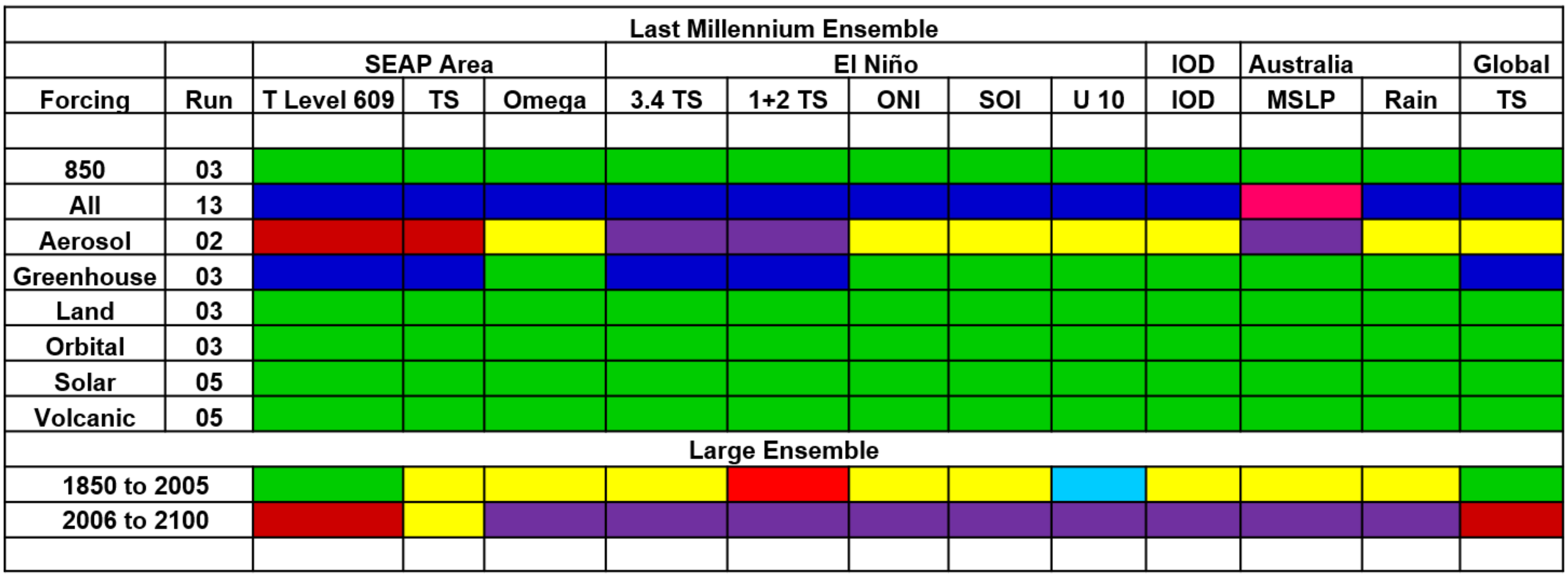

Figure 35: Processing route for each parameter including time series and segmented data.

	Time Series			Segmented	
	Annual	Apr-Oct	SON	Annual	monthly
	None			None	None
	Normalised			None	None
	Normalised			Normalised	None
	Normalised			Normalised	Normalised
	Normalised			Normalised	Normalised & Smoothed 12 Av.
	Normalised			Normalised	Deseasonalised & normalised
	Normalised			Normalised	Averaged 12 points

Figure 36: Key for processing routes

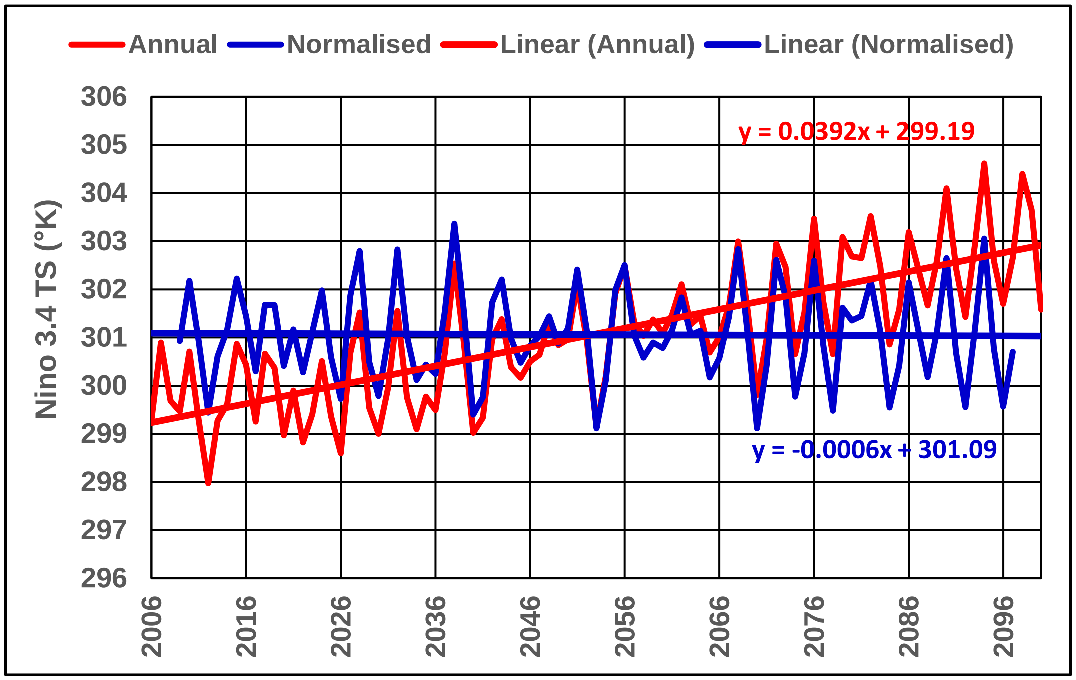

Figure 37: Effect of normalising Nino 3.4 TS data from the LE RCP 8.5 data.

The effect of the normalization process is described in [*Dettling*, 2014] p34 and is shown in Figure 37 where the trend in TS under RCP 8.5 has been reduced from 3.72°K to -0.057°K across the data set and the interannual variation is virtually unchanged.

10 APPENDIX C – CORRELATION MATRIX FOR LME, LE AND MERRA-2

	850	All	GHG	Land Use R3	Orbital R3	Ozone Aerosol R2	Solar	Volcanic R5	MERRA 2
850	1.00	0.02	0.03	-0.04	0.08	-0.08	0.07	-0.02	-0.37
All	0.02	1.00	0.02	0.00	-0.02	0.54	-0.04	-0.02	0.12
GHG	0.03	0.02	1.00	0.00	0.09	-0.06	0.04	0.01	-0.05
Land Use R3	-0.04	0.00	0.00	1.00	0.00	0.02	0.00	0.02	-0.03
Orbital R3	0.08	-0.02	0.09	0.00	1.00	0.12	-0.01	0.03	-0.09
Ozone Aerosol R2	-0.08	0.54	-0.06	0.02	0.12	1.00	-0.15	0.12	-0.09
Solar	0.07	-0.04	0.04	0.00	-0.01	-0.15	1.00	-0.07	0.25
Volcanic R5	-0.02	-0.02	0.01	0.02	0.03	0.12	-0.07	1.00	-0.39
MERRA 2	-0.37	0.12	-0.05	-0.03	-0.09	-0.09	0.25	-0.39	1.00
Average	-0.04	0.08	0.01	0.00	0.03	0.05	0.01	-0.04	-0.08

Figure 38: Correlation matrix for LME and MERRA-2 CSEAP AOD/AODVIS. The average excludes the self-correlations which return 1.00.

There is only one significant positive correlation between the All and Ozone Aerosol data in Figure 38 hence 8 of the 9 data sets are independent.

Acknowledgments and Data

I acknowledge:

NASA: Analyses and visualizations used in this paper were produced with the Giovanni online data system, developed and maintained by the NASA GES DISC; the mission scientists and Principal Investigators who provided the data used in this paper including the CALIPSO data; and Dr Robert Schmunk for the Panoply data viewer;

The Hadley Centre for the HadISST_1 dataset;

Google Earth^{TM} and the copyright holders noted on the images for the images of the Earth and gas flares;

The Global Forest Watch at https://data.globalforestwatch.org/datasets/de1fe5832831464cbd64aaa8f2d54781_0/data for the fire data;

Oak Ridge National Laboratory and NASA for the Global Fire Emissions Database (GFED4.1s) for the BC Emissions for the Equatorial Asian Region at https://daac.ornl.gov/cgi-bin/dsviewer.pl?ds_id=1293

The Climate and Global Dynamics Division of ESSL at NCAR for the SEAP SST, Omega and Niño 1+2 and 3.4 SST data;

The Indonesian burned areas data from NASA at https://search.earthdata.nasa.gov/projects?p=C1457414586-SEDAC!C1457414586-SEDAC&q=burned%20area%20indonesia&tl=1563231391!4!!

NOAA: Data and images provided by the NOAA/OAR/ESRL PSD, Boulder, Colorado, USA, from their Web site at http://www.esrl.noaa.gov/psd/ ; the Trade Wind data by the Climate Prediction Centre;

The CESM1(CAM5) Last Millennium Ensemble Community Project and supercomputing resources provided by NSF/CISL/Yellowstone;

The CESM Large Ensemble Community Project and supercomputing resources provided by NSF/CISL/Yellowstone;

The United Nations Department of Economic and Social Affairs Population Division for the world population statistics;

The United Nations Forest Resources Assessment reports for the burned area data

The Australian Bureau of Meteorology for the Walker Circulation images, SOI data and SOI formula at http://www.bom.gov.au;

The U.S. Geological Survey for the earthquake information at: https://www.usgs.gov/natural-hazards/earthquake-hazards/science/20-largest-earthquakes-world?qt-science_center_objects=0#qt-science_center_objects ;

BP for the oil production statistics at http://www.bp.com/en/global/corporate/energy-economics/statistical-review-of-world-energy.html;

The Global Volcanism Program at the Smithsonian Institution for the volcano eruption data at http://volcano.si.edu/

Warwick Goldsworthy and Andrew Metcalfe for discussion and comments;

The anonymous reviewers whose comments greatly improved the paper.

All data supporting the conclusions is available from the sources shown in the text.

This research project was funded personally by the author and his wife Julie.

References

Ammann, C. M., G. A. Meehl, W. M. Washington, and C. S. Zender (2003), A monthly and latitudinally varying volcanic forcing dataset in simulations of 20th century climate, *Geophysical Research Letters*, *30*(12), n/a-n/a, doi:10.1029/2003GL016875.

Applegate, G., U. Chokkalingam, and Suyanto (2001), The Underlying Causes and Impacts of Fires in South-east Asia, *Center for International Forestry Research and International Centre for Research in Agroforestry*.

Barry, R. G., and R. J. Chorley (2010), *Atmosphere Weather and Climate* Routledge, Abingdon UK.

Blake, S. A. P., S. C. Lewis, A. N. LeGrande, and R. L. Miller (2018), Assessing the impact of large volcanic eruptions of the last millennium (850–1850 CE) on Australian rainfall regimes, *Clim. Past*, *14*(6), 811-824, doi:10.5194/cp-14-811-2018.

Booth, B. B., N. J. Dunstone, P. R. Halloran, T. Andrews, and N. Bellouin (2012), Aerosols implicated as a prime driver of twentieth-century North Atlantic climate variability, *Nature*, *484*(7393), 228-232, doi:10.1038/nature10946.

Brown, J. N., and A. V. Fedorov (2010), How Much Energy Is Transferred from the Winds to the Thermocline on ENSO Time Scales?, *Journal of Climate*, *23*(6), 1563-1580, doi:10.1175/2009JCLI2914.1.

Cane, M. A. (2005), The evolution of El Niño, past and future, *Earth and Planetary Science Letters*, *230*(3–4), 227-240, doi:http://dx.doi.org/10.1016/j.epsl.2004.12.003.

Center for International Earth Science Information Network - CIESIN - Columbia University (2018), Global Fire Emissions Indicators, Country-Level Tabular Data: 1997-2015, edited, NASA Socioeconomic Data and Applications Center (SEDAC), Palisades, NY.

Cook, E. R., K. J. Anchukaitis, B. M. Buckley, R. D. D'Arrigo, G. C. Jacoby, and W. E. Wright (2010), Asian Monsoon Failure and Megadrought During the Last Millennium, *Science*, *328*(5977), 486-489, doi:10.1126/science.1185188.

Dettling, D. M. (2014), Applied Time Series Analysis, *Zurich University of Applied Sciences*, *https://stat.ethz.ch/education/semesters/ss2014/atsa/Scriptum_v140523.pdf*.

Duncan, B. N., I. Bey, M. Chin, L. J. Mickley, T. D. Fairlie, R. V. Martin, and H. Matsueda (2003), Indonesian wildfires of 1997: Impact on tropospheric chemistry, *Journal of Geophysical Research: Atmospheres*, *108*(D15), 4458, doi:10.1029/2002JD003195.

Emile-Geay, J., R. Seager, M. A. Cane, E. R. Cook, and G. H. Haug (2008), Volcanoes and ENSO over the Past Millennium, *Journal of Climate*, *21*(13), 3134-3148.

Enfield, D. B. (1989), El Niño, past and present, *Reviews of Geophysics*, *27*(1), 159-187, doi:10.1029/RG027i001p00159.

Foster, G., and S. Rahmstorf (2011), Global temperature evolution 1979–2010, *Environ. Res. Lett.*, *6*, doi:doi:10.1088/1748-9326/6/4/044022.

Gao, C., A. Robock, and C. Ammann (2008), Volcanic forcing of climate over the past 1500 years: An improved ice core-based index for climate models, *Journal of Geophysical Research: Atmospheres*, *113*(D23), doi:10.1029/2008jd010239.

Gelaro, R., et al. (2017), The Modern-Era Retrospective Analysis for Research and Applications, Version 2 (MERRA-2), *Journal of Climate*, *30*(14), 5419-5454, doi:10.1175/jcli-d-16-0758.1.

Hammer, Ø., D. A. T. Harper, and P. D. Ryan (2001), PAST: Paleontological statistics software package for education and data analysis. , *Palaeontologia Electronica 4(1): 9pp*, 9pp.

Handler, P., and K. Andsager (1990), Volcanic aerosols, El Niñmo and the Southern Oscillation, *International Journal of Climatology*, *10*(4), 413-424, doi:10.1002/joc.3370100409.
Hansell, R. A., S. C. Tsay, Q. Ji, K. N. Liou, and S. C. Ou (2003), Surface aerosol radiative forcing derived from collocated ground-based radiometric observations during PRIDE, SAFARI, and ACE-Asia, *Appl Opt*, *42*(27), 5533-5544.
Hirono, M. (1988), On the trigger of El Niño Southern Oscillation by the forcing of early El Chichón volcanic aerosols, *Journal of Geophysical Research: Atmospheres*, *93*(D5), 5365-5384, doi:10.1029/JD093iD05p05365.
Huang, B., P. W. Thorne, V. F. Banzon, T. Boyer, G. Chepurin, J. H. Lawrimore, M. J. Menne, T. M. Smith, R. S. Vose, and H.-M. Zhang (2017), Extended Reconstructed Sea Surface Temperature, Version 5 (ERSSTv5): Upgrades, Validations, and Intercomparisons, *Journal of Climate*, *30*(20), 8179-8205, doi:10.1175/jcli-d-16-0836.1.
Kajikawa, Y., B. Wang, and J. Yang (2010), A multi-time scale Australian monsoon index, *International Journal of Climatology*, *30*(8), 1114-1120, doi:10.1002/joc.1955.
Kaufman, Y. J., B. N. Holben, D. Tanré, I. Slutsker, A. Smirnov, and T. F. Eck (2000), Will aerosol measurements from Terra and Aqua Polar Orbiting satellites represent the daily aerosol abundance and properties?, *Geophysical Research Letters*, *27*(23), 3861-3864, doi:10.1029/2000GL011968.
Kay, J. E., et al. (2015), The Community Earth System Model (CESM) Large Ensemble Project: A Community Resource for Studying Climate Change in the Presence of Internal Climate Variability, *Bulletin of the American Meteorological Society*, *96*(8), 1333-1349, doi:10.1175/bams-d-13-00255.1.
Maher, N., S. McGregor, M. H. England, and A. S. Gupta (2015), Effects of volcanism on tropical variability, *Geophysical Research Letters*, *42*(14), 6024-6033, doi:10.1002/2015GL064751.
Mann, M. E., M. A. Cane, S. E. Zebiak, and A. Clement (2005), Volcanic and Solar Forcing of the Tropical Pacific over the Past 1000 Years, *Journal of Climate*, *18*(3), 447-456, doi:10.1175/JCLI-3276.1.
Maraun, D., and J. Kurths (2005), Epochs of phase coherence between El Niño/Southern Oscillation and Indian monsoon, *Geophysical Research Letters*, *32*(15), n/a-n/a, doi:10.1029/2005GL023225.
McGregor, S., A. Timmermann, M. F. Stuecker, M. H. England, M. Merrifield, F.-F. Jin, and Y. Chikamoto (2014), Recent Walker circulation strengthening and Pacific cooling amplified by Atlantic warming, *Nature Clim. Change*, *4*(10), 888-892, doi:10.1038/nclimate2330
http://www.nature.com/nclimate/journal/v4/n10/abs/nclimate2330.html#supplementary-information.
McPhaden, M. J., et al. (1998), The Tropical Ocean-Global Atmosphere observing system: A decade of progress, *Journal of Geophysical Research: Oceans*, *103*(C7), 14169-14240, doi:10.1029/97JC02906.
McPhaden, M. J., S. E. Zebiak, and M. H. Glantz (2006), ENSO as an Integrating Concept in Earth Science, *Science*, *314*(5806), 1740-1745, doi:10.1126/science.1132588.
Mieville, A., C. Granier, C. Liousse, B. Guillaume, F. Mouillot, J. F. Lamarque, J. M. Grégoire, and G. Pétron (2010), Emissions of gases and particles from biomass burning during the 20th century using satellite data and an historical reconstruction, *Atmospheric Environment*, *44*(11), 1469-1477, doi:http://dx.doi.org/10.1016/j.atmosenv.2010.01.011.

Morice, C. P., J. J. Kennedy, N. A. Rayner, and P. D. Jones (2012), Quantifying uncertainties in global and regional temperature change using an ensemble of observational estimates: The HadCRUT4 data set, *Journal of Geophysical Research: Atmospheres*, *117*(D8), n/a-n/a, doi:10.1029/2011JD017187.

Newhall, C. G., and S. Self (1982), The volcanic explosivity index (VEI) an estimate of explosive magnitude for historical volcanism, *Journal of Geophysical Research: Oceans*, *87*(C2), 1231-1238, doi:10.1029/JC087iC02p01231.

Nicholls, N. (1988), Low latitude volcanic eruptions and the El Niño-Southern Oscillation, *Journal of Climatology*, *8*(1), 91-95, doi:10.1002/joc.3370080109.

Nicholls, N. (1990), Low-latitude volcanic eruptions and the El Niñmo/Southern Oscillation: A reply, *International Journal of Climatology*, *10*(4), 425-429, doi:10.1002/joc.3370100410.

Nozawa, T., T. Nagashima, H. Shiogama, and S. A. Crooks (2005), Detecting natural influence on surface air temperature change in the early twentieth century, *Geophysical Research Letters*, *32*(20), n/a-n/a, doi:10.1029/2005GL023540.

Otto-Bliesner, B. L., E. C. Brady, J. Fasullo, A. Jahn, L. Landrum, S. Stevenson, N. Rosenbloom, A. Mai, and G. Strand (2016), Climate Variability and Change since 850 CE: An Ensemble Approach with the Community Earth System Model, *Bulletin of the American Meteorological Society*, *97*(5), 735-754, doi:10.1175/bams-d-14-00233.1.

Potts, K. A. (2020), How Extreme Apparitions of the Volcanic and Anthropogenic South East Asian Aerosol Plume caused the Millennium Drought in South Eastern Australian. First Attribution and Mechanism using data from the Last Millennium Ensemble, Large Ensemble, MERRA-2 Reanalysis, four Satellites and the Global Volcanism Program.

Predybaylo, E., G. L. Stenchikov, A. T. Wittenberg, and F. Zeng (2017), Impacts of a Pinatubo-size volcanic eruption on ENSO, *Journal of Geophysical Research: Atmospheres*, *122*(2), 925-947, doi:doi:10.1002/2016JD025796.

Ramanathan, V. (2006), ATMOSPHERIC BROWN CLOUDS: HEALTH, CLIMATE AND AGRICULTURE IMPACTS, *Scripta Varia 106*.

Randerson, J. T., G. R. Van Der Werf, L. Giglio, G. J. Collatz, and P. S. Kasibhatla (2017), Global Fire Emissions Database, Version 4.1 (GFEDv4), edited, ORNL Distributed Active Archive Center, doi:10.3334/ORNLDAAC/1293.

Rayner, N. A., D. E. Parker, E. B. Horton, C. K. Folland, L. V. Alexander, D. P. Rowell, E. C. Kent, and A. Kaplan (2003), Global analyses of sea surface temperature, sea ice, and night marine air temperature since the late nineteenth century, *Journal of Geophysical Research: Atmospheres*, *108*(D14), doi:doi:10.1029/2002JD002670.

Remer, L. A., et al. (2009), Executive Summary, in Atmospheric Aerosol Properties and Climate Impacts, A Report by the U.S. Climate Change Science Program and the Subcommittee on Global Change Research [Mian Chin, Ralph A. Kahn, and Stephen E. Schwartz (eds.)]. National Aeronautics and Space Administration, Washington, D.C., USA.

Robock, A., K. E. Taylor, G. L. Stenchikov, and Y. Liu (1995), GCM evaluation of a mechanism for El Niño triggering by the El Chichón ash cloud, *Geophysical Research Letters*, *22*(17), 2369-2372, doi:10.1029/95GL02065.

Self, S., M. R. Rampino, J. Zhao, and M. G. Katz (1997), Volcanic aerosol perturbations and strong El Niño events: No general correlation, *Geophysical Research Letters*, *24*(10), 1247-1250, doi:10.1029/97GL01127.

Shukla, J., and D. A. Paolino (1983), The Southern Oscillation and Long-Range Forecasting of the Summer Monsoon Rainfall over India, *Monthly Weather Review*, *111*(9), 1830-1837, doi:doi:10.1175/1520-0493(1983)111<1830:TSOALR>2.0.CO;2.

Simkin, T., and L. Siebert (2000), Earth's volcanoes and eruptions: an overview p. 249-261. , in *Encyclopedia of Volcanoes,* , edited by S. H, Academic Press, San Diego.

Solomon, S., et al. (2007), Technical Summary. In: Climate Change 2007: The Physical Science Basis. Contribution of Working Group I to the Fourth Assessment Report of the Intergovernmental Panel on Climate Change [Solomon, S., D. Qin, M. Manning, Z. Chen, M. Marquis, K.B. Averyt, M. Tignor and H.L. Miller (eds.)]. Cambridge University Press, Cambridge, United Kingdom and New York, NY, USA.

Stocker, T. F., et al. (2013), Technical Summary. In: Climate Change 2013: The Physical Science Basis. Contribution of Working Group I to the Fifth Assessment Report of the Intergovernmental Panel on Climate Change*Rep.*, Intergovernmental Panel on Climate Change, Cambridge, United Kingdom and New York, NY, USA.

Sturman, A. P., and N. J. Tapper (1996), The Weather and Climate of Australia and New Zealand. Oxford University Press Australia 476.

Takemura, T., T. Nozawa, S. Emori, T. Y. Nakajima, and T. Nakajima (2005), Simulation of climate response to aerosol direct and indirect effects with aerosol transport-radiation model, *Journal of Geophysical Research: Atmospheres*, *110*(D2), n/a-n/a, doi:10.1029/2004JD005029.

Timbal, B., and W. Drosdowsky (2013), The relationship between the decline of Southeastern Australian rainfall and the strengthening of the subtropical ridge, *International Journal of Climatology*, *33*(4), 1021-1034, doi:10.1002/joc.3492.

Timmreck, C. (2012), Modeling the climatic effects of large explosive volcanic eruptions, *Wiley Interdisciplinary Reviews: Climate Change*, *3*(6), 545-564, doi:doi:10.1002/wcc.192.

Tosca, M. G., D. J. Diner, M. J. Garay, and O. V. Kalashnikova (2015), Human-caused fires limit convection in tropical Africa: First temporal observations and attribution, *Geophysical Research Letters*, *42*(15), 2015GL065063, doi:10.1002/2015GL065063.

Trenberth, K. E., J. M. Caron, D. P. Stepaniak, and S. Worley (2002), Evolution of El Niño–Southern Oscillation and global atmospheric surface temperatures, *Journal of Geophysical Research: Atmospheres*, *107*(D8), AAC 5-1-AAC 5-17, doi:10.1029/2000JD000298.

Trenberth, K. E., D. P. Stepaniak, and J. M. Caron (2000), The Global Monsoon as Seen through the Divergent Atmospheric Circulation, *Journal of Climate*, *13*(22), 3969-3993, doi:doi:10.1175/1520-0442(2000)013<3969:TGMAST>2.0.CO;2.

Venzke, E. (2013), Volcanoes of the World v. 4.4.3, edited by S. I. G. V. Program, doi: http://dx.doi.org/10.5479/si.GVP.VOTW4-2013.

Wang, B., and S. An (2002), A mechanism for decadal changes of ENSO behavior: roles of background wind changes, *Climate Dynamics*, *18*(6), 475-486, doi:10.1007/s00382-001-0189-5.

Wang, B., and Z. Fan (1999), Choice of South Asian Summer Monsoon Indices, *Bulletin of the American Meteorological Society*, *80*(4), 629-638, doi:doi:10.1175/1520-0477(1999)080<0629:COSASM>2.0.CO;2.

Wang, B., R. Wu, and K.-M. Lau (2001), Interannual Variability of the Asian Summer Monsoon: Contrasts between the Indian and the Western North Pacific–East Asian Monsoons, *Journal of Climate*, *14*(20), 4073-4090, doi:doi:10.1175/1520-0442(2001)014<4073:IVOTAS>2.0.CO;2.

Wang, C. (2002), Atmospheric Circulation Cells Associated with the El Nin˜o–Southern Oscillation, *Journal of Climate*.

Webster, P. J., and S. Yang (1992), Monsoon and Enso: Selectively Interactive Systems, *Quarterly Journal of the Royal Meteorological Society*, *118*(507), 877-926, doi:10.1002/qj.49711850705.

Winker, D. M., M. A. Vaughan, A. Omar, Y. Hu, K. A. Powell, Z. Liu, W. H. Hunt, and S. A. Young (2009), Overview of the CALIPSO Mission and CALIOP Data Processing Algorithms, *Journal of Atmospheric and Oceanic Technology*, *26*(11), 2310-2323, doi:10.1175/2009jtecha1281.1.

Zebiak, S. E., and M. A. Cane (1987), A Model El Ni&ntilde–Southern Oscillation, *Monthly Weather Review*, *115*(10), 2262-2278, doi:doi:10.1175/1520-0493(1987)115<2262:AMENO>2.0.CO;2.

Zhang, D., R. Blender, and K. Fraedrich (2013), Volcanoes and ENSO in millennium simulations: global impacts and regional reconstructions in East Asia, *Theoretical & Applied Climatology*, *111*(3/4), 437-454, doi:10.1007/s00704-012-0670-6.

How Extreme Apparitions of the Volcanic and Anthropogenic South East Asian Aerosol Plume caused the Millennium Drought in South Eastern Australian. First Attribution and Mechanism using data from the Last Millennium Ensemble, Large Ensemble, MERRA-2 Reanalysis, four Satellites and the Global Volcanism Program.

K. A. Potts[1]

[1] Kyna Keju Pty Ltd.

Corresponding author: Keith Potts (Keith.Potts@bigpond.com)

Key Points:

- Drought in SE Australia, ENSO and IOD events are caused by apparitions of the South East Asian aerosol Plume (SEAP)
- Volcanoes are and always have been the major source of the aerosols
- Post 1980 the anthropogenic SEAP has intensified the volcanic plume, drought, ENSO and the IOD especially in Sep-Nov

Abstract

The Last Millennium Ensemble, Large Ensemble, MERRA-2, four satellite data sets and the Global Volcanism Program database all show independently that drought in south eastern Australia (SEAus) is created by apparitions of the natural and anthropogenic aerosol plume over south east Asia which simultaneously create ENSO and IOD events. From 1997 to 2008 SEAus endured an exceptionally severe drought - the Millennium Drought. The River Murray, the major waterway in the region, experienced inflows at record low levels in 2006-07 which were more than 40% below the previous low. As the literature, Inter Governmental Panel on Climate Change (IPCC) and the USA Climate Change Science Program suggest that aerosols can affect the large-scale atmospheric circulation and hydrologic cycle I examine the relationship between aerosols and Australian droughts. The global aerosol coverage is highly inhomogeneous and variable at daily, monthly, annual and decadal scales. I show that the aerosol optical depth (AOD) and aerosol index (AI) of the South East Asian Plume (SEAP) and the volume of aerosols ejected by volcanoes (tephra) in south east Asia correlate with drought in Australia and conclude that the SEAP causes drought in Australia by Aerosol Regional Dimming (ARD), which, by altering the surface radiation budget under the plume and warming the upper atmosphere, forces the regional Inter Tropical Convergence Zone and Hadley Cells into abnormal seasonal positions. These effects alter the regional atmospheric circulation systems and hydrologic cycle thereby causing drought and, as the SEAP has intensified over time, created climate change.

1 INTRODUCTION

1.1 HYPOTHESIS AND PHYSICAL MODEL

This paper explores an explicit physical model and hypothesis to explain how the South East Asia aerosol Plume (SEAP) causes drought in south eastern Australia (SEAus) and simultaneously causes ENSO, described in the companion paper [*K.A. Potts*, 2020b], and IOD events.

Droughts in SEAus have always has been triggered and sustained by the natural volcanic aerosol plume over south east Asia (SEAsia) which has, in recent decades, been intensified by the anthropogenic aerosol plume especially from August to November (SON).

The sequence of events is:

12. The volcanic tephra aerosol plume forms over SEAsia and, in recent decades, is intensified by the anthropogenic plume which is most intense from August to November (ASON);
13. The aerosols absorb (and reflect) solar radiation which heats the atmosphere;
14. The aerosols reduce the solar radiation at the surface under the plume which cools the surface;
15. 2 and 3 create a temperature inversion compared to times without a plume and this reduces convection in the region;
16. The region to the south of the SEAP is now the driving force of the convective leg of the southern regional Hadley cell;
17. This southerly move in convection shifts the entire southern Hadley Cell south;
18. This results in a southerly shift in the sub-tropical high over SEAus;
19. This results in higher pressure over SEAus;
20. This forces the cold fronts south and reduces rainfall over SEAus;
21. The cooler sea surface temperature (SST) in SEAsia reduces evaporation in the area which supplies moisture to SEAus;
22. This results in less water vapour in the atmosphere over SEAus;
23. The combination of 9 and 11 above causes drought in SEAus.

1.2 Drought in south eastern Australia

An exceptional and extended drought occurred in South Eastern Australia (SEAus) at the turn of the century, the Millennium Drought [*Timbal et al.*, 2010] and [*Ummenhofer et al.*, 2009], and Figure 1 shows the rainfall deficit from 1997 to 2008 when parts of SEAus received the lowest rainfall on record. In this period all major cities in Australia were forced to build seawater desalination plants to guarantee the urban water supply and the River Murray, the major waterway in SEAus, received the lowest inflows on record [*Murray Darling Basin Authority*, 2011].

Whilst the Millennium Drought was exceptionally strong, drought has always occurred in SEAus and must therefore be a natural phenomenon as historically anthropogenic forcing was insufficient to impact the climate.

The drivers of such SEAus droughts have been identified as: El Niño – Southern Oscillation Index (SOI) (ENSO) events by *Neville Nicholls et al.* [1996], *Power et al.* [1998] and *G Wang and Hendon* [2007]; as Indian Ocean Dipole (IOD) events by *Ummenhofer et al.* [2009] and as variations in the location and intensity of the sub-tropical ridge over SEAus by *Timbal and Drosdowsky* [2013]. *Meyers et al.* [2007] investigated the effects of various combinations of ENSO and IOD events on Australian rainfall concluding there is a need to develop the "capability to predict interannual SST anomalies in the seas north of Australia in both the Pacific and the Indian Oceans."

The Centre for Australian Weather and Climate Research (CAWCR) in *Timbal et al.* [2010] reported the relationship between rainfall in south eastern Australia and the indices and parameters in Figure 2 which shows that in Sept. Oct. and Nov (SON) the Niño 4 Sea Surface Temperature (SST) and the local Mean Sea Level Pressure (SLP) exhibit the most significant and negative correlation with rainfall. However, the climate model used for the analysis did not include carbonaceous aerosols or small volcanic eruptions (personal communication).

I show that the element which must be included in the analysis of drought in SEAus is the South East Asian aerosol Plume (SEAP) which simultaneously creates drought, ENSO and IOD events

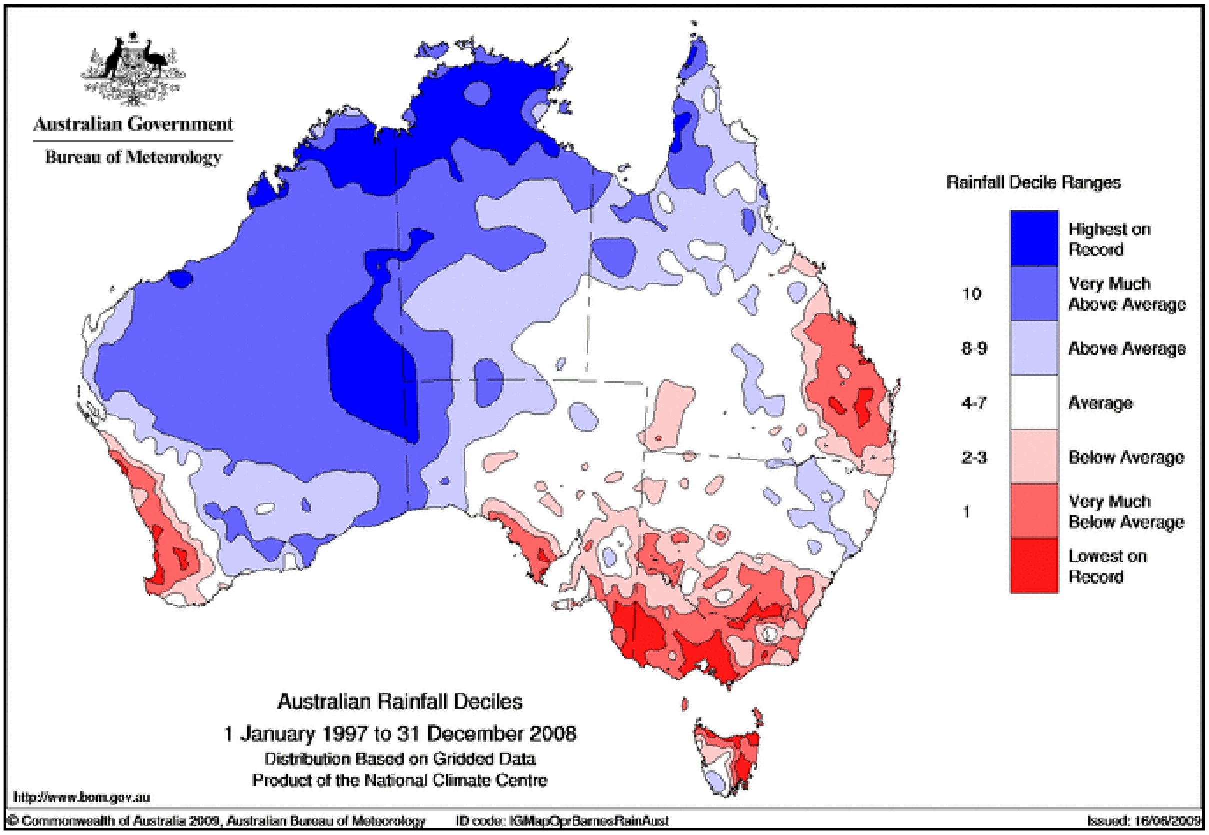

Figure 1: Figure 57 in *Timbal et al.* [2010] Australian rainfall deciles 1997 to 2008.

Correlation of Rainfall in Southern Hemisphere seasons with:	**Autumn (MAM)**	**Winter (JJA)**	**Spring (SON)**	**Summer (DJF)**
Local MSLP	-0.29	-0.74	-0.39	0.14
Niño 4 SST	-0.16	-0.20	-0.37	-0.18
NWS (North West Shelf) SST	0.07	0.30	0.26	-0.09
SAM (Southern Annular Mode)	-0.02	-0.27	0.31	0.31
NTS (Near Tasman Sea) SST	0.25	0.07	0.16	0.19

Figure 2: Correlations of parameters shown and rainfall south eastern Australia from Table 1 in *Timbal et al.* [2010].

1.3 Aerosols and Climate

The IPCC Assessment Report 4 (AR4) [*Solomon et al.*, 2007] identifies the two main anthropogenic contributors to climate change as Long Lived Green House Gases (LLGHG) and aerosols and defines Radiative Forcing (RF) as the global annual average of "the change in the net, downward minus upward, irradiance (expressed in W m^{-2}) at the tropopause". The IPCC AR4 also discusses Surface Forcing (SF), the effects of the forcing agents at the surface of the Earth and Figure 3 from that report shows the evolution of RF and SF from 1850 to the present day. It can be clearly seen that the net anthropogenic RF effect, black line – panel (A), follows the red line of LLGHG reasonably closely. However, the net anthropogenic SF effect, black line – panel (B), clearly follows the evolution of the aerosol direct effect which is much larger than the aerosol direct RF effect. The SF graph also shows that the anthropogenic aerosol direct effect in 2000 at -1.6W/m^2 is comparable to the explosive volcanic eruptions of Krakatau (1883) -2.2W/m^2 and Pinatubo (1991) -1.8W/m^2 which are considered to affect the mid to high latitude atmospheric circulation patterns [*Solomon et al.*, 2007].

Absorbing aerosols, particularly black carbon, a product of incomplete combustion [*Novakov et al.*, 2003], and organic carbon [*Kirchstetter*, 2004], have been linked to variations in the vertical temperature profile of the atmosphere and the large scale atmospheric circulation [*Solomon et al.*, 2007], [*Menon et al.*, 2002] and [*Chien Wang*, 2004]. Aerosols may also have a greater influence on the hydrologic cycle than other forcing agents through their SF effects [*Solomon et al.*, 2007].

Aerosols were believed to have mainly affected the northern hemisphere due to the greater annually averaged aerosol optical depth north of the equator however *Rotstayn et al.* [2009b] reviewed the impact of natural and anthropogenic aerosols on the Australian climate and suggested that regional aerosol plumes with their associated large reductions in short wave flux at the surface such as that derived from biomass burning in Indonesia may be important in understanding climate variation in Australia and recommended that further research should be undertaken on a limited number of topics including biomass burning in Indonesia as current aerosol inventories from this region are poorly treated. *Solomon et al.* [2007] expressed the same concern that the distribution and evolution of aerosol emissions during the 20th century were not well understood and *Hegerl et al.* [2007] noted that most studies used in the IPCC AR4 omitted carbonaceous aerosols which could have significant effects at regional scales.

The effects of short lived gases and aerosols were found to be substantial compared to LLGHG and to account for as much as 40% of the warming over the summertime United States and the climate response to these forcing agents was not confined to the area of their emission [*Levy II et al.*, 2008].

The global aerosol coverage and forcing is highly variable geographically and temporally and it is "insufficient or even misleading" to emphasise the global average and the aerosol SF is greater than the RF at the top of the atmosphere. Such SF affects the atmospheric circulation and the hydrologic cycle [*Remer et al.*, 2009].

Rotstayn et al. [2007] concluded that anthropogenic aerosol forcing should be included in modelling the Australian climate and that Asian anthropogenic aerosols may have affected the hydrologic cycle in the Australian region.

Menon et al. [2002] investigating the climate of China and India found precipitation and temperature changes in their model that were comparable to those observed only if the aerosol ensemble included a large proportion of absorbing black carbon ("soot") which was similar to observed amounts and noted that absorbing aerosols heat the atmosphere and alter the regional atmospheric stability and vertical motions which affects the large-scale circulation and hydrologic cycle with significant regional climate effects.

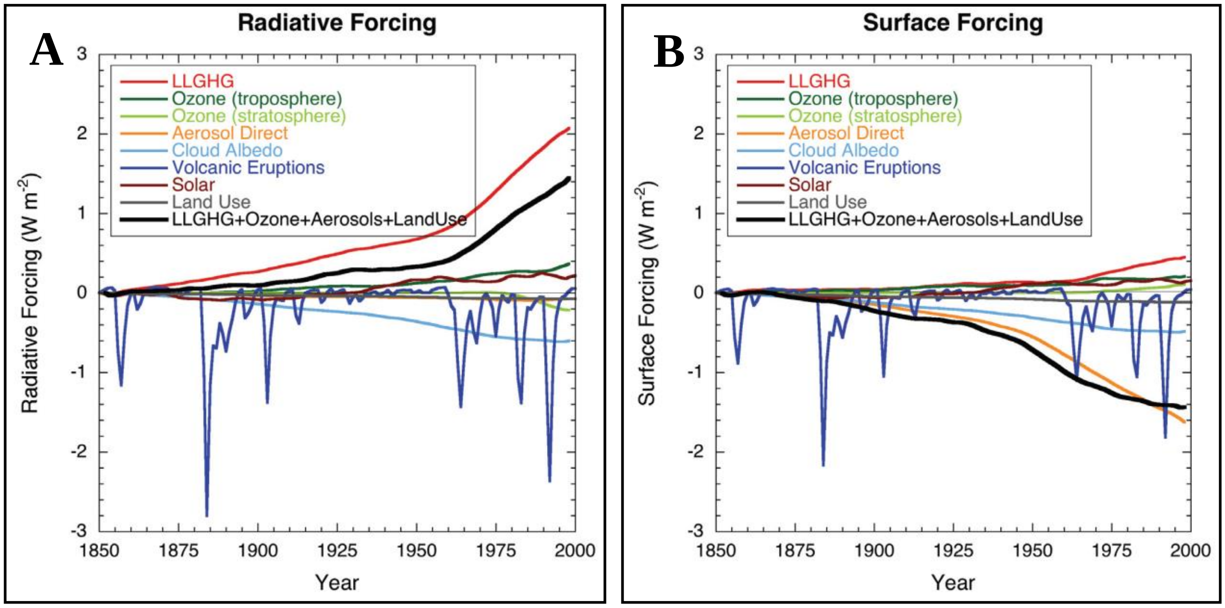

Figure 3: IPCC AR4 Figure 2.23 Chapter 2 page 208 [Forster et al., 2007]. Globally and annually averaged temporal evolution of the instantaneous all-sky RF (A) and SF (B) due to various agents, as simulated in the MIROC+SPRINTARS model (Nozawa et al., 2005; Takemura et al., 2005). This is an illustrative example of the forcings as implemented and computed in one of the climate models participating in the AR4. Note that there could be differences in the RFs among models. Most models simulate roughly similar evolution of the LLGHGs' RF.

In a review of the simulation of the Australian climate with the new CSIRO global climate model (GCM) Mark 3.6 which includes an interactive aerosol scheme *Rotstayn et al.* [2009a] found that "Compared to its predecessors and several international GCMs, Mk 3.6 is best able to capture the spatial pattern of the leading rainfall mode, which represents variability due to the El Niño Southern Oscillation (ENSO)".

Anthropogenic aerosols have been linked to: the decadal variance in the North Atlantic SST and thus to drought in the Sahel and the Amazon with the dominant mechanism being the reduction in short wave surface radiation [*Booth et al.*, 2012]; and the expansion of the tropics in the northern hemisphere evidenced by a poleward shift of the Hadley Cells, subtropical dry zones and extra-tropical storm tracks [*Allen et al.*, 2012]. SE Asia is identified as one of the regions of the globe which has demonstrated the largest rates of increase in black carbon emissions from 1970 to 2009 [*Allen et al.*, 2012] and it is noted that future emissions of anthropogenic aerosols are "directly addressable by policy actions" [*Booth et al.*, 2012]. However *R Zhang et al.* [2013b] investigated the claims in [*Booth et al.*, 2012] and concluded that “key aspects of the HadGEM2-ES simulation exhibit substantial discrepancies with observations.” Whilst noting that “Anthropogenic and natural aerosols have likely played some role in forcing the observed Atlantic mutidecadal variability.”

[*Ott et al.*, 2010] investigated the extreme biomass burning episode in the SEAP Area in 2006 and found that “temperatures over Indonesia were strongly modified by increased diabatic heating during the period of burning. The largest increases were found in October and November between 150 and 400 hPa. In some regions, increases exceeded 0.7 K during SON.” and that It is necessary for GCMs to include realistic representations of aerosols which fully represent the interannual variability of biomass burning emissions in order to capture the effects discussed in the paper.

The carbonaceous aerosol emission inventories for the Coupled Model Intercomparison Project phase 5 (CMIP5) are based on *Lamarque et al.* [2010] and are decadal averages designed to investigate long term (decadal to century) climate change and *Lamarque et al.* [2010] specifically state the emission inventories for CMIP5 are not designed to investigate “rapid” (i.e. less than a few years) pollution changes which this paper addresses. The base year for the CMIP5 Representative Concentration Pathways (RCP)’s is 2005 which was a low emission year in the SEAP Area and contrasts starkly with 2006, a very high emission year, the effects of which would not be captured in the CMIP5 analysis.

Finally [*K.A. Potts*, 2018] and [*K.A. Potts*, 2017] reported results that showed that drought and local MSLP in SEAus are forced by the SEAP.

In summary then the literature states aerosols affect:

1. The hydrologic cycle;
2. The large-scale atmospheric circulation systems; and
3. are not well understood;

and that carbonaceous aerosols:

1. Are an essential parameter in climate models to correctly model observed changes in precipitation;
2. Were omitted from most studies used in the IPCC AR4;
3. Have recently been linked to significant climate events; and
4. Are only included in the CMIP 5 RCP’s as decadal averages which cannot model the effects this paper addresses.

1.4 The Anthropogenic South East Asian Aerosol Plume

The major anthropogenic aerosol plume in the Australian region occurs over SE Asia and is referred to as the South East Asian aerosol Plume (SEAP).

The SEAP is one of eight great aerosol plumes which occur annually. It can be identified on the monthly mean 0.55 micron AOD data from MODIS [*Kaufman et al.*, 2000] on the NASA Terra and Aqua satellites distributed via the NASA MODIS Giovanni System (NMGS). *Remer et al.* [2005] confirm that the uncertainty in the AOD measured by these two satellites is “$\Delta\tau=\pm 0.05 \pm 0.15\tau$ over land” and that the AOD retrievals can be used in monitoring the aerosol radiative forcing of the global climate. Two areas shown in Figure 4 are used to describe the SEAP: the “SEAP Area” (latitude 10ºS to 10ºN and longitude 90ºE to 160ºE); and the Central SEAP (CSEAP) Area (latitude 5ºS to 5ºN and longitude 100ºE to 120ºE) where the SEAP is most intense. The monthly average AOD of the CSEAP Area is shown in Figure 5 to demonstrate the peak anthropogenic aerosol emission season is ASON, the end of the dry season in SE Asia, and was extremely high in 2002, 2004, 2006, 2009, 2014 and 2015 compared with the intervening years. In this analysis the AOD in the SON season has been used as it matches the seasonal analysis by CAWCR in *Timbal et al.* [2010] although in some years the AOD of the CSEAP Area is greater in August than in November. However, the CSEAP Area AOD in SON correlates with the ASON and ASO AOD at over 0.99 and 0.98 respectively. Figure 6 shows the geographic extent of the October 2006 apparition of the SEAP when the drought in SEAus was at its height (This image was included in the inaugural NASA Giovanni Image Hall of Fame in 2013.) This paper therefore focuses on the anthropogenic SEAP in SON because it is at its most intense in this season when it contains a preponderance of carbonaceous aerosols from biomass burning and will therefore have its greatest effect at this time.

The average AI from the Total Ozone Mapping Spectrometer (TOMS) on the Nimbus 7 (N7) and Earth Probe (EP) satellite platforms and from the Ozone Monitoring Instrument (OMI) on NASA Aura and the AOD of the CSEAP Area from the Terra Platform from 1979 to 2018 in SON are shown in Figure 7 which exhibits extreme interannual and interdecadal variation. The maximum AOD and AI for the CSEAP Area was 1.60 (Oct 2015) and 1.811 (Sept 1997) and the AI of the CSEAP Area increased from 0.038 in SON in 1979 to 0.193 in 1992 and to 0.296 in 2000 a 408% and 679% increase respectively in years without extensive biomass burning. From 1979 to 1997, a major biomass burning event year, the increase in AI in September was 3,499%.

1.5 The Natural South East Asian Aerosol Plume

Indonesia, in the SEAP Area, is the most “is the most volcanically active nation on Earth” (USGS at https://www.usgs.gov/center-news/revolutionizing-volcano-monitoring-indonesia) and the Global Volcanism Program (GVP) database shows the SEAP Area hosts 18% of the total number of volcanic eruptions in the World in about 3% of the global surface. *Simkin and Siebert* [2000] identify 16 volcanoes which have been erupting nearly continuously for 30 years and 5 (31%) are in the SEAP Area.

Appendix A describes in detail how the three major aerosol sources in the SEAP Area: biomass burning; gas flares; and volcanoes contributed to the extreme increases in the AOD or AI of the SEAP Area in 1997, 2002, 2006, 2014 and 2015 and in the decade 2000 to 2009.

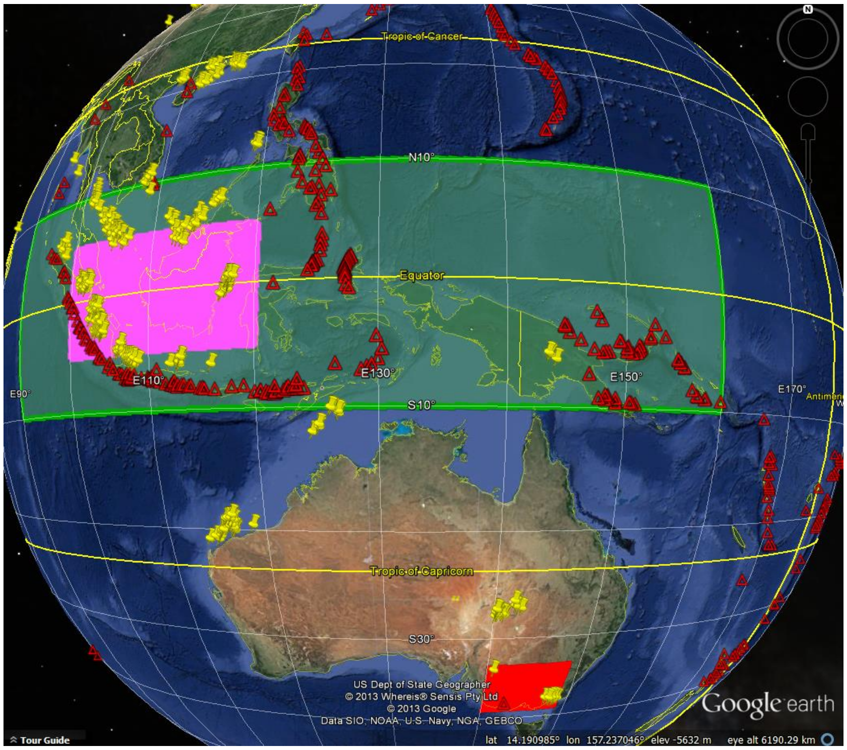

Figure 4: Google Earth image showing SEAP Area in Green, CSEAP Area in pink and the area used to analyse rainfall in SEAus in red with the locations of gas flares (National Oceanic and Atmospheric Administration (NOAA) and the Global Gas Flaring Reduction Partnership (GGFRP)) in yellow and volcanoes (GVP) in red.

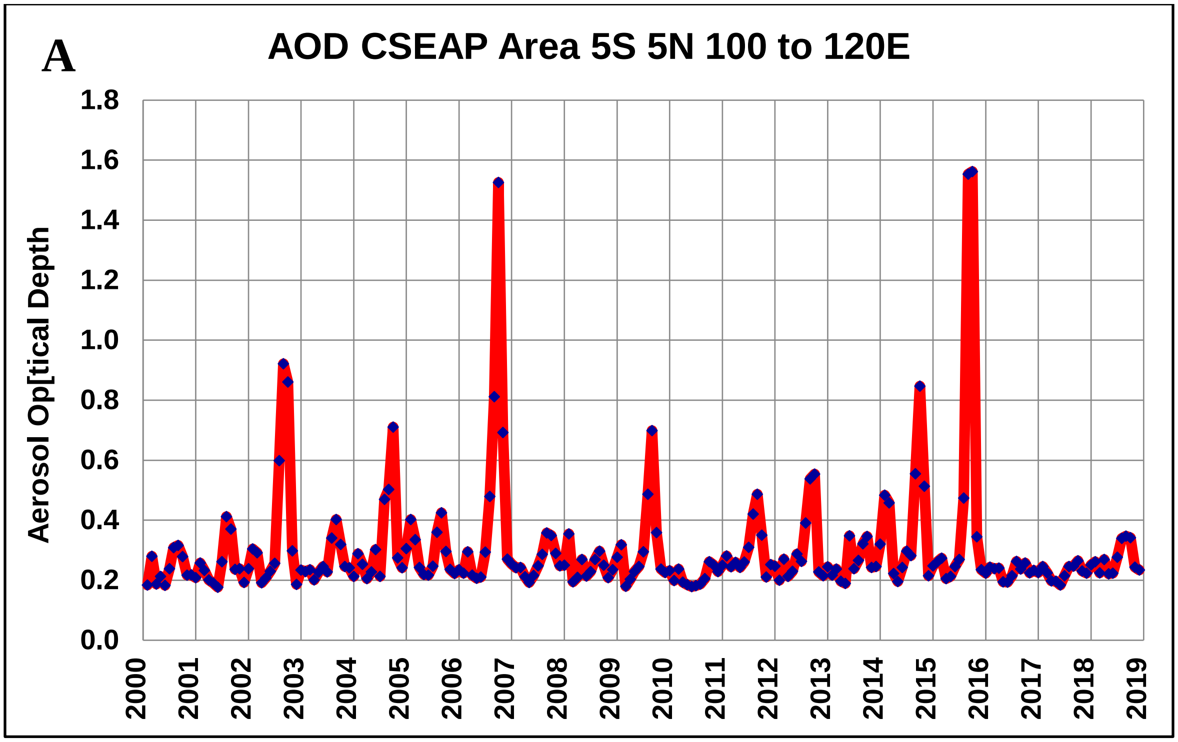

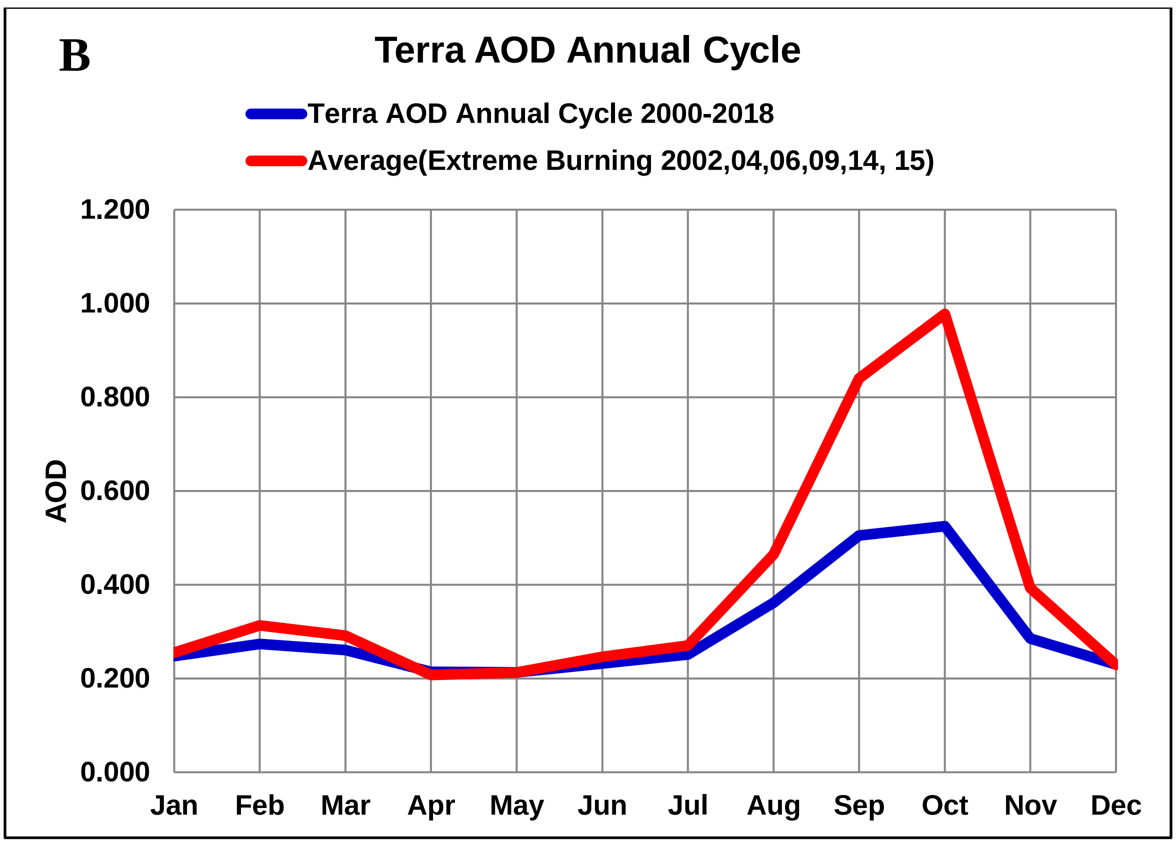

Figure 5: Terra AOD CSEAP Area. A: Monthly Average. B: Average annual cycle and cycle during years of extreme burning in SE Asia.

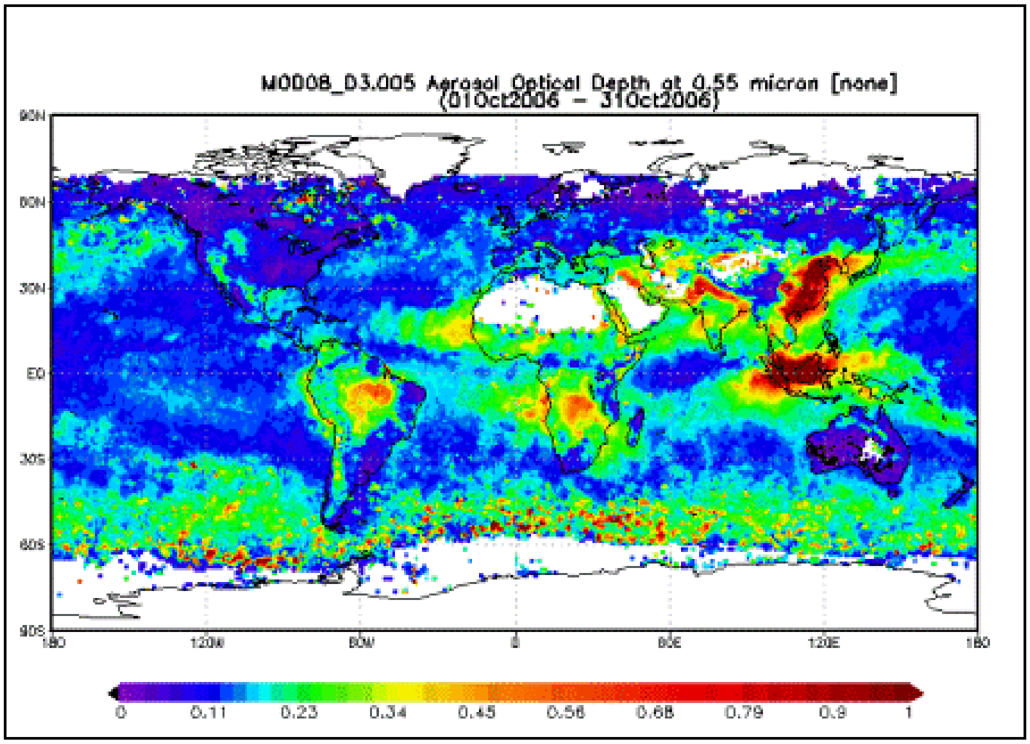

Figure 6: NASA Terra monthly mean AOD data October 2006.

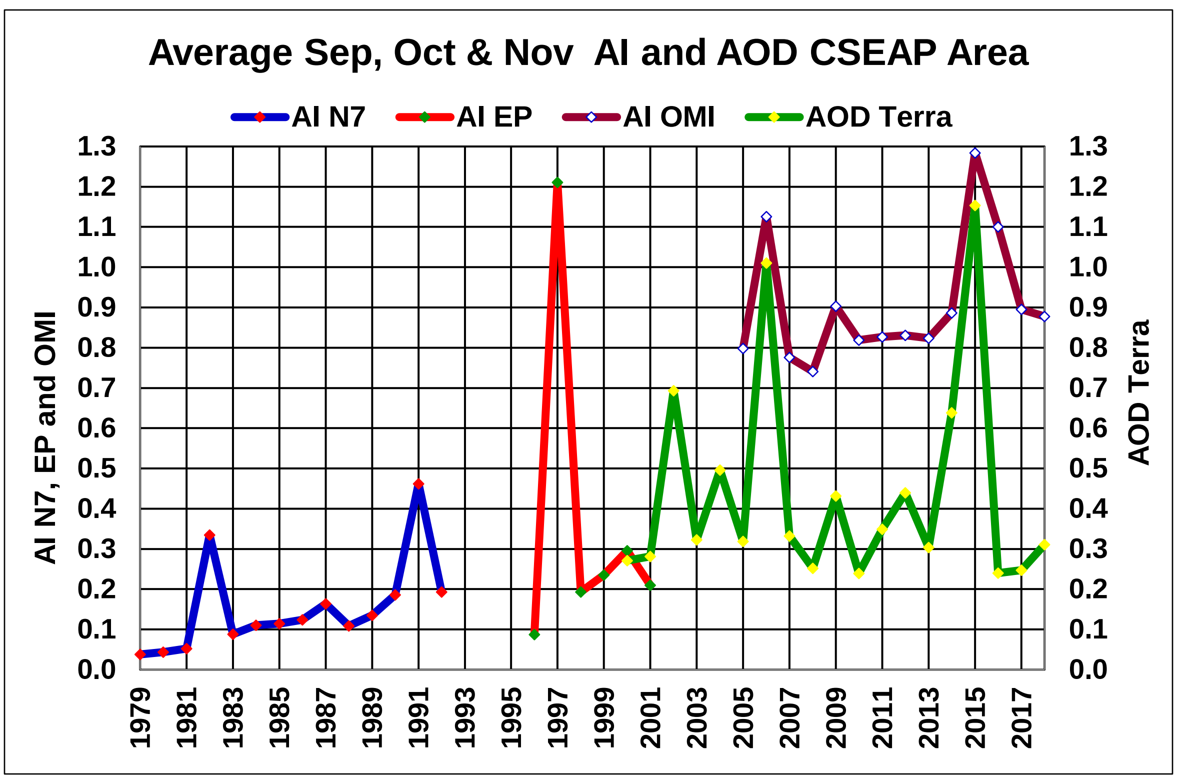

Figure 7: Average SON AI and AOD CSEAP Area.

1.6 Surface Radiative Forcing by the South East Asian Plume

The SF of aerosols is significant and the literature includes:

1. a 10% to 30% reduction of Photosynthetically Active Radiation recorded during INDOEX in the Indian Ocean in 1999 [Ramanathan, 2006];
2. -150 W m^{-2} in an analysis of the Indonesian wildfires which occurred in 1997 in [Duncan et al., 2003]; and
3. ~-286.0(W/ m^2)/$\tau\alpha$ recorded during the Aerosol Characterization Experiment -Asia in 2001 [Hansell et al., 2003] ($\tau\alpha$ is the aerosol optical depth and its derivation is described in the paper).

The idealised change in direct surface radiation when the SEAP is present is shown in Figure 8 with a plume AOD estimated at 0.52 compared with background 0.3 (Terra data Figure 7) giving a 20% reduction in surface radiation noting that 0.52 is much less than the maxima shown in the Terra data in Figure 7. In this figure the sun is assumed to be over the equator and the phase lag between the sun and the position of the ITCZ is ignored. It is clear that the highest level of surface solar radiation is at the edges of the plume and that these regions will drive convection which, in turn, drive the Hadley Cells. With the convective drive of the regional southern Hadley Cell moving south the entire southern regional Hadley Cell moves south which in turn moves the regional sub-tropical ridge south and creates anomalous, persistent high pressure over south eastern Australia as a direct consequence of the SEAP.

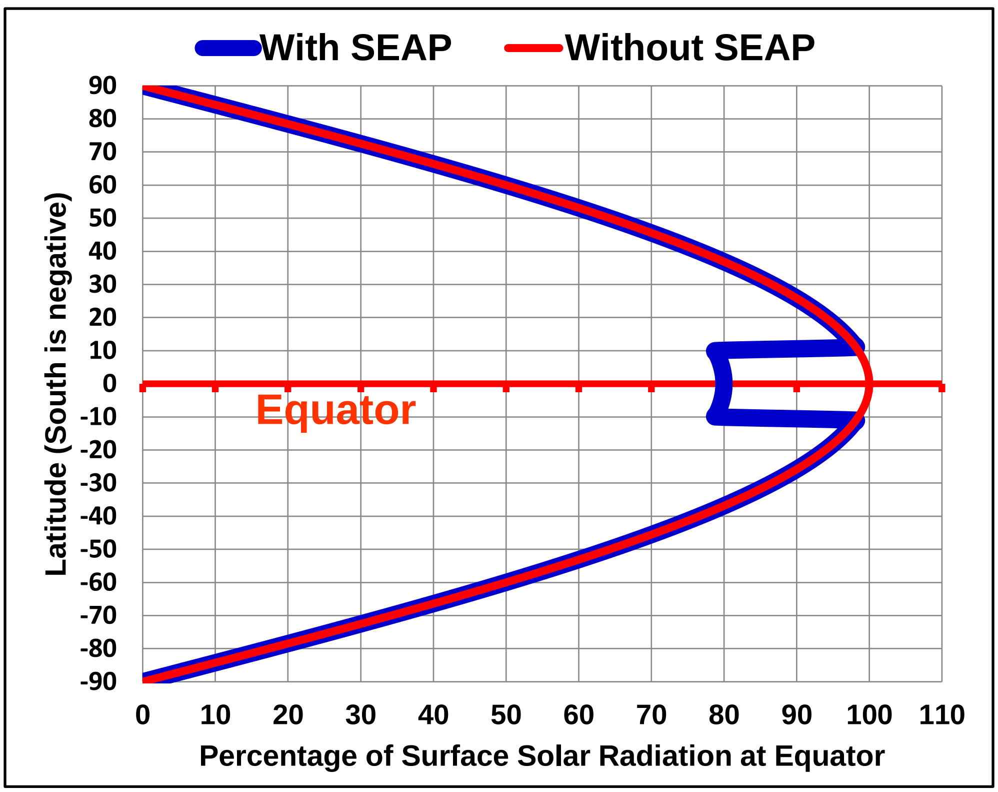

Figure 8: Idealised surface solar radiation with and without the SEAP assuming an increase in AOD from 0.3 to 0.52 which gives a 20% reduction under the SEAP.

The term Aerosol Regional Dimming (ARD) describes the surface radiative forcing effect of continental scale aerosol plumes which immediately alters the large-scale atmospheric circulation systems and regional hydrologic cycle and, crucially, only occurs when the plume exists.

1.7 The Connection Between the IOD and ENSO

The Australian Bureau of Meteorology (BOM) shows images of the atmospheric circulation during IOD and ENSO events in its website at http://www.bom.gov.au/climate/iod/ and http://www.bom.gov.au/climate/about/australian-climate-influences.shtml?bookmark=enso .

From the diagrams of the IOD and ENSO it is clear that the connection between the two effects is the SEAP Area. When the SST in the SEAP Area is warmer and convection occurs there ENSO is in the neutral/La Nina phase and the IOD in the neutral/negative phase whilst when the SST is cooler and convection reverses ENSO is in the El Niño phase and the IOD is in the positive phase. Hence aerosol changes in the SEAP Area which affect convection and the SST can impact both indices simultaneously.

2 METHOD and DATA

2.1 Modelling Data

The Last Millennium Ensemble (LME) [*Otto-Bliesner et al.*, 2016] data is available at https://www.earthsystemgrid.org/ . One member of each of the eight LME forcing simulations with run number in () (850 (3), All (13), Ozone and Aerosol (Aero) (2), Green House Gas (GHG) (3), Land use (Land) (3), Orbital (3), Solar (5) and Volcanic (5)) was used to create time series of 1,156 years and 13,872 months of: AOD; surface temperature; precipitation and omega; as well as indices for: the Indian Ocean Dipole (IOD); Nino 3.4 SST and SOI (which the IPCC AR5 shows at Table 1 in Box 2.5 are used to monitor the status of ENSO). This LME data was processed as shown in Appendix B and correlated as a time series to demonstrate that these indices and parameters are directly connected to aerosols in the SEAP area.

The data was also segmented and averaged on the basis of AOD and then correlated and is also presented graphically to show the effects of changes in AOD without using correlation.

Areas used for the LME and LE data were:

1. Rainfall: 137° 160°E 30° 40°S
2. Pressure: 130° 145°E 25° 40°S

A similar approach was used for:

1. The Large Ensemble (LE) [*Kay et al.*, 2015] using data from 1850 to 2005 with historic forcings and from 2006 to 2100 using RCP 8.5 projections (run 001) Data as for LME.
2. The NASA Modern Era Retrospective analysis for Research and Applications release two (MERRA-2) reanalysis dataset [*Gelaro et al.*, 2017] . Data http://giovanni.gsfc.nasa.gov/giovanni/

2.2 Satellite Data

Figure 5 shows the anthropogenic SEAP is at its height in SON, the end of the dry season in SE Asia, and will therefore have its greatest impact in this season. Aerosol data from four NASA satellites, N7 (AI), EP (AI), Terra (AOD) and OMI (AI) was downloaded from the NASA Giovanni system and correlated on an average SON basis with the following datasets:

1. **Rainfall:** Data NASA MERRA-2 reanalysis, area 36° to 39°S 140° to 149°E;
2. **MSLP:** Data NCEP reanalysis [*Kalnay et al.*, 1996]; area 30° to 35°S 140° to 147.4°E
3. **SEAP Area SST:** to the north and northwest of Australia reported by the BOM to influence the hydrologic cycle over SEAus (ENSO Wrap-Up Sept 2007) at http://www.bom.gov.au/climate/search/enso-wrap-up.shtml?bookmark=no-rm. Data NCEP reanalysis;
4. **Omega**: Data from NCEP reanalysis at http://www.esrl.noaa.gov/psd/data/timeseries/
5. **IOD:** Data from NOAA ESRL at https://www.esrl.noaa.gov/psd/gcos_wgsp/Timeseries/Data/dmi.long.data
6. **ENSO:** ENSO Nino 3.4 index from NOAA at http://www.cpc.ncep.noaa.gov/data/indices/ersst4.nino.mth.81-10.ascii

   SOI: The Southern Oscillation Index from the BOM at ftp://ftp.bom.gov.au/anon/home/ncc/www/sco/soi/soiplaintext.html

to demonstrate the connection between the SEAP, SON drought in SE Australia, ENSO and the IOD. As some aerosol datasets exhibit significant trends the data was also detrended using the PAST software version 3.22 [*Hammer et al.*, 2001].

Note: AI, unlike AOD, is "only sensitive to desert dust and elevated smoke layers. Therefore, it does not account for aerosols of industrial origin or any kind of aerosol in the lowest 2 km of the atmosphere" (Personal Communication - NASA). However in the SEAP Area it is useful as we are investigating biomass burning "smoke" in SON and the CALIPSO data at https://eosweb.larc.nasa.gov/project/calipso/calipso_table shows smoke at an altitude of 3Km in October 2015, above the lower limit of AI data.

2.3 Global Volcanism Program Data

Volcanoes are the major source of natural aerosols in the SEAP Area which existed prior to the anthropogenic SEAP of recent decades as described in Appendix A.

The Global Volcanism Program (GVP) database [*Venzke*, 2013] includes the Volcanic Explosivity Index (VEI) for most eruptions. The VEI was converted to tephra using the table in [*Newhall and Self*, 1982] which relates the VEI of an eruption to an estimated volume of Tephra (VEIT), the material explosively ejected into the atmosphere during the eruption. The IPCC AR5 [*Stocker et al.*, 2013] shows that tropospheric, tropical/sub-tropical, volcanic aerosols have a residence time of one to three weeks in the atmosphere and *Simkin and Siebert* [2000] state that the median duration of a volcanic eruption is seven weeks which results in a median plume duration of eight to ten weeks. Under the plume the eruption produces "Cooling because reduction of sunlight overwhelms any increased downward energy emitted by volcanic cloud" [*Kirtman et al*., 2013].

Simkin and Siebert [2000] state that 16 volcanoes have been erupting nearly continuously for 24 years and that 5 of them are in the SEAP Area.

Appendix A describes the processing route for the GVP eruption data which is available at http://volcano.si.edu/list_volcano_holocene.cfm. This data was then correlated with:

1. **Rainfall in the Riverina West Rainfall District**: Data: BOM CD and 2009 -2016 data by personal communication;
2. **Rainfall in Melbourne, Adelaide and Echuca:** data from BOM;
3. **The inflows into the River Murray:** Data: Murray Darling Basin Authority (MDBA) (personal communication) 1892 to 2015;
4. **Convection in the SEAP Area:** Data NCEP reanalysis1948 to 2016
5. **Mean SLP in Echuca and Melbourne:** Data BOM Australian Climate data CD

3 RESULTS

The climate is highly variable with more than one agent usually contributing to any variation and therefore whilst useful information can be extracted from such data using only time series analysis it is preferable to also analyse the data by segmenting the data on the basis of the forcing agent being investigated, averaging and then correlating as the averaging process improves the signal to noise ratio in the data significantly and the range of the forced parameter from the lowest to the highest forcing segment is a good indicator of the effects of the forcing agent without relying on correlation.

Some of the correlations from the LME and LE show significance levels that are much less than 0.01 due to the correlation magnitude and the length of the time series.

Note: Colour coding for the correlation significance in all results is Blue < 0.1, Green <0.05, Orange <0.02, Yellow < 0.01.

3.1 Modelling Data

3.1.1 Last Millennium Ensemble

Segment analysis results in the extraordinary correlations shown in the last two rows of Figure 9, the majority are 0,97 or greater magnitude. The segments boundaries for all runs except the "All" and "Aero" were set at AODVIS levels of: 0, 0.025, 0.028, 0.032, 0.038, 0.046, 0.055, 0.065 and 25 for all the CSEAP Area correlations and 0, 0.043, 0.046, 0.049, 0.053, 0.059, 0.068, 0.078 and 25 for the SEAP Area correlations. The AODVIS levels in the SEAP and CSEAP Areas are different with annual averages of 0.100 and 0.077 respectively and hence require different segments for analysis. The "All" and "Aero" runs show very different aerosol levels and therefore very different segments have to be used and, although they show similar levels of correlation with the IOD, and PSL and PRECL in SEAus they were not included in this analysis for simplicity. A graph of annual average SE Australian rainfall (PRECL), SLP (PSL) and AODVIS is at Figure 10 and shows that precipitation falls from an average of 398 to 162 mm/annum from the segment with the lowest AODVIS to the segment with the highest, a fall of 59%.

The AODVIS and the IOD graph is at Figure 11 showing an IOD rise from -1.2 to 1.0 from the lowest AODVIS segment to the highest. This compares well with the NOAA IOD data which has a range of -1.2 to 1.5 noting that the highest monthly maximum of the LME AODVIS (Aero (2)) at 0.28 is much lower than the Terra AOD at 1.56 with only three years showing maximum monthly AOD in the Terra data less than 0.28. Correcting this bias in the LME data would be expected to increase the maximum of the IOD in the LME data to at least the level in the instrument record.

Graphs of the Nino 3.4 SST, the SOI and omega in the SEAP Area are in the companion paper [*K.A. Potts*, 2020b].

Note: The volcanic forcing data in the LME cannot of itself demonstrate the connection between the natural volcanic SEAP and rainfall and SLP in SEAus, the IOD and ENSO as it does not have the resolution required to do so. It is derived from ice cores in the Arctic and Antarctic [*Otto-Bliesner et al.*, 2016] and [*Gao et al.*, 2008] who provide the data as only stratospheric sulfate forcing in latitude bands (ten degrees wide), by altitude and month. For volcanic tephra to travel to the polar regions the tephra must be injected into the stratosphere requiring a minimum VEI of 3 to 4. Hence all the VEI 0,1,2 and some (50% assumed) of the VEI 3 eruptions in the SEAP Area must be missing from the dataset. Since this excludes over 94% of the eruptions in the SEAP Area since 1850 which are used in this paper the resolution of this LME volcanic forcing dataset is inadequate in itself in terms of eruption size, geospace and aerosol type to prove the causation of the effects of volcanic tephra described in this paper. Although these volcanic forcing runs do provide another independent LME aerosol forcing dataset which is used.

AODVIS	Omega (609mb)	SST Nino 3.4 TS	SOI	IOD	Pressure SEAus	Rainfall SEAus
Monthly (Segmented)						
CSEAP Area	0.95	0.96	-0.97	0.94	0.82	-0.83
SEAP Area	0.76	0.93	-0.98	0.94	0.84	-0.98
September to November Averages						
CSEAP Area	0.82	0.79	-0.79	0.85	0.42	-0.76
SEAP Area	0.87	0.77	-0.78	0.82	0.50	-0.72
April to October Averages						
CSEAP Area	0.80	0.85	-0.89	0.88	0.68	-0.79
SEAP Area	0.81	0.83	-0.80	0.83	0.75	-0.65
Annual Averages						
CSEAP Area	0.79	0.90	-0.86	0.89	0.70	-0.78
SEAP Area	0.83	0.84	-0.79	0.76	0.78	-0.59
Annual Average - Segmented						
CSEAP Area	0.92	1.00	-1.00	0.97	0.97	-0.95
SEAP Area	0.98	0.99	-0.97	0.90	0.99	-0.87

Figure 9 LME correlations of AODVIS in the CSEAP and SEAP Areas with the parameters shown.

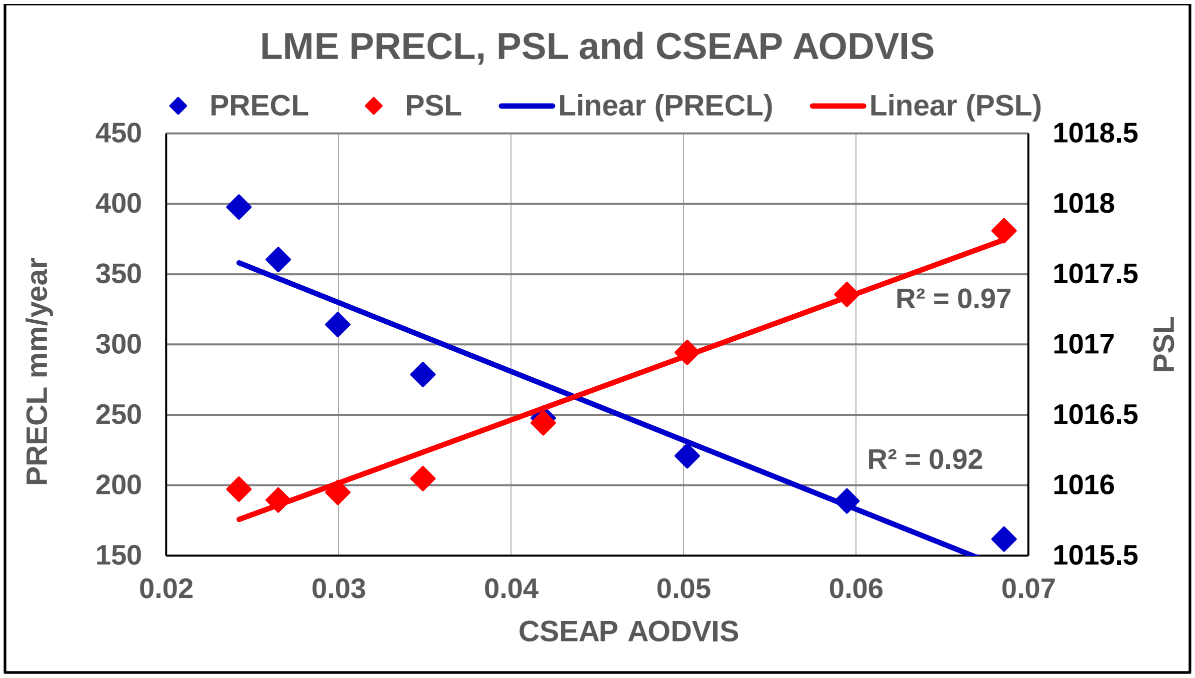

Figure 10: Segmented Annual LME AODVIS with SEAus Precipitation and SLP. Averaged using the 850 GHG, Land, Orbital, Solar and Volcanic runs.

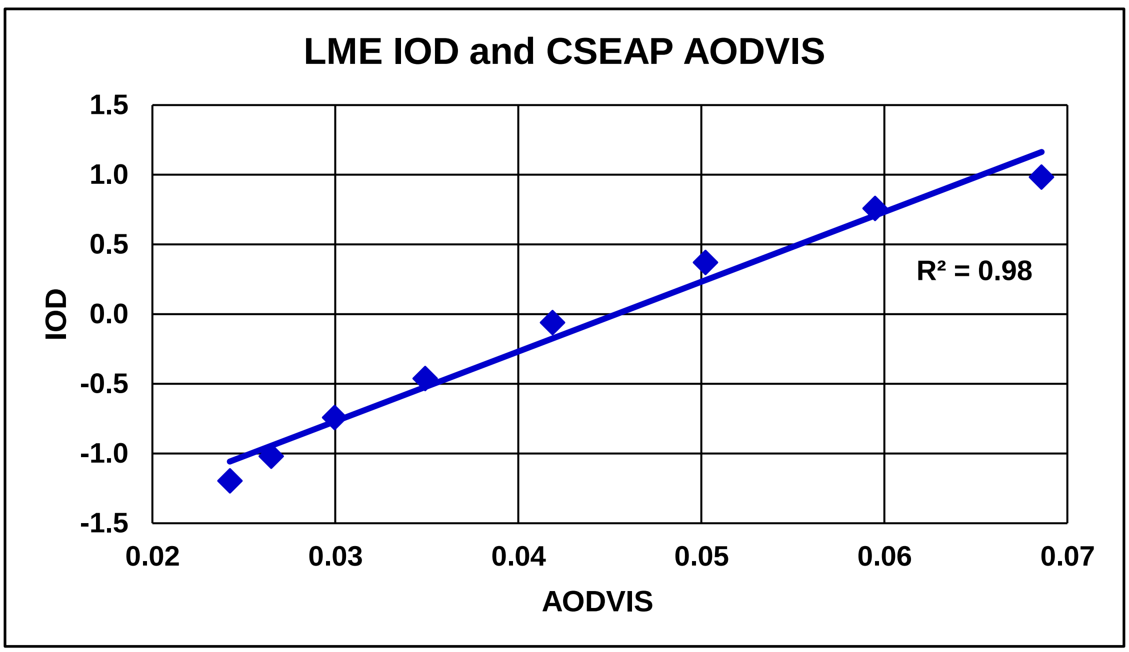

Figure 11: Segmented Annual LME AODVIS and the Indian Ocean Dipole. Averaged using the 850, GHG, Land, Orbital Solar and Volcanic runs.

3.1.2 Large Ensemble

The LE data was analysed in the same way as the LME data for the historic data from 1850 to 2005 and the RCP 8.5 data from 2006 to 2100 separately and the results were then averaged and are shown in Figure 12.

AODVIS	Omega (609mb)	SST Nino 3.4 TS	SOI	IOD	Pressure SEAus	Rainfall SEAus
Monthly (Segmented)						
CSEAP Area	0.96	0.90	-0.86	0.85	0.96	-0.76
SEAP Area	0.83	0.93	-0.95	0.91	0.82	-0.89
September to November Averages						
CSEAP Area	0.90	0.78	-0.73	0.78	0.41	-0.75
SEAP Area	0.85	0.63	-0.72	0.80	0.42	-0.66
April to October Averages						
CSEAP Area	0.91	0.88	-0.84	0.81	0.71	-0.78
SEAP Area	0.83	0.76	-0.76	0.87	0.73	-0.70
Annual Averages						
CSEAP Area	0.92	0.92	-0.82	0.84	0.70	-0.74
SEAP Area	0.91	0.86	-0.77	0.87	0.78	-0.73
Annual Average – Segmented						
CSEAP Area	0.98	0.99	-0.97	0.96	0.97	-0.96
SEAP Area	0.98	0.99	-0.97	0.99	0.98	-0.96

Figure 12 LE average correlations of AODVIS in the CSEAP and SEAP Areas with the parameters shown.

3.1.3 MERRA-2

The NASA MERRA-2 reanalysis is an atmospheric reanalysis of the modern satellite era produced by NASA’s Global Modelling and Assimilation Office. MERRA-2 is especially useful for the analysis in this paper as it includes the assimilation of aerosol observations and extended for 39 years in 2019. The aerosol loading in the CSEAP area is highly variable with significant spikes at near random intervals making it especially useful in correlation analysis. Results from the analysis of the MERRA-2 data are shown in Figure 13 (right hand column) where all the data is derived from the MERRA-2 dataset. These results support the LME and LE analysis. The areas used for the MERRA-2 analysis SLP and rainfall analysis are longitude 140° 149°E and latitude 36° 39°S.

Graphs of the MERRA-2 SON AOD, precipitation in SEAus, the IOD and SLP in SEAus are at Figures 14 and 15 which show a fall in precipitation of 39% from the segment with lowest AOD to the highest whilst the IOD rises from -0.38 to 0.74 across the same segments.

A	**Sept Oct Nov – Correlations**							
		AOD Terra 2000-18	AI Nimbus 7 1979-1992	AI E Probe 1996-2001	AI OMI 2004 - 18	AI N7 + EP 1979...2001	AI N7+EP+OMI 1979…2018	MERRA-2 MERRA-2 1980-2018
1	**MERRA Rainfall**	**-0.66**	**-0.41**	**-0.45**	**-0.23**	**-0.24**	**-0.17**	**-0.52**
2	**MSL Pressure**	**0.69**	**0.26**	**0.69**	**0.46**	**0.49**	**0.47**	**0.42**
3	**SST SEAP Area**	**-0.66**	**-0.68**	**-0.85**	**-0.20**	**-0.41**	**0.11**	**-0.54**
4	**CSEAP Omega**	**0.91**	**0.57**	**0.96**	**0.62**	**0.56**	**0.31**	**0.79**
5	**IOD**	**0.57**	**0.62**	**0.95**	**0.30**	**0.79**	**0.63**	**0.62**
6	**Nino 3.4 SST**	**0.77**	**0.56**	**0.91**	**0.65**	**0.61**	**0.34**	**0.73**
7	**SOI**	**-0.75**	**-0.64**	**-0.85**	**-0.69**	**-0.45**	**-0.13**	**-0.73**

B	**Sept Oct Nov - Detrended (PAST 3) Correlations**							
		AOD Terra 2000-18	**AI Nimbus 7** 1979-1992	**AI E Probe** 1996-2001	**AI OMI** 2004 - 18	**AI N7 + EP** 1979...2001	**AI N7+EP+OMI** 1979…2018	MERRA-2 MERRA-2 1980-2018
1	**MERRA Rainfall**	**-0.66**	**-0.69**	**-0.46**	**-0.29**	**-0.37**	**-0.39**	**-0.52**
2	**MSL Pressure**	**0.70**	**0.42**	**0.67**	**0.48**	**0.54**	**0.51**	**0.45**
3	**SST SEAP Area**	**-0.67**	**-0.83**	**-0.83**	**-0.33**	**-0.75**	**-0.65**	**-0.58**
4	**CSEAP Omega**	**0.92**	**0.79**	**0.98**	**0.68**	**0.74**	**0.71**	**0.78**
5	**IOD**	**0.58**	**0.69**	**0.92**	**0.25**	**0.83**	**0.66**	**0.67**
6	**Nino 3.4 SST**	**0.77**	**0.67**	**0.92**	**0.61**	**0.73**	**0.63**	**0.75**
7	**SOI**	**-0.74**	**-0.76**	**-0.87**	**-0.65**	**-0.65**	**-0.60**	**-0.73**

Figure 13: Correlations of time series (A) and detrended (using PAST 3) time series (B) AI and AOD over the CSEAP Area with characteristics of Australian drought, CSEAP Area Omega and the IOD in SON. In the MERRA-2 MERRA-2 column only data from the MERRA-2 reanalysis is used using the same areas as is used in all the other columns.

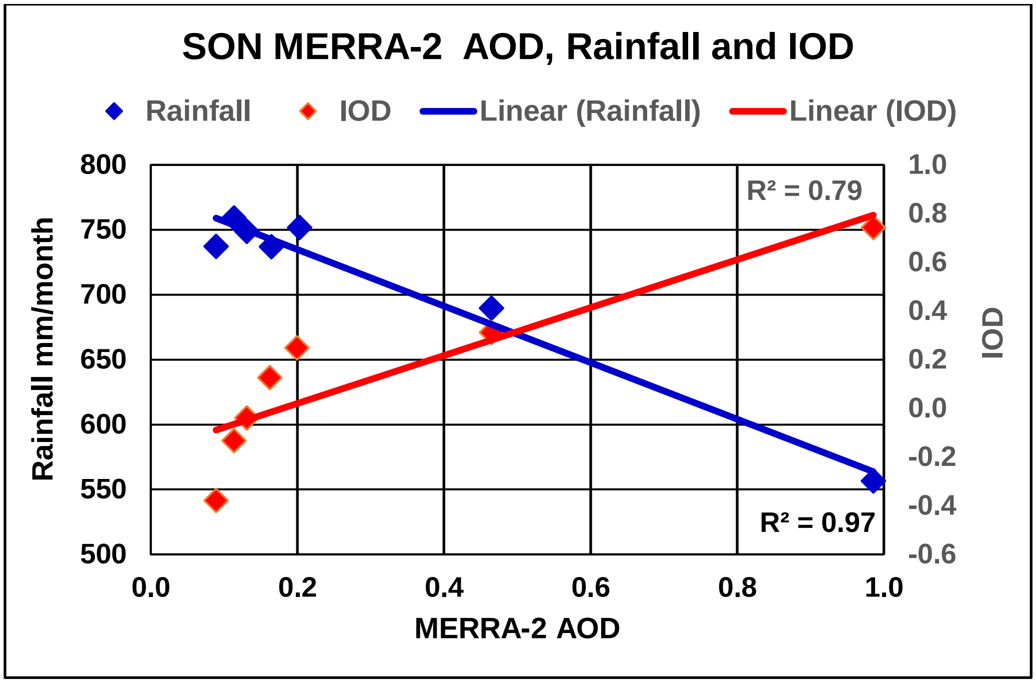

Figure 14: SON MERRA-2 AOD CSEAP Area, Rainfall SEAus and the IOD segmented and averaged

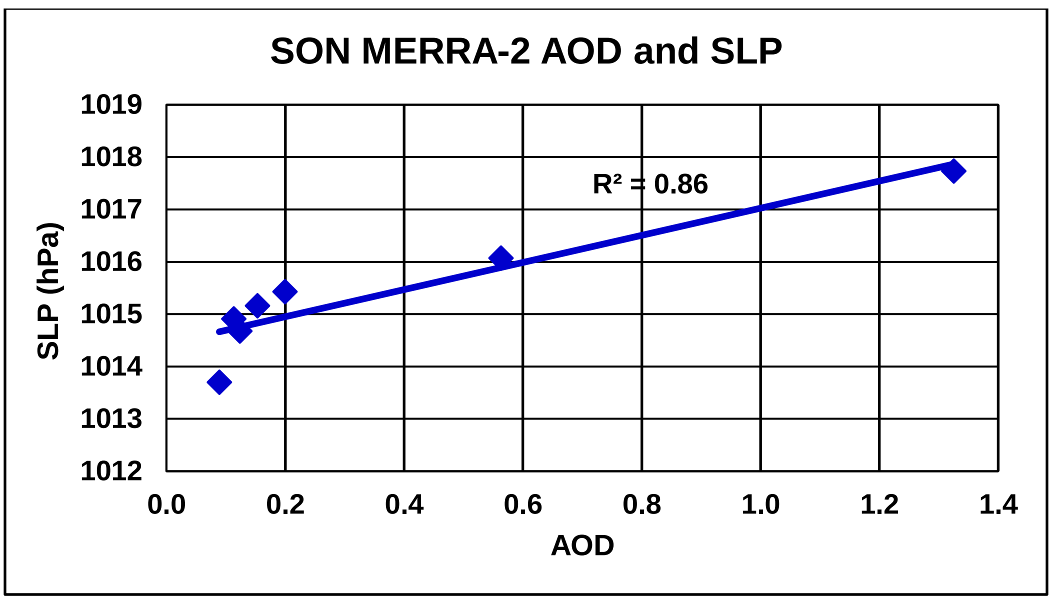

Figure 15: SON MERRA-2 AOD CSEAP Area and SLP segmented and averaged

3.2 Satellite Data

As shown in Figure 7 the CSEAP AI data contains a significant trend and therefore the SON AI, AOD and other data was detrended using PAST 3 [*Hammer et al.*, 2001] and then correlated both as a times series and a detrended time series. The results are shown in Figures 13(A) and (B) which show statistically significant correlations with all seven (AOD) and six of seven (N7 AI) detrended parameters respectively. The EP and OMI AI data are shown correlated alone and the EP data with the N7 data and the OMI data with both the N7 and EP data. Due to the short duration of the EP data, the extreme 1997 biomass burning event in Indonesia and the very unusual 1997 biomass burning event in north western Australia the EP data should be interpreted with caution. However, it is considered to support the N7, OMI and AOD correlations. The EP data was detrended with PAST 3 by detrending the data without the extreme 1997 data and then reinserting the 1997 data as detrending with the 1997 data introduces a different, significant trend.

The lower correlation coefficients for the N7 AI time series data cf. the Terra AOD data are suggested to relate to the much lower AI level in the SEAP Area in the early years of the data when the effects of the plume would have been much smaller and to the effects of the significant trend in the AI data which is demonstrated by the higher correlation coefficients of the detrended data.

The OMI AI data shows lower correlation magnitudes than the AOD data with reduced significance caused at least partially by the shorter duration of this data. The detrended OMI AI and Terra AOD data correlate at 0.85 and the significance of the OMI data is therefore expected to increase as its duration increases.

The detrended time series of the AI and AOD of the CSEAP Area with SEAus rainfall and pressure are shown in Figures 16 and 17. The AI and AOD are shown on the same scale in these graphs to minimise the number of graphs although the AI and AOD measure different aspects of the aerosol plume.

Segmenting the Terra AOD and rainfall data in the same way as the MERRA-2 data shows a decline in rainfall in SON of 47% from the segment with the lowest AOD to the highest.

Note: The AI derived from OMI is significantly higher than that derived from the N7 and EP satellites at about 0.8 base level compared with 0.2 (EP) and 0.1 (N7). This disparity is not seen in data from the aerosol plumes over the Amazon and West Africa. It may be due to several causes including instrumentation differences, aerosol height, the actual increase in aerosol loading over time, volcanic aerosols in the SEAP which are not present in the other areas and the non-volcanic aerosol types present. The OMI data is therefore useful as an independent dataset and detrended in combination with the detrended N7 and EP data. In Figure 13A the combined N7, EP and OMI data has been retained for completeness but should be viewed with caution due to the discontinuity discussed above.

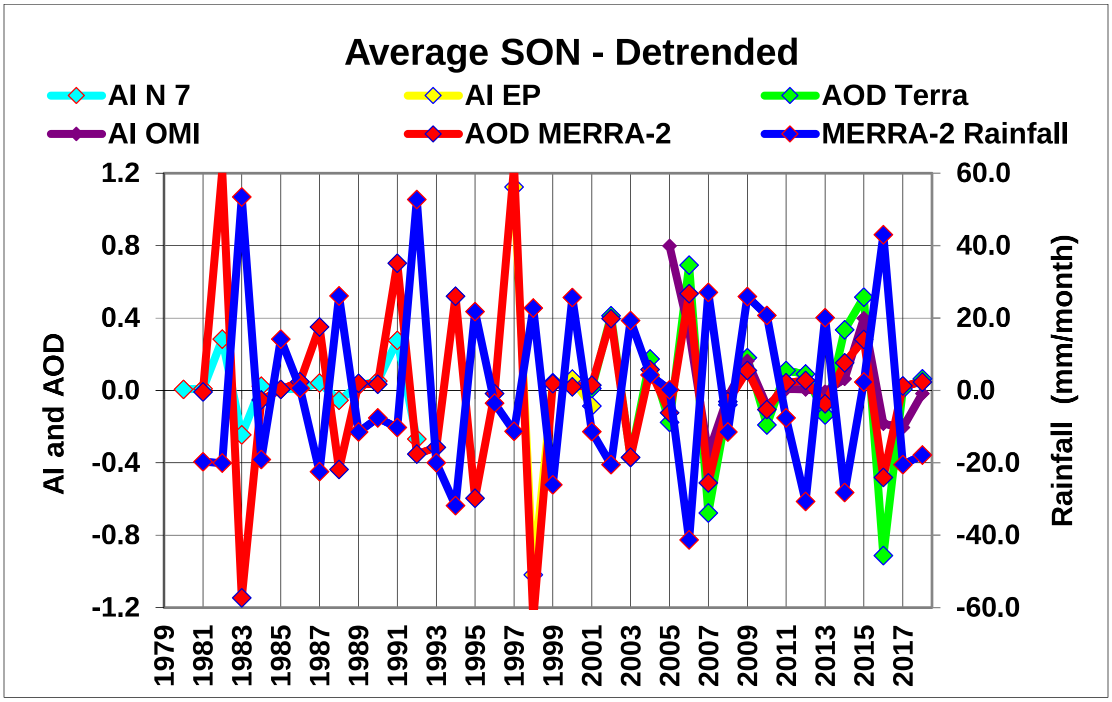

Figure 16: Average SON AI and AOD CSEAP Area and Rainfall south eastern Australia (from NASA MERRA converted to mm/month.) PAST 3 detrended

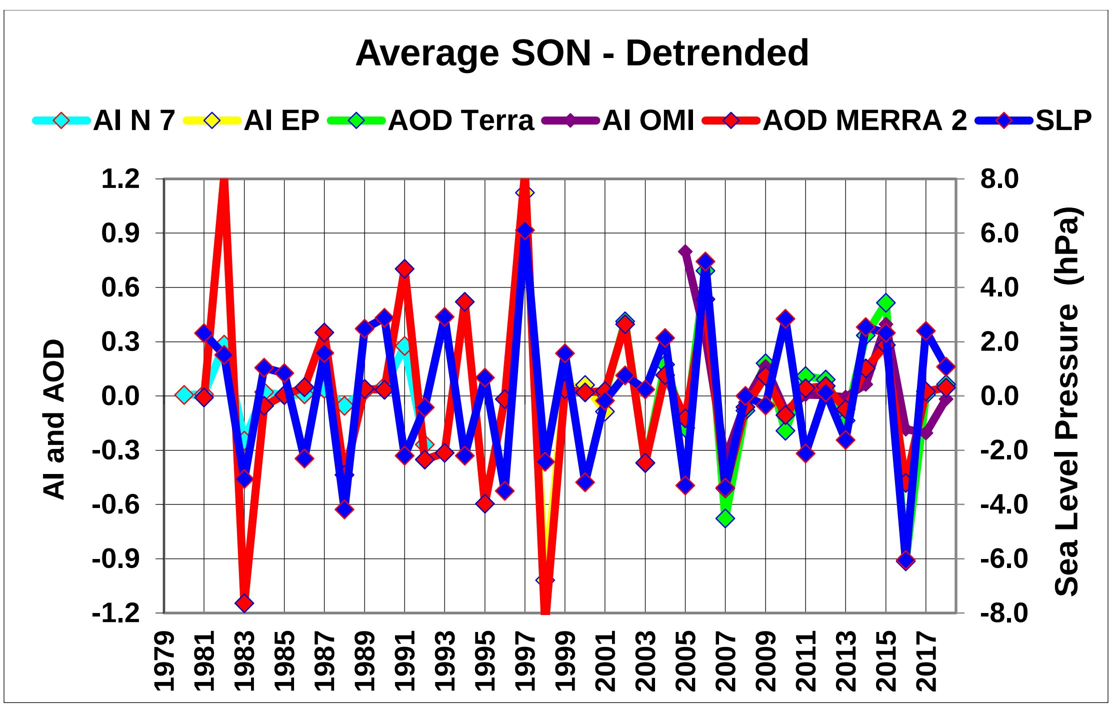

Figure 17: Average SON AOD and AI CSEAP Area and MERRA-2 SLP south eastern Australia PAST 3 detrended.

3.3 Global Volcanism Program Data

The SEAP Area VEIT data was processed into monthly totals as shown in Appendix A, then smoothed with a 12-month running average before segmenting and averaging which is expected to improve the signal to noise level in the data as both the VEI(T) and Murray River data have caveats on accuracy.

Figure 18 shows the correlations of the segmented and averaged SEAP Area VEIT with rainfall, pressure, inflows into the River Murray and CSEAP Area omega and demonstrates statistically significant correlations exists. The three locations, Adelaide, Melbourne and Echuca, are spread across the area used in the analysis of the satellite data from north to south and east to west to demonstrate the spread of reduced rainfall across SEAus using measured rainfall data.

It is worth noting here that the SEAP Area covers 70º of longitude, 19% of the Earth's circumference, and the effect of volcanic tephra ejected in the eastern part of the SEAP Area on SEAus may be different to volcanic tephra ejected in the central or western part.

The plots of the segmented and averaged data are shown in Figure 19 (RWRD rainfall) and Figure 20 (Murray River inflows). It is worth noting that from the lowest VEIT at 0.000167Km^3 to the fourth segment with VEIT at 0.0011 Km^3 the inflows into the River Murray declined by 15% to 820 Gl/month and with VEIT at 0.017, the highest, by 63% to 360 Gl/month.

Index	Correlation (Monthly)	Period
RWRD Rainfall (BOM)	**-0.99**	1890 – 2016
Adelaide Rainfall (BOM)	**-0.89**	1870 - 2018
Melbourne Rainfall (BOM)	**-0.91**	1890 - 2018
Echuca Rainfall (BOM)	**-0.97**	1890 - 2018
Murray River Inflow (MDBA)	**-0.98**	1892 – 2015
SLP Melbourne	**0.96**	1903 - 2008
SLP Echuca	**0.84**	1908 - 2008
CSEAP Area Omega (NCEP/NCAR)	**0.98**	1948 – 2018

Figure 18: Correlations of segmented and averaged SEAP Area VEIT with parameters shown for the periods shown. All annual data except for SLP which is April to October average.

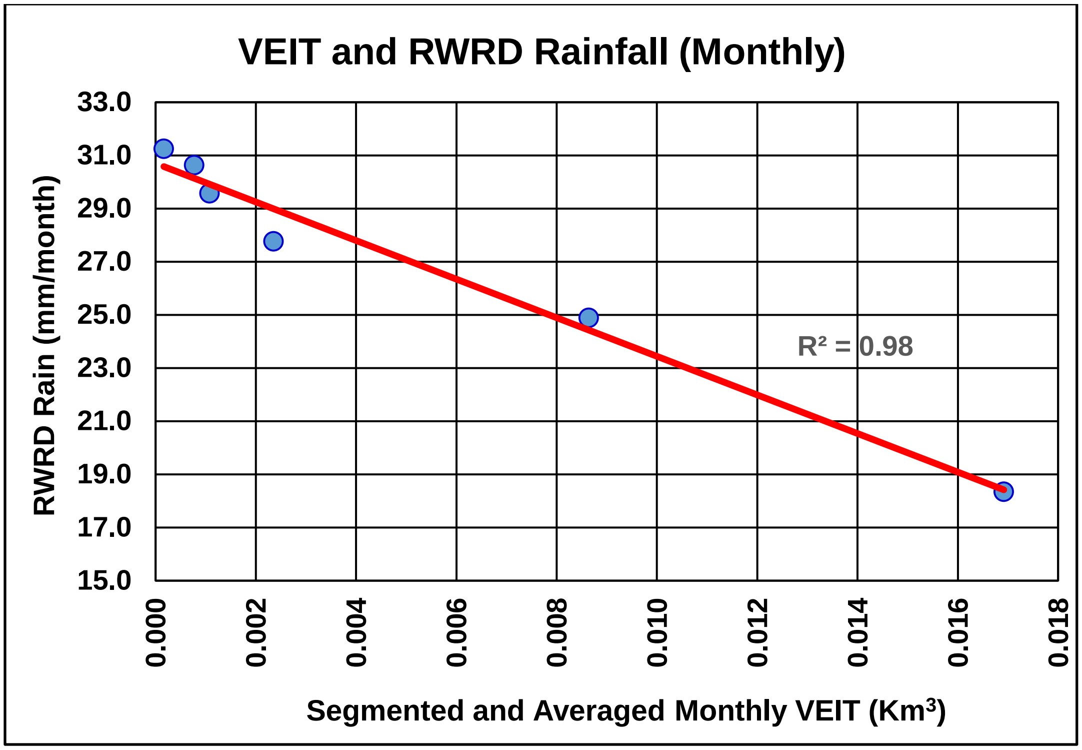

Figure 19: Monthly RWRD Rainfall and SEAP Area VEIT 1890 to 2016 data segmented and averaged.

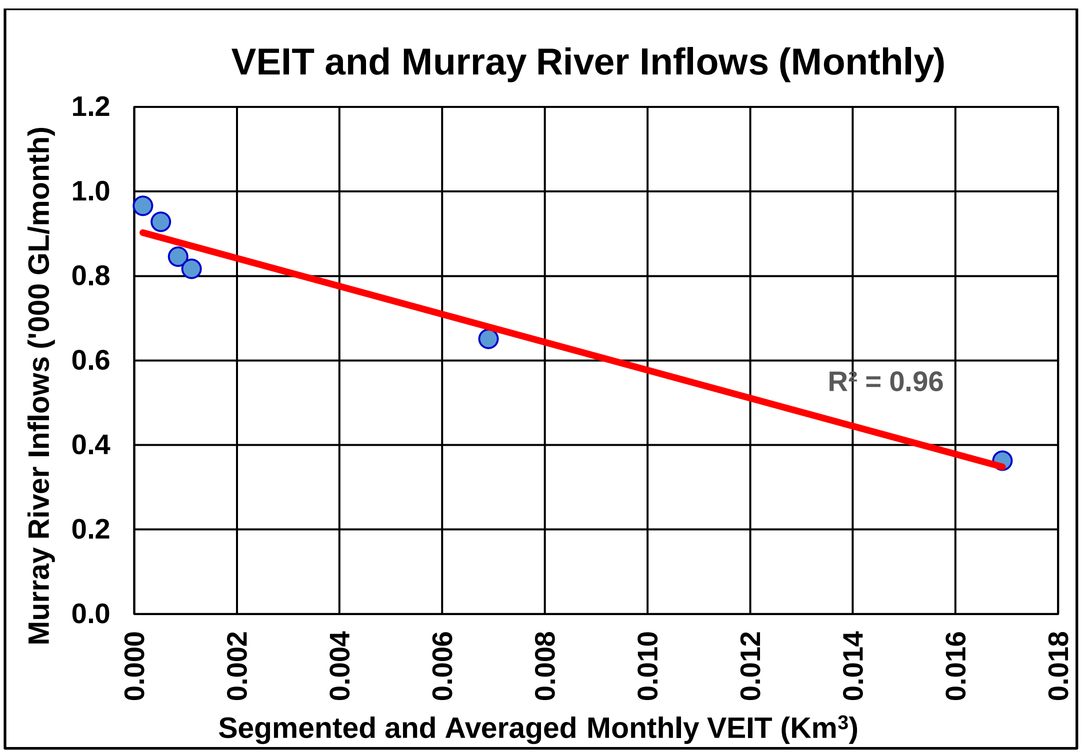

Figure 20: Annual Murray River Inflows and VEIT from the SEAP Area. 1892 to 2015 data segmented and averaged.

3.4 Convection in the CSEAP Area

Radical changes in convection occur in the CSEAP Area when the SEAP exists and the detrended AOD and AI of this area was correlated with the detrended NCEP/NCAR reanalysis omega at the 400hPa level in the same area. Omega is a measure of vertical velocity in the atmosphere at specific pressure levels. Positive values indicate falling motion and negative values rising and a reduction in convection produces a positive change in omega. The correlations of the detrended data are shown in Figure 13 (B) (4) at 0.68 or greater magnitude showing that when an aerosol plume is present over the CSEAP area convection decreases. The segmented and averaged VEIT data was also correlated with the CSEAP Area omega. Figure 18 shows the statistically significant correlation. Graphs of the data are in the companion paper [*K.A. Potts*, 2020b].

4 MECHANISMS – FOLLOWING THE HYPOTHESIS

Timbal et al. [2010] state that “Many of the influences of the climate indices on SEA (South Eastern Australia) come about through modulations of the atmospheric circulation”. This section explains how ARD caused by apparitions of the SEAP drives these modulations of rainfall and SLP in SEAus and the IOD via the effects outlined in the hypothesis and physical model. ENSO is addressed in the companion paper [*K.A. Potts*, 2020b].

The extreme interannual variation in the AOD of the SEAP is used to show the changes wrought by the SEAP using the NCEP/NCAR reanalysis and MERRA-2 data by subtracting the SON data in 2016, low AOD, from 2015, high AOD (as shown in Figures 5 and 7), which shows the effect of the 2015 apparition of the SEAP.

4.1 The SEAP Forms

In recent decades the AOD of the SEAP Area has increased as Figures 5 and 7 and Appendix A show due to increases in both the natural and anthropogenic plumes. In SON the anthropogenic SEAP has increased significantly in some years as Figure 7 also shows. Figure 21 shows the extreme change in the SEAP in SON between 2015 to 2016. The actual extent of the 2015 apparition of the SEAP is similar to the 2006 apparition shown in Figure 6.

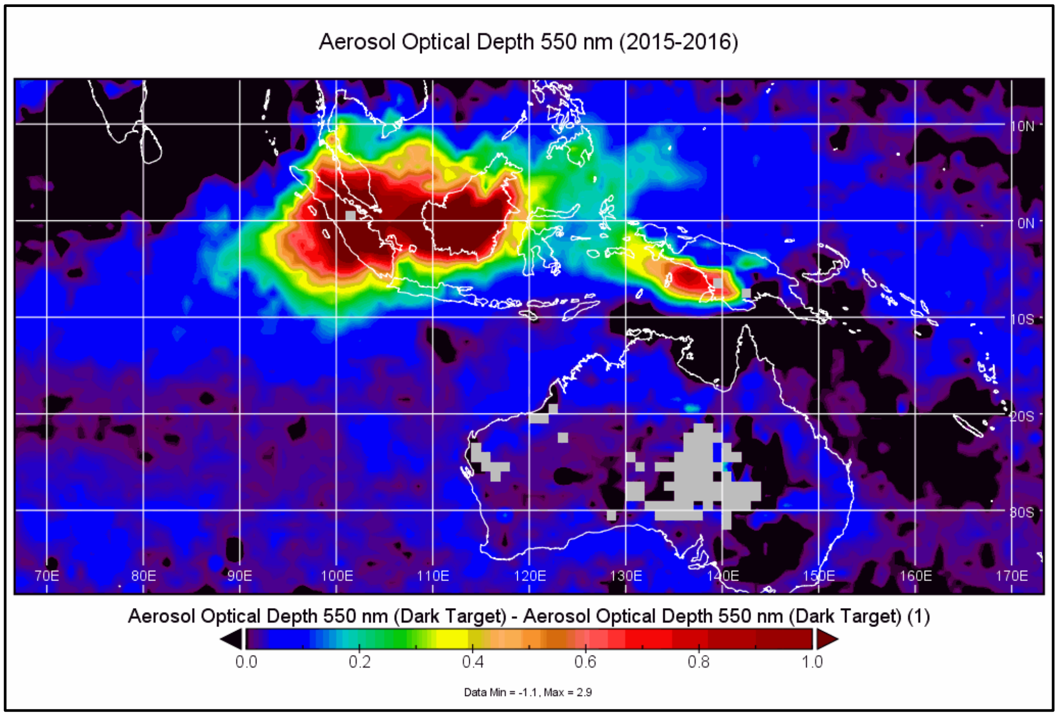

Figure 21: Terra AOD SON 2015-2016 (NASA Panoply)

4.2 The SEAP absorbs solar radiation and heats the atmosphere

Figure 22 shows the MERRA-2 air temperature averaged across the CSEAP Area longitudes from 30°S to 30°N and it can be clearly seen that in the high AOD year the air temperature within the plume at 400hPa and 650hPa is higher which correlates with estimated aerosol height from the Calipso data reasonably well.

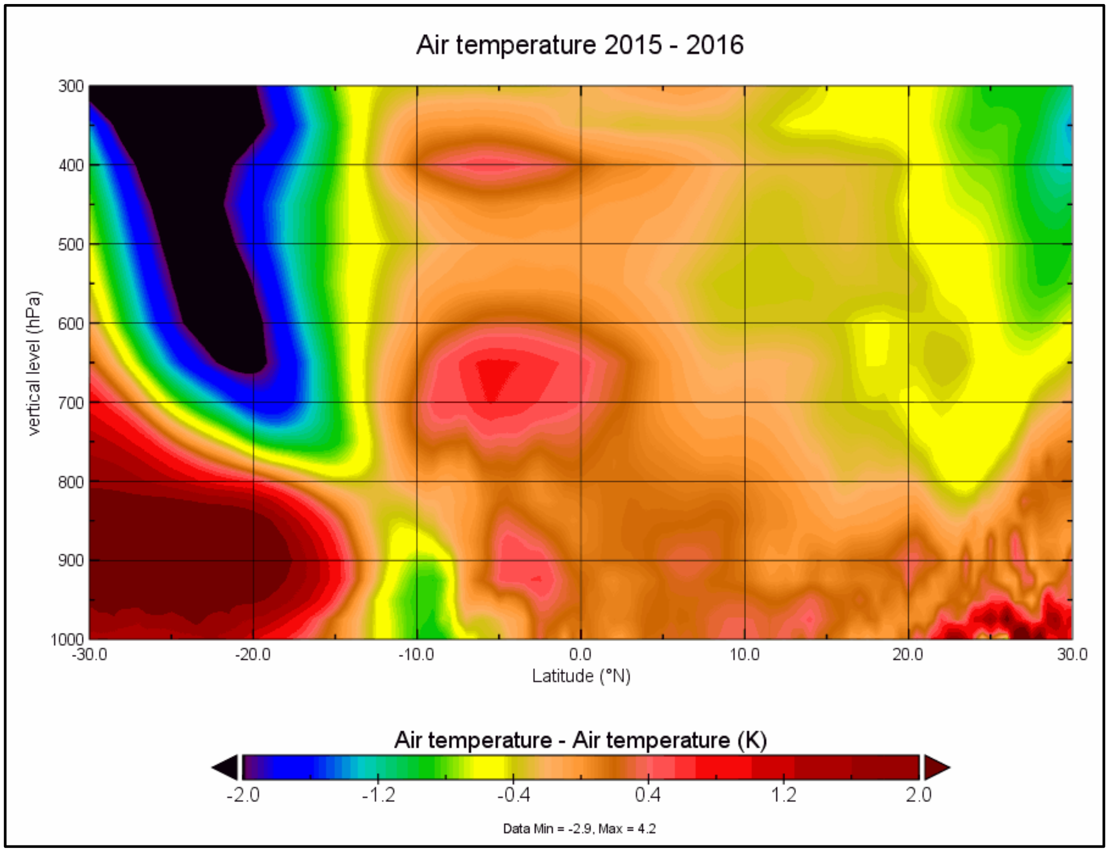

Figure 22: MERRA-2 SON Air Temperature averaged across the CSEAP Longitudes 2015-2016

4.3 The SEAP reduces surface solar radiation which cools the surface

The NCEP/NCAR reanalysis dataset SON SST in Figure 23 with 2016 subtracted from 2015 shows nearly all the SEAP Area sea surface is cooler except the extreme north and west.

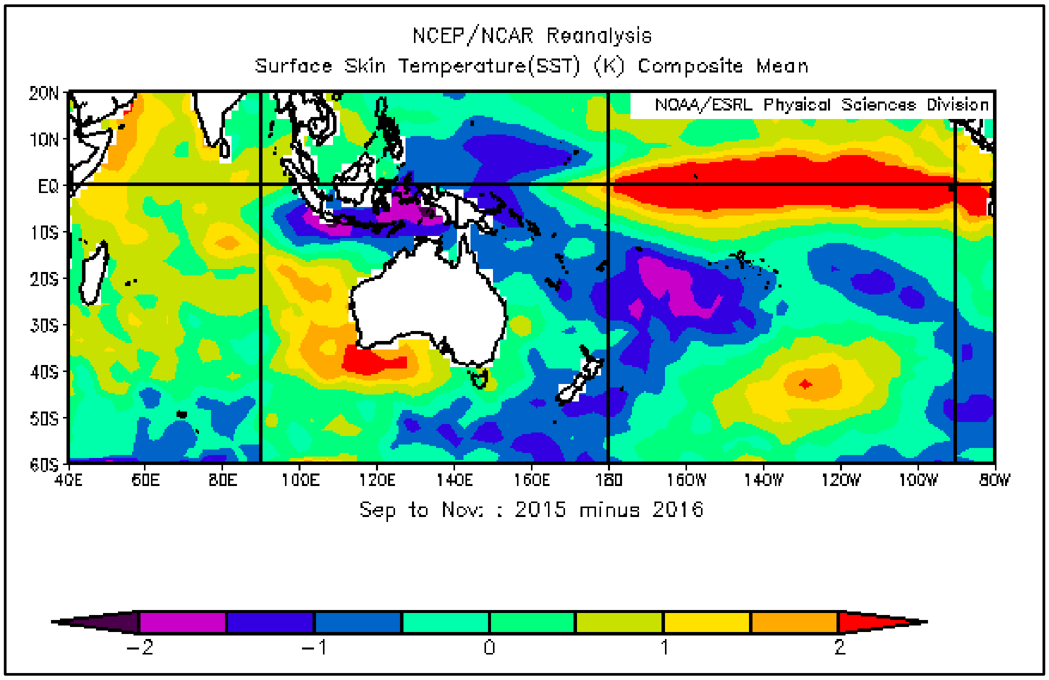

Figure 23: NCEP/NCAR SST 2015-2016

4.4 Convection in the SEAP Area:

The effects of aerosols on convection and atmospheric circulation have been extensively described in the literature as discussed in the introduction. The SEAP absorbs solar radiation which warms the upper atmosphere and reduces solar radiation at the surface which cools the lower atmosphere. This alters the vertical temperature profile of the atmosphere with warmer air above cooler air (relative to the temperatures without the plume) and this stabilises the atmosphere and reduces convection. This well understood process is confirmed in the SEAP Area in this paper with the demonstrated correlation of omega with the AOD, AI and ejected volcanic ash in the area and in Figures 13, 18 and 24 where again nearly all the SEAP Area is affected except the extreme north and west.

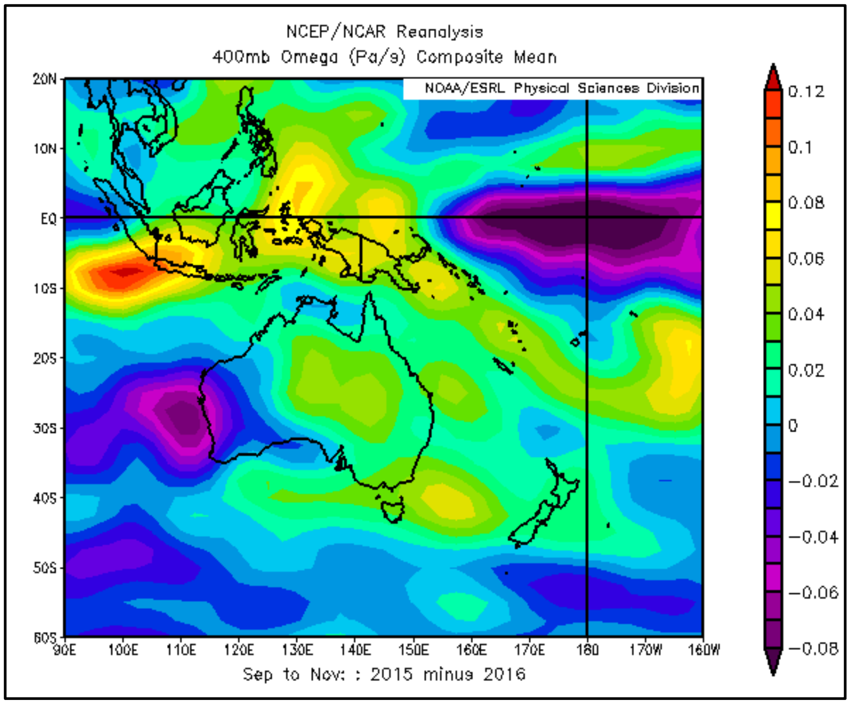

Figure 24: NCEP/NCAR convection at the 400 mb level 2015-2016

4.5 Hadley Cells:

The Hadley Cells are thermally driven [*G R McGregor and Nieuwolf*, 1977], [*Barry and Chorley*, 2010] and [*IPCC*, 2007]. Reduced convection in the SEAP Area alters the regional Hadley Cells and this can be clearly seen in Figure 25 where the rising limb of the southern Hadley Cell has been altered in the year of high AI or AOD in the SEAP Area relative to the low AI or AOD years and the region driving the greatest convection is between 20° and 30° south.

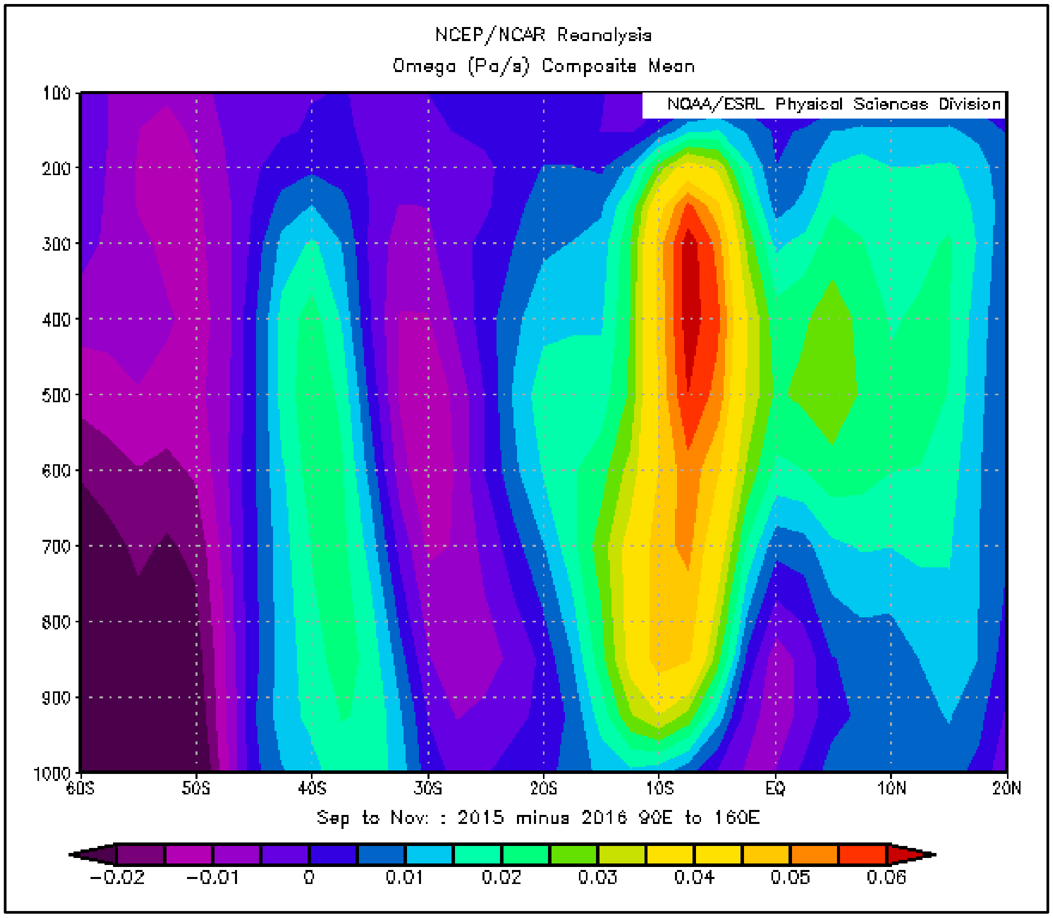

Figure 25: NCEP/NCAR omega averaged across the SEAP Area longitudes 2015-2016

4.6 High Pressure over SE Australia

The perturbation of the "Southern Hadley Cell" shown in Figure 25 creates falling motion and therefore anomalous high pressure over SEAus as Figure 26 shows.

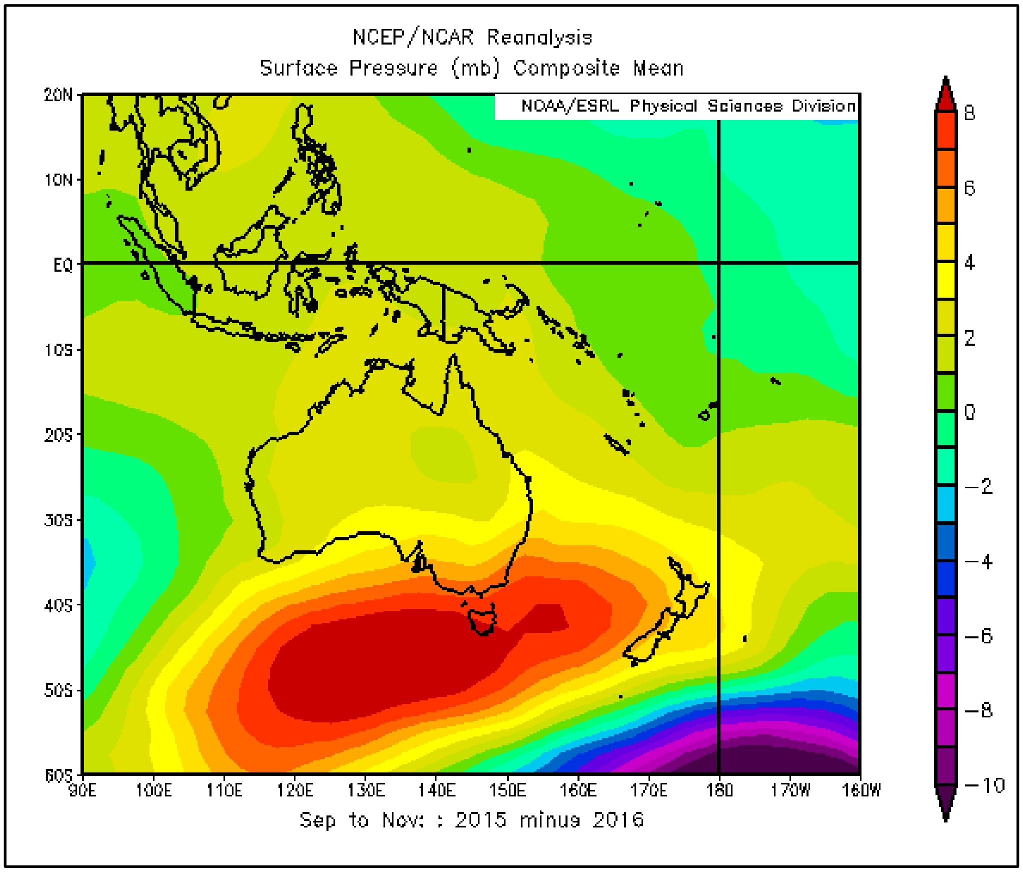

Figure 26: NCEP/NCAR Surface Pressure 2016 -2015.

4.7 Rainfall in SE Australia

Rainfall reduces in SEAus when ARD occurs in the SEAP Area because: The SEAP reduces the SST in the SEAP Area and this reduces evaporation in an area which is a major source of precipitation for SEAus; and the SEAP also forces the perturbation of the "Southern Hadley Cell" which creates a persistent high pressure system over SEAus which then forces the low pressure systems and cold fronts to the south resulting in fewer rain events and, as each rain event deposits less rain due to the lower humidity, drought ensues as Figure 27 shows. Note the band of reduced rainfall extends from SEAus to the NNW and points directly at the CSEAP Area, the southern part of which is also experiencing a significant reduction in rainfall.

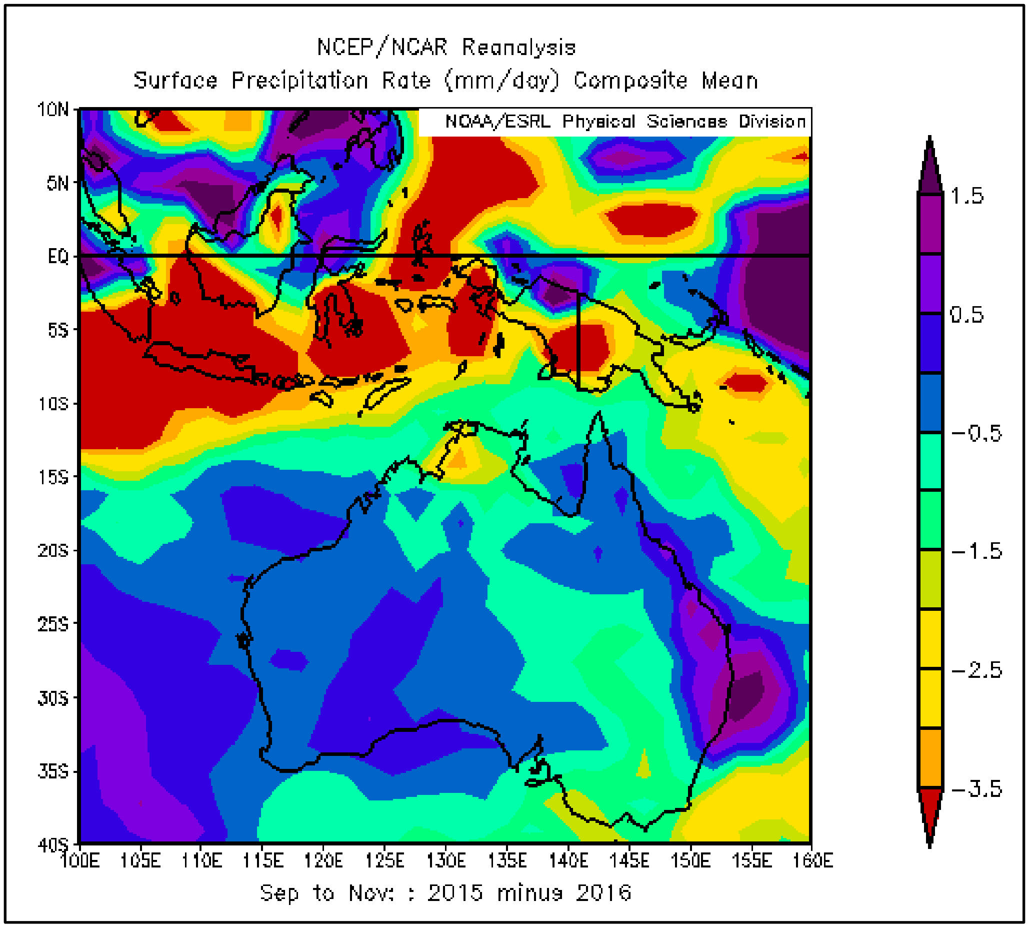

Figure 27: NCEP/NCAR Reanalysis surface precipitation 2015-2016.

4.8 The IOD

In Figure 23 the SST (2015-2016) is cooler in the eastern IOD Area, as it is shaded by the SEAP, and warmer in the western IOD Area as the surface wind speed reduces which drives the IOD into a positive phase when the AOD in the SEAP Area is high.

5 CAUSATION ANALYSIS

It is clearly understood that correlation between events A and B does not prove causation from A to B or vice versa. Thus, the causal relationship between the SEAP and the ENSO must be demonstrated in other ways.

5.1 Volcanic Eruptions

Volcanic eruptions are caused by deep earth tectonic processes and cannot be caused by rainfall or SLP thirty degrees of latitude away. Therefore, given the clear correlation between volcanic tephra, rainfall and SLP demonstrated in this paper the causal relationship must be from the volcanic tephra to the rainfall and SLP.

5.2 Analysis without Correlation

Figure 10 shows that the LME annual precipitation in SEAus falls from 398mm to 162 mm a fall of 59% from the segment with the lowest AODVIS to the one with the highest and this is comparable to the fall in the measured annual RWRD rainfall in 2006 from 2005 of -56% without using correlation.

5.3 ENSO and the IOD

This paper and its companion [*K.A. Potts*, 2020b] show that the SEAP is simultaneously the cause of drought in SEAus, and the IOD and ENSO events which have historically been cited as the cause of drought in SEAus. The IOD and ENSO are therefore not the drivers of drought in SEAus.

5.4 Modelling

LME: there is no physical mechanism by which drought or SLP in SEAus can create aerosols in the LME over south east Asia hence the causal direction must run from the aerosols to the rainfall and SLP.

In addition, the aerosol forcings in all LME runs are fixed at 1850 values except for the “ozone and aerosol” and “all” runs and there can therefore be no forcing of the aerosols by any agent within these six runs and the causal direction must flow from the aerosols to the rainfall and SLP.

LE: Aerosols are included as forcing agents in the LE and rainfall and SLP in SEAus cannot therefore affect the aerosols over SEAsia and the causal direction must run from the aerosols to rainfall and SLP.

MERRA-2 reanalysis assimilates measured aerosol data and therefore the causal direction must be from the aerosols to the rainfall and SLP.

5.5 Multiple Independent Datasets

Seven of eight LME modelling runs (excluding the aerosol forced run as it correlates with the All forcing run) and the MERRA-2 reanalysis exhibit very low or negative correlations between the CSEAP AODVIS in the individual runs as shown in the correlation matrix in Appendix C with an overall average 0.0016. Hence the datasets are independent. The LE is excluded as it correlates with the LME ALL forcing run.

All the datasets show correlations with the rainfall and SLP at significance of <0.01 or less and the chance that all these eight independent datasets show the same result and are wrong is the product of the significance i.e. 0.01^{-8} or 10.0^{-16}, a vanishingly small number.

5.6 Companion Paper

The companion paper [*K.A. Potts*, 2020b] demonstrates that ENSO events which have commonly been linked to drought in south eastern Australia are also caused by the SEAP and this further confirms that the causal relationship flows from the SEAP to all these events.

5.7 Segmented Data

The climate is a chaotic system and my preferred way to analyse climate data is to segment, average the data as the averaging process will improve the signal to noise ratio of the analysis. When the LME CSEAP annual AODVIS and rainfall and SLP data in SEAus is segmented on the basis of the AODVIS data and then averaged and correlated R^2 values of 0.92 and 0.97 (Figure 10) are found. This demonstrates clearly that the SEAP is the major and possibly the only driver of reduced rainfall and increased SLP in SEAus.

The difference between the lowest LME CSEAP Area AODVIS segment and the highest shows a reduction in annual precipitation in SEAus of 236mm or 59% in Figure 10 with an obvious, well-established trend. Similarly, the same Figure shows and increase in SLP of 1.8 hPa also with a well-established trend. This analysis does not depend on correlation.

5.8 Causal Direction

Therefore with:

3. The volcanic aerosols demonstrating conclusively that SEAP Area aerosols must be the cause of reduced rainfall and increased SLP in SEAus;
4. The segmented LME data showing a reduction in rainfall in SEAus as the AODVIS level of the SEAP rises without using correlation;
5. The LME and MERRA-2 time series analysis showing the same results across multiple independent datasets with a vanishingly small chance of error;
6. The LME data showing, by a preferred analysis method, extremely high correlations of AODVIS, PRECL and PSL (R^2 = 0.92 and 0.97) which leave no possibility of other significant drivers;

7. The demonstration that IOD and ENSO (in the companion paper) events which are commonly cited as the cause of drought in SEAus are also caused by the SEAP;
8. The support of four satellite datasets showing the same results;

The inevitable conclusion is that the hypothesis is proven and the SEAP is the primary driver of reduced rainfall and increased SLP in SEAus and may even be the sole driver.

6 THE CAUSE OF THE MILLENNIUM DROUGHT IN SOUTH EASTERN AUSTRALIA

This paper shows that volcanic and anthropogenic aerosol plumes in the SEAP Area are the primary cause of drought in SEAus and this allows the causes of the Millennium Drought to be determined.

6.1 Changes in the Natural SEAP

The level of tectonic activity in the SEAP Area during the Millennium Drought was at an extremely high level (Figure 28) with five of the twenty largest earthquakes (magnitude 8.4+) in the world between 1900 and 2015 occurring in the SEAP Area and four of them occurring between 2000 and 2015 (United States Geological Survey (USGS) database). In concert with this increased tectonic activity the volcanic activity in the SEAP Area also intensified significantly and Figure 29 shows that in the decade from 2000 to 2009 there were 79 eruptions and 0.50 km^3 of tephra ejected against averages of 40.9 and 0.17 km^3 per decade over the twentieth century an approximate doubling and trebling respectively.

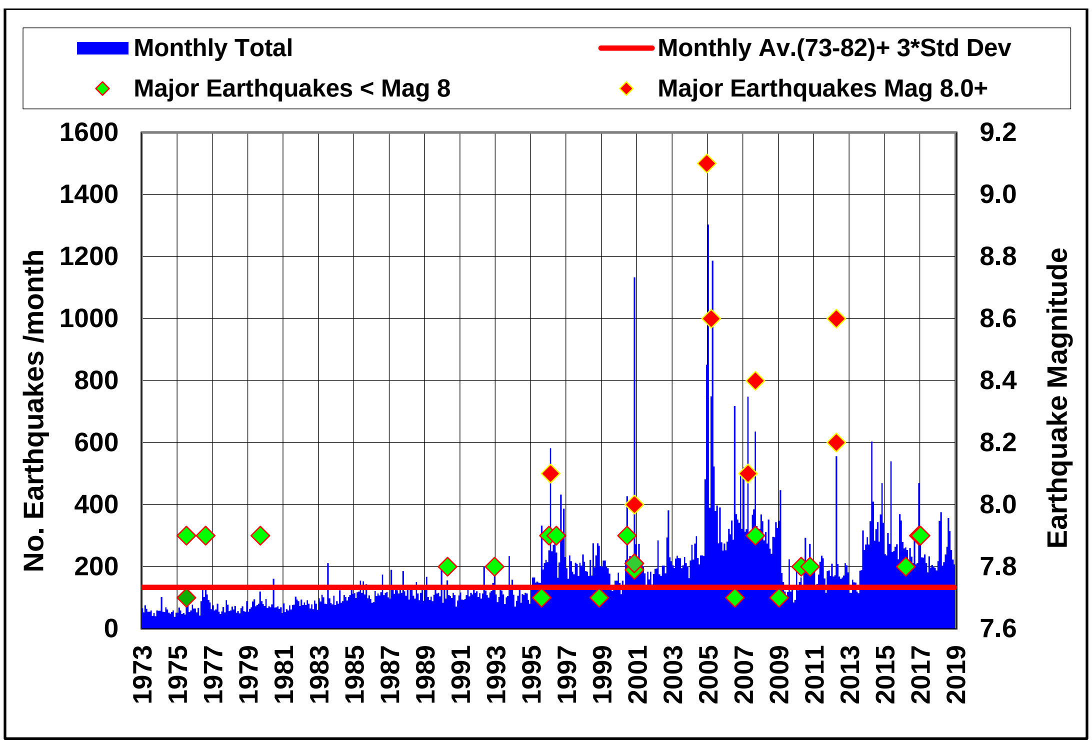

Figure 28: Total Monthly Earthquakes SEAP Area with major events Magnitude 7.7+ shown. USGS Earthquake database.

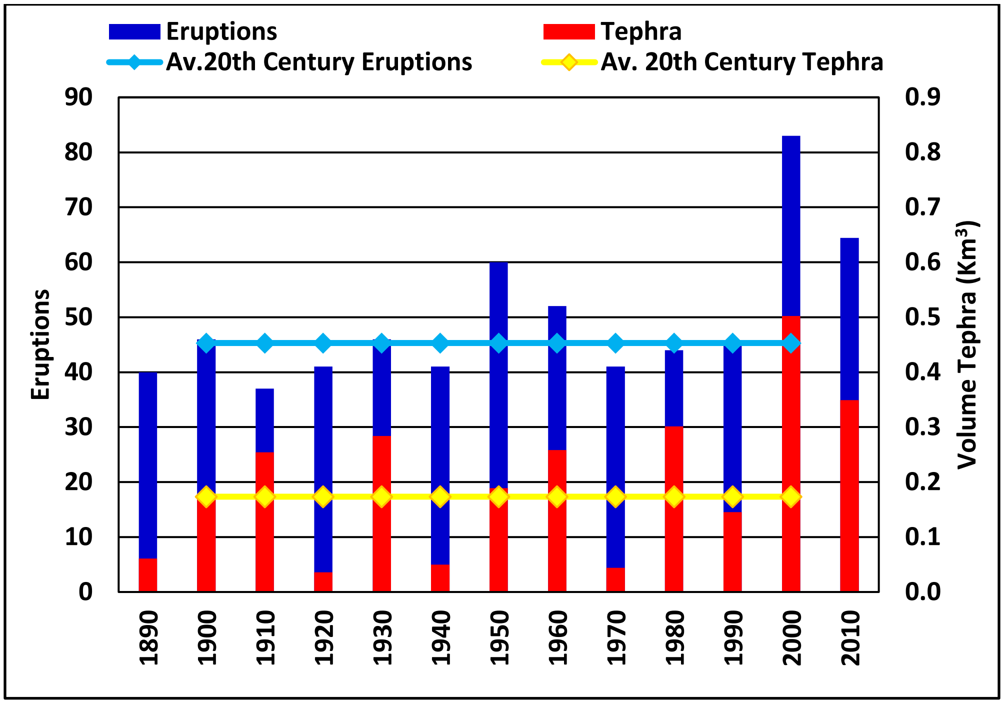

Figure 29: Decadal total and average volcanic eruptions and tephra volume in the SEAP Area from April to October. Averages from 1900 to 1999. The 2010 data has been increased pro rata to enable comparison with other decades.

6.2 Changes in the Anthropogenic SEAP

The background level of AOD in the SEAP Area was significantly higher during the Millennium Drought having increased by 679% in SON from 1979 to 2000 and it is worth noting here that this background level has not reduced in the last decade (Figures 5 and 7). There was also a large increase in the frequency and intensity of rainforest clearing events in the SEAP Area (seen as the AI and AOD peaks in 1997, 2002, 2004, 2006 and 2009 in Figures 5 and 7) with the associated increased extent and AOD of the carbonaceous aerosol plume in the SEAP Area in SON.

6.3 The Cause

In the segmented model data the correlations of the LME CSEAP AODVIS and precipitation and SLP data for SEAus in Figure 9 are -0.95 and 0.97 respectively (LE correlations -0.96 and 0.97) which give r^2 = 0.90 and 0.94 and conclusively shows that the SEAP is the prime cause of drought in SEAus.

During the Millennium Drought I have shown there was a significant increase in volcanic activity, background AOD levels and rainforest clearing in the SEAP Area which drove the AOD of the SEAP Area higher and which:

1. Cooled the sea surface under the plume resulting in lower evaporation in the region where the water which falls as rain in SEAus evaporates;

2. Perturbed the southern, regional Hadley Cell resulting in anomalous high pressure over SEAus; which
3. Forced cold fronts, which normally cross SEAus, to the south and away from the continent.

Therefore, large increase in the natural and anthropogenic SEAP during the years of the Millennium Drought was the cause of the Millennium Drought in SEAus.

7 FUTURE RESEARCH

To finally confirm the findings above I suggest that a further LME analysis is undertaken in which an aerosol plume is created in the model which ramps up from the naturally low level in January to reach the same AOD as the extreme SEAP of October 2006 or 2015 in February, continues at the same level to October and ramps down in November to the naturally low level in December. This plume to be applied in the model with random returns from 2 to 10 years to mimic the actual known return frequency of ENSO events with all other forcing agents held constant.

This modelling should be repeated with AOD levels reduced by perhaps 0.1 between runs to determine the level of AOD in the SEAP Area which is required to create the effects outlined in this paper.

This will confirm the analysis in this paper and conclusively demonstrate that reduced rainfall and increased SLP in SEAus and IOD and ENSO events are caused by the SEAP.

8 CONCLUSIONS

The LME with 1.156 annual and 13,872 monthly time series data points, the LE including the RCP 8.5 forcing to 2100, MERRA-2, measured aerosol datasets from four satellites and the GVP volcanic eruption data all confirm the direct connection between the SEAP and drought in SEAus in multiple independent ways and my analysis clearly shows that the relationship must be causal.

I therefore conclude that Aerosol Regional Dimming by apparitions of the SEAP is the prime trigger for and sustaining influence on drought in SEAus, ENSO and IOD events.

Applying this conclusion to the Millennium Drought, it is obvious that this unprecedented drought was caused by:

1. The increased level of tectonic activity, earthquakes and volcanic eruptions which led to a tripling of the volcanic tephra ejected in the SEAP Area;
2. The increase in background AOD in the SEAP Area; and
3. The increase in the intensity and frequency of the anthropogenic SEAP in SON

These conclusions demonstrate the importance of accurately modelling in climate analysis:

1. The natural volcanic tephra plumes from both small and large volcanic eruptions;
2. The other seven continental scale, anthropogenic, carbonaceous, aerosol plumes in Africa the Americas, the Middle East and Asia;

at adequate spatial and temporal resolutions.

Finally I concur with *Booth et al.* [2012] that emissions of carbonaceous aerosols are directly addressable by government policy actions and suggest that this is an urgent necessity to avoid future anthropogenic droughts in the Austral spring in south eastern Australia.

9 APPENDICES

9.1 Appendix A: The Three Major Sources of the SEAP and the Volcanic Data Processing Route

9.2 Appendix B: The LME and LE Processing Route

9.3 Appendix C: LME and MERRA-2 Aerosol Correlation Matrix

The appendices are included in the companion paper [*K.A. Potts*, 2020b].

ACKNOWLEDGEMENTS

I acknowledge:

NASA: Analyses and visualizations used in this paper were produced with the Giovanni online data system, developed and maintained by the NASA GES DISC; the mission scientists and Principal Investigators who provided the data used in this paper including the CALIPSO data; and Dr Robert Schmunk for the Panoply data viewer;

The CESM1(CAM5) Last Millennium Ensemble Community Project and supercomputing resources provided by NSF/CISL/Yellowstone;

The CESM Large Ensemble Community Project and supercomputing resources provided by NSF/CISL/Yellowstone;

Google Earth™ and the copyright holders noted on the image for the image of the Earth;

The Murray Darling Basin Authority, Australia for the Murray River inflow data;

The Climate and Global Dynamics Division of ESSL at NCAR for the SEAP SST and Omega data;

NOAA: Data and images provided by the NOAA/OAR/ESRL PSD, Boulder, Colorado, USA, from their Web site at http://www.esrl.noaa.gov/psd/ and the IOD at https://www.esrl.noaa.gov/psd/gcos_wgsp/Timeseries/DMI/

The United Nations Department of Economic and Social Affairs Population Division for the world population statistics;

The Australian Bureau of Meteorology for the Australian climate information and data at http://www.bom.gov.au

The U.S. Geological Survey for the earthquake and volcano information at: https://www.usgs.gov/natural-hazards/earthquake-hazards/science/20-largest-earthquakes-world?qt-science_center_objects=0#qt-science_center_objects

BP for the oil production statistics at https://www.bp.com/en/global/corporate/energy-economics/statistical-review-of-world-energy.html

The Global Volcanism Program at the Smithsonian Institution for the volcano eruption data. http://dx.doi.org/10.5479/si.GVP.VOTW4-2013 ;

Warwick Goldsworthy and Andrew Metcalfe for discussion and comments;

The anonymous reviewers whose comments greatly improved the paper.

All data supporting the conclusions is available from the sources shown in the text.

This research project was funded personally by the author and his wife Julie..

References

Allen, R. J., S. C. Sherwood, J. R. Norris, and C. S. Zender (2012), Recent Northern Hemisphere tropical expansion primarily driven by black carbon and tropospheric ozone, *Nature*, *485*(7398), 350-354, doi:10.1038/nature11097.

Ammann, C. M., G. A. Meehl, W. M. Washington, and C. S. Zender (2003), A monthly and latitudinally varying volcanic forcing dataset in simulations of 20th century climate, *Geophysical Research Letters*, *30*(12), n/a-n/a, doi:10.1029/2003GL016875.

Applegate, G., U. Chokkalingam, and Suyanto (2001), The Underlying Causes and Impacts of Fires in South-east Asia, *Center for International Forestry Research and International Centre for Research in Agroforestry*.

Barry, R. G., and R. J. Chorley (2010), *Atmosphere Weather and Climate* Routledge, Abingdon UK.

Blake, S. A. P., S. C. Lewis, A. N. LeGrande, and R. L. Miller (2018), Assessing the impact of large volcanic eruptions of the last millennium (850–1850 CE) on Australian rainfall regimes, *Clim. Past*, *14*(6), 811-824, doi:10.5194/cp-14-811-2018.

Booth, B. B., N. J. Dunstone, P. R. Halloran, T. Andrews, and N. Bellouin (2012), Aerosols implicated as a prime driver of twentieth-century North Atlantic climate variability, *Nature*, *484*(7393), 228-232, doi:10.1038/nature10946.

Brown, J. N., and A. V. Fedorov (2010), How Much Energy Is Transferred from the Winds to the Thermocline on ENSO Time Scales?, *Journal of Climate*, *23*(6), 1563-1580, doi:10.1175/2009JCLI2914.1.

Cane, M. A. (2005), The evolution of El Niño, past and future, *Earth and Planetary Science Letters*, *230*(3–4), 227-240, doi:http://dx.doi.org/10.1016/j.epsl.2004.12.003.

Center for International Earth Science Information Network - CIESIN - Columbia University (2018), Global Fire Emissions Indicators, Country-Level Tabular Data: 1997-2015, edited, NASA Socioeconomic Data and Applications Center (SEDAC), Palisades, NY.

Cook, E. R., K. J. Anchukaitis, B. M. Buckley, R. D. D'Arrigo, G. C. Jacoby, and W. E. Wright (2010), Asian Monsoon Failure and Megadrought During the Last Millennium, *Science*, *328*(5977), 486-489, doi:10.1126/science.1185188.

Dettling, D. M. (2014), Applied Time Series Analysis, *Zurich University of Applied Sciences*, *https://stat.ethz.ch/education/semesters/ss2014/atsa/Scriptum_v140523.pdf*.

Duncan, B. N., I. Bey, M. Chin, L. J. Mickley, T. D. Fairlie, R. V. Martin, and H. Matsueda (2003), Indonesian wildfires of 1997: Impact on tropospheric chemistry, *Journal of Geophysical Research: Atmospheres*, *108*(D15), 4458, doi:10.1029/2002JD003195.

Emile-Geay, J., R. Seager, M. A. Cane, E. R. Cook, and G. H. Haug (2008), Volcanoes and ENSO over the Past Millennium, *Journal of Climate*, *21*(13), 3134-3148.

Enfield, D. B. (1989), El Niño, past and present, *Reviews of Geophysics*, *27*(1), 159-187, doi:10.1029/RG027i001p00159.

Forster, P., et al. (2007), Changes in Atmospheric Constituents and in Radiative Forcing. In: Climate Change 2007: The Physical Science Basis. Contribution of Working Group I to the Fourth Assessment Report of the Intergovernmental Panel on Climate Change [Solomon, S., D. Qin, M. Manning, Z. Chen, M. Marquis, K.B. Averyt, M.Tignor and H.L. Miller (eds.)] Cambridge University Press, Cambridge, United Kingdom and New York, NY, USA.

Foster, G., and S. Rahmstorf (2011), Global temperature evolution 1979–2010, *Environ. Res. Lett.*, *6*, doi:doi:10.1088/1748-9326/6/4/044022.

Gao, C., A. Robock, and C. Ammann (2008), Volcanic forcing of climate over the past 1500 years: An improved ice core-based index for climate models, *Journal of Geophysical Research: Atmospheres*, *113*(D23), doi:10.1029/2008jd010239.

Gelaro, R., et al. (2017), The Modern-Era Retrospective Analysis for Research and Applications, Version 2 (MERRA-2), *Journal of Climate*, *30*(14), 5419-5454, doi:10.1175/jcli-d-16-0758.1.

Hammer, Ø., D. A. T. Harper, and P. D. Ryan (2001), PAST: Paleontological statistics software package for education and data analysis. , *Palaeontologia Electronica 4(1): 9pp*, 9pp.

Handler, P., and K. Andsager (1990), Volcanic aerosols, El Niñmo and the Southern Oscillation, *International Journal of Climatology*, *10*(4), 413-424, doi:10.1002/joc.3370100409.

Hansell, R. A., S. C. Tsay, Q. Ji, K. N. Liou, and S. C. Ou (2003), Surface aerosol radiative forcing derived from collocated ground-based radiometric observations during PRIDE, SAFARI, and ACE-Asia, *Appl Opt*, *42*(27), 5533-5544.

Hegerl, G. C., F. W. Zwiers, P. Braconnot, N. P. Gillett, Y. Luo, J. A. Marengo Orsini, N. Nicholls, J. E. Penner, and P. A. Stott (2007), Understanding and Attributing Climate Change. In: Climate Change 2007: The Physical Science Basis. Contribution of Working Group I to the Fourth Assessment Report of the Intergovernmental Panel on Climate Change [Solomon, S., D. Qin, M. Manning, Z. Chen, M. Marquis, K.B. Averyt, M. Tignor and H.L. Miller (eds.)]. Cambridge University Press, Cambridge, United Kingdom and New York, NY, USA.

Hirono, M. (1988), On the trigger of El Niño Southern Oscillation by the forcing of early El Chichón volcanic aerosols, *Journal of Geophysical Research: Atmospheres*, *93*(D5), 5365-5384, doi:10.1029/JD093iD05p05365.

Huang, B., P. W. Thorne, V. F. Banzon, T. Boyer, G. Chepurin, J. H. Lawrimore, M. J. Menne, T. M. Smith, R. S. Vose, and H.-M. Zhang (2017), Extended Reconstructed Sea Surface Temperature, Version 5 (ERSSTv5): Upgrades, Validations, and Intercomparisons, *Journal of Climate*, *30*(20), 8179-8205, doi:10.1175/jcli-d-16-0836.1.

IPCC (2007), IPCC Assessment Report 4 Glossary.

Kajikawa, Y., B. Wang, and J. Yang (2010), A multi-time scale Australian monsoon index, *International Journal of Climatology*, *30*(8), 1114-1120, doi:10.1002/joc.1955.

Kalnay, E., et al. (1996), The NCEP/NCAR 40-Year Reanalysis Project, *Bulletin of the American Meteorological Society*, *77*(3), 437-471, doi:10.1175/1520-0477(1996)077<0437:TNYRP>2.0.CO;2.

Kaufman, Y. J., B. N. Holben, D. Tanré, I. Slutsker, A. Smirnov, and T. F. Eck (2000), Will aerosol measurements from Terra and Aqua Polar Orbiting satellites represent the daily aerosol abundance and properties?, *Geophysical Research Letters*, *27*(23), 3861-3864, doi:10.1029/2000GL011968.

Kay, J. E., et al. (2015), The Community Earth System Model (CESM) Large Ensemble Project: A Community Resource for Studying Climate Change in the Presence of Internal Climate Variability, *Bulletin of the American Meteorological Society*, *96*(8), 1333-1349, doi:10.1175/bams-d-13-00255.1.

Kirchstetter, T. W. (2004), Evidence that the spectral dependence of light absorption by aerosols is affected by organic carbon, *Journal of Geophysical Research*, *109*(D21), doi:10.1029/2004jd004999.

Kirtman, B., et al. (2013), Near-term Climate Change: Projections and Predictability. In: Climate Change 2013: The Physical Science Basis. Contribution of Working Group I to the Fifth Assessment Report of the Intergovernmental Panel on Climate Change Stocker, T.F., D. Qin, G.-

K. Plattner, M. Tignor, S.K. Allen, J. Boschung, A. Nauels, Y. Xia, V. Bex and P.M. Midgley (eds.)].*Rep.*, IPCC, Cambridge, United Kingdom and New York, NY, USA.

Lamarque, J. F., et al. (2010), Historical (1850–2000) gridded anthropogenic and biomass burning emissions of reactive gases and aerosols: methodology and application, *Atmospheric Chemistry and Physics*, *10*(15), 7017-7039, doi:10.5194/acp-10-7017-2010.

Levy II, H., D. T. Shindell, A. Gilliland, M. D. Schwarzkopf, and L. W. Horowitz (2008), Executive Summary in Climate Projections Based on Emissions Scenarios for Long-Lived and Short-Lived Radiatively Active Gases and Aerosols. H. Levy II, D.T. Shindell, A. Gilliland, M.D. Schwarzkopf, L.W. Horowitz, (eds.). A Report by the U.S. Climate Change Science Program and the Subcommittee on Global Change Research, Washington, D.C.

Maher, N., S. McGregor, M. H. England, and A. S. Gupta (2015), Effects of volcanism on tropical variability, *Geophysical Research Letters*, *42*(14), 6024-6033, doi:10.1002/2015GL064751.

Mann, M. E., M. A. Cane, S. E. Zebiak, and A. Clement (2005), Volcanic and Solar Forcing of the Tropical Pacific over the Past 1000 Years, *Journal of Climate*, *18*(3), 447-456, doi:10.1175/JCLI-3276.1.

Maraun, D., and J. Kurths (2005), Epochs of phase coherence between El Niño/Southern Oscillation and Indian monsoon, *Geophysical Research Letters*, *32*(15), n/a-n/a, doi:10.1029/2005GL023225.

McGregor, G. R., and S. Nieuwolf (1977), *Tropical Climatology*, 207 pp., John Wiley and Sons.

McGregor, S., A. Timmermann, M. F. Stuecker, M. H. England, M. Merrifield, F.-F. Jin, and Y. Chikamoto (2014), Recent Walker circulation strengthening and Pacific cooling amplified by Atlantic warming, *Nature Clim. Change*, *4*(10), 888-892, doi:10.1038/nclimate2330 http://www.nature.com/nclimate/journal/v4/n10/abs/nclimate2330.html#supplementary-information.

McPhaden, M. J., et al. (1998), The Tropical Ocean-Global Atmosphere observing system: A decade of progress, *Journal of Geophysical Research: Oceans*, *103*(C7), 14169-14240, doi:10.1029/97JC02906.

McPhaden, M. J., S. E. Zebiak, and M. H. Glantz (2006), ENSO as an Integrating Concept in Earth Science, *Science*, *314*(5806), 1740-1745, doi:10.1126/science.1132588.

Menon, S., J. Hansen, L. Nazarenko, and Y. Luo (2002), Climate Effects of Black Carbon Aerosols in China and India, *Science*, *297*(5590), 2250-2253, doi:10.1126/science.1075159.

Meyers, G., P. McIntosh, L. Pigot, and M. Pook (2007), The Years of El Niño, La Niña, and Interactions with the Tropical Indian Ocean, *Journal of Climate*, *20*(13), 2872-2880, doi:10.1175/jcli4152.1.

Mieville, A., C. Granier, C. Liousse, B. Guillaume, F. Mouillot, J. F. Lamarque, J. M. Grégoire, and G. Pétron (2010), Emissions of gases and particles from biomass burning during the 20th century using satellite data and an historical reconstruction, *Atmospheric Environment*, *44*(11), 1469-1477, doi:http://dx.doi.org/10.1016/j.atmosenv.2010.01.011.

Morice, C. P., J. J. Kennedy, N. A. Rayner, and P. D. Jones (2012), Quantifying uncertainties in global and regional temperature change using an ensemble of observational estimates: The HadCRUT4 data set, *Journal of Geophysical Research: Atmospheres*, *117*(D8), n/a-n/a, doi:10.1029/2011JD017187.

Murray Darling Basin Authority (2011), Annual Report 2010-11*Rep.*

Newhall, C. G., and S. Self (1982), The volcanic explosivity index (VEI) an estimate of explosive magnitude for historical volcanism, *Journal of Geophysical Research: Oceans*, *87*(C2), 1231-1238, doi:10.1029/JC087iC02p01231.
Nicholls, N. (1988), Low latitude volcanic eruptions and the El Niño-Southern Oscillation, *Journal of Climatology*, *8*(1), 91-95, doi:10.1002/joc.3370080109.
Nicholls, N. (1990), Low-latitude volcanic eruptions and the El Niñmo/Southern Oscillation: A reply, *International Journal of Climatology*, *10*(4), 425-429, doi:10.1002/joc.3370100410.
Nicholls, N., B. Lavery, C. Frederiksen, W. Drosdowsky, and S. Torok (1996), Recent apparent changes in relationships between the El Niño-Southern Oscillation and Australian rainfall and temperature, *Geophysical Research Letters*, *23*(23), 3357-3360, doi:10.1029/96GL03166.
Novakov, T., V. Ramanathan, J. E. Hansen, T. W. Kirchstetter, M. Sato, J. E. Sinton, and J. A. Sathaye (2003), Large historical changes of fossil-fuel black carbon aerosols, *Geophysical Research Letters*, *30*(6), 1324, doi:10.1029/2002GL016345.
Nozawa, T., T. Nagashima, H. Shiogama, and S. A. Crooks (2005), Detecting natural influence on surface air temperature change in the early twentieth century, *Geophysical Research Letters*, *32*(20), n/a-n/a, doi:10.1029/2005GL023540.
Ott, L., B. Duncan, S. Pawson, P. Colarco, M. Chin, C. Randles, T. Diehl, and E. Nielsen (2010), Influence of the 2006 Indonesian biomass burning aerosols on tropical dynamics studied with the GEOS-5 AGCM, *Journal of Geophysical Research: Atmospheres*, *115*(D14), D14121, doi:10.1029/2009JD013181.
Otto-Bliesner, B. L., E. C. Brady, J. Fasullo, A. Jahn, L. Landrum, S. Stevenson, N. Rosenbloom, A. Mai, and G. Strand (2016), Climate Variability and Change since 850 CE: An Ensemble Approach with the Community Earth System Model, *Bulletin of the American Meteorological Society*, *97*(5), 735-754, doi:10.1175/bams-d-14-00233.1.
Potts, K. A. (2017), Poster: The South East Asian Aerosol Plume: The Cause of All El Niño Events, in *AGU 2017 Fall Meeting*, edited, Earth and Space Science Open Archive (ESSOAr, New Orleans, USA, doi:https://doi.org/10.1002/essoar.10500075.1.
Potts, K. A. (2018), Poster: How the Natural & Anthropogenic Aerosol Plume over S. E. Asia caused the Millennium Drought, in *AMOS-ICSHMO 2018*, edited, Sydney, Australia, doi:https://doi.org/10.1002/essoar.10500083.1.
Potts, K. A. (2020a), How Extreme Apparitions of the Volcanic and Anthropogenic South East Asian Aerosol Plume caused the Millennium Drought in South Eastern Australian. First Attribution and Mechanism using data from the Last Millennium Ensemble, Large Ensemble, MERRA-2 Reanalysis, four Satellites and the Global Volcanism Program.
Potts, K. A. (2020b), How Extreme Apparitions of the Volcanic and Anthropogenic South East Asian Aerosol Plume Trigger and Sustain El Niño Events. First Attribution and Mechanism using data from the Last Millennium Ensemble, Large Ensemble, MERRA-2 Reanalysis, four Satellites and the Global Volcanism Program.
Power, S., F. Tseitkin, S. Torok, B. Lavery, R. Dahni, and B. McAvaney (1998), Australian temperature, Australian rainfall and the Southern Oscillation, 1910-1992: coherent variability and recent changes, *Aust. Met. Mag.*, *47*.
Predybaylo, E., G. L. Stenchikov, A. T. Wittenberg, and F. Zeng (2017), Impacts of a Pinatubo-size volcanic eruption on ENSO, *Journal of Geophysical Research: Atmospheres*, *122*(2), 925-947, doi:doi:10.1002/2016JD025796.
Ramanathan, V. (2006), ATMOSPHERIC BROWN CLOUDS: HEALTH, CLIMATE AND AGRICULTURE IMPACTS, *Scripta Varia 106*.

Randerson, J. T., G. R. Van Der Werf, L. Giglio, G. J. Collatz, and P. S. Kasibhatla (2017), Global Fire Emissions Database, Version 4.1 (GFEDv4), edited, ORNL Distributed Active Archive Center, doi:10.3334/ORNLDAAC/1293.

Rayner, N. A., D. E. Parker, E. B. Horton, C. K. Folland, L. V. Alexander, D. P. Rowell, E. C. Kent, and A. Kaplan (2003), Global analyses of sea surface temperature, sea ice, and night marine air temperature since the late nineteenth century, *Journal of Geophysical Research: Atmospheres*, *108*(D14), doi:doi:10.1029/2002JD002670.

Remer, L. A., et al. (2009), Executive Summary, in Atmospheric Aerosol Properties and Climate Impacts, A Report by the U.S. Climate Change Science Program and the Subcommittee on Global Change Research [Mian Chin, Ralph A. Kahn, and Stephen E. Schwartz (eds.)]. National Aeronautics and Space Administration, Washington, D.C., USA.

Remer, L. A., et al. (2005), The MODIS Aerosol Algorithm, Products, and Validation, *Journal of the Atmospheric Sciences*, *62*(4), 947-973, doi:10.1175/JAS3385.1.

Robock, A., K. E. Taylor, G. L. Stenchikov, and Y. Liu (1995), GCM evaluation of a mechanism for El Niño triggering by the El Chichón ash cloud, *Geophysical Research Letters*, *22*(17), 2369-2372, doi:10.1029/95GL02065.

Rotstayn, L. D., et al. (2007), Have Australian rainfall and cloudiness increased due to the remote effects of Asian anthropogenic aerosols?, *Journal of Geophysical Research: Atmospheres*, *112*(D9), D09202, doi:10.1029/2006JD007712.

Rotstayn, L. D., M. A. Collier, M. R. Dix, Y. Feng, H. B. Gordon, S. P. O'Farrell, I. N. Smith, and J. Syktus (2009a), Improved simulation of Australian climate and ENSO-related rainfall variability in a global climate model with an interactive aerosol treatment, *International Journal of Climatology*, n/a-n/a, doi:10.1002/joc.1952.

Rotstayn, L. D., M. D. Keywood, B. W. Forgan, A. J. Gabric, I. E. Galbally, J. L. Gras, A. K. Luhar, G. H. McTainsh, R. M. Mitchell, and S. A. Young (2009b), Possible impacts of anthropogenic and natural aerosols on Australian climate: a review, *International Journal of Climatology*, *29*(4), 461-479, doi:10.1002/joc.1729.

Self, S., M. R. Rampino, J. Zhao, and M. G. Katz (1997), Volcanic aerosol perturbations and strong El Niño events: No general correlation, *Geophysical Research Letters*, *24*(10), 1247-1250, doi:10.1029/97GL01127.

Shukla, J., and D. A. Paolino (1983), The Southern Oscillation and Long-Range Forecasting of the Summer Monsoon Rainfall over India, *Monthly Weather Review*, *111*(9), 1830-1837, doi:doi:10.1175/1520-0493(1983)111<1830:TSOALR>2.0.CO;2.

Simkin, T., and L. Siebert (2000), Earth's volcanoes and eruptions: an overview p. 249-261. , in *Encyclopedia of Volcanoes*, , edited by S. H, Academic Press, San Diego.

Solomon, S., et al. (2007), Technical Summary. In: Climate Change 2007: The Physical Science Basis. Contribution of Working Group I to the Fourth Assessment Report of the Intergovernmental Panel on Climate Change [Solomon, S., D. Qin, M. Manning, Z. Chen, M. Marquis, K.B. Averyt, M. Tignor and H.L. Miller (eds.)]. Cambridge University Press, Cambridge, United Kingdom and New York, NY, USA.

Stocker, T. F., et al. (2013), Technical Summary. In: Climate Change 2013: The Physical Science Basis. Contribution of Working Group I to the Fifth Assessment Report of the Intergovernmental Panel on Climate Change*Rep.*, Intergovernmental Panel on Climate Change, Cambridge, United Kingdom and New York, NY, USA.

Sturman, A. P., and N. J. Tapper (1996), The Weather and Climate of Australia and New Zealand. Oxford University Press Australia 476.

Takemura, T., T. Nozawa, S. Emori, T. Y. Nakajima, and T. Nakajima (2005), Simulation of climate response to aerosol direct and indirect effects with aerosol transport-radiation model, *Journal of Geophysical Research: Atmospheres*, *110*(D2), n/a-n/a, doi:10.1029/2004JD005029.

Timbal, B., et al. (2010), Understanding the anthropogenic nature of the observed rainfall decline across south-eastern Australia, *Centre for Australian Weather and Climate Research*, *Technical Report 026*.

Timbal, B., and W. Drosdowsky (2013), The relationship between the decline of Southeastern Australian rainfall and the strengthening of the subtropical ridge, *International Journal of Climatology*, *33*(4), 1021-1034, doi:10.1002/joc.3492.

Timmreck, C. (2012), Modeling the climatic effects of large explosive volcanic eruptions, *Wiley Interdisciplinary Reviews: Climate Change*, *3*(6), 545-564, doi:doi:10.1002/wcc.192.

Tosca, M. G., D. J. Diner, M. J. Garay, and O. V. Kalashnikova (2015), Human-caused fires limit convection in tropical Africa: First temporal observations and attribution, *Geophysical Research Letters*, *42*(15), 2015GL065063, doi:10.1002/2015GL065063.

Trenberth, K. E., J. M. Caron, D. P. Stepaniak, and S. Worley (2002), Evolution of El Niño–Southern Oscillation and global atmospheric surface temperatures, *Journal of Geophysical Research: Atmospheres*, *107*(D8), AAC 5-1-AAC 5-17, doi:10.1029/2000JD000298.

Trenberth, K. E., D. P. Stepaniak, and J. M. Caron (2000), The Global Monsoon as Seen through the Divergent Atmospheric Circulation, *Journal of Climate*, *13*(22), 3969-3993, doi:doi:10.1175/1520-0442(2000)013<3969:TGMAST>2.0.CO;2.

Ummenhofer, C. C., M. H. England, P. C. McIntosh, G. A. Meyers, M. J. Pook, J. S. Risbey, A. S. Gupta, and A. S. Taschetto (2009), What causes southeast Australia's worst droughts?, *Geophysical Research Letters*, *36*(4), doi:10.1029/2008gl036801.

Venzke, E. (2013), Volcanoes of the World v. 4.4.3, edited by S. I. G. V. Program, doi: http://dx.doi.org/10.5479/si.GVP.VOTW4-2013.

Wang, B., and S. An (2002), A mechanism for decadal changes of ENSO behavior: roles of background wind changes, *Climate Dynamics*, *18*(6), 475-486, doi:10.1007/s00382-001-0189-5.

Wang, B., and Z. Fan (1999), Choice of South Asian Summer Monsoon Indices, *Bulletin of the American Meteorological Society*, *80*(4), 629-638, doi:doi:10.1175/1520-0477(1999)080<0629:COSASM>2.0.CO;2.

Wang, B., R. Wu, and K.-M. Lau (2001), Interannual Variability of the Asian Summer Monsoon: Contrasts between the Indian and the Western North Pacific–East Asian Monsoons, *Journal of Climate*, *14*(20), 4073-4090, doi:doi:10.1175/1520-0442(2001)014<4073:IVOTAS>2.0.CO;2.

Wang, C. (2002), Atmospheric Circulation Cells Associated with the El Nin˜o–Southern Oscillation, *Journal of Climate*.

Wang, C. (2004), A modeling study on the climate impacts of black carbon aerosols, *Journal of Geophysical Research: Atmospheres*, *109*(D3), D03106, doi:10.1029/2003JD004084.

Wang, G., and H. H. Hendon (2007), Sensitivity of Australian Rainfall to Inter–El Niño Variations, *Journal of Climate*, *20*(16), 4211-4226, doi:10.1175/jcli4228.1.

Webster, P. J., and S. Yang (1992), Monsoon and Enso: Selectively Interactive Systems, *Quarterly Journal of the Royal Meteorological Society*, *118*(507), 877-926, doi:10.1002/qj.49711850705.

Winker, D. M., M. A. Vaughan, A. Omar, Y. Hu, K. A. Powell, Z. Liu, W. H. Hunt, and S. A. Young (2009), Overview of the CALIPSO Mission and CALIOP Data Processing Algorithms, *Journal of Atmospheric and Oceanic Technology*, *26*(11), 2310-2323, doi:10.1175/2009jtecha1281.1.

Zebiak, S. E., and M. A. Cane (1987), A Model El Ni&ntilde–Southern Oscillation, *Monthly Weather Review*, *115*(10), 2262-2278, doi:doi:10.1175/1520-0493(1987)115<2262:AMENO>2.0.CO;2.

Zhang, D., R. Blender, and K. Fraedrich (2013a), Volcanoes and ENSO in millennium simulations: global impacts and regional reconstructions in East Asia, *Theoretical & Applied Climatology*, *111*(3/4), 437-454, doi:10.1007/s00704-012-0670-6.

Zhang, R., et al. (2013b), Have Aerosols Caused the Observed Atlantic Multidecadal Variability?, *Journal of the Atmospheric Sciences*, *70*(4), 1135-1144, doi:doi:10.1175/JAS-D-12-0331.1.